BEHAVIOR OF RC BEAMS STRENGTHENED WITH CFRP LAMINATES

UNDER FIRE -A FINITE ELEMENT SIMULATION

A THESIS IN CIVIL ENGINEERING

Presented to the faculty of the American University of Sharjah
College of Engineering
in partial fulfillment of
the requirements for the degree

MASTER OF SCIENCE

by
Mohannad Z. Naser
B.S. 2008

Sharjah, U.A.E
March 2011

We approve the thesis of Mohannad Z. Naser | Date of signature

_____ _____

Dr. Rami Hawileh
Assistant Professor
Civil Engineering
Thesis Advisor

_____ _____

Dr. Hayder Rasheed
Associate Professor
Civil Engineering
Kansas State University
Thesis Co-Advisor

_____ _____

Dr. Jamal Abdalla
Professor
Civil Engineering
Graduate Committee

_____ _____

Dr. Elias Saqan
Associate Professor
Civil Engineering
American University in Dubai
Graduate Committee

_____ _____

Dr. Essam Wahba
Assistant Professor
Mechanical Engineering
Graduate Committee

_____ _____

Dr. Jamal Abdalla
Professor
Department Head
Civil Engineering

_____ _____

Dr. Hany El-Kadi
Associate Dean
College of Engineering

_____ _____

Dr. Yousef Al-Assaf
Dean
College of Engineering

_____ _____

Dr. Gautam Sen
Vice Provost, Research and Graduate Studies

BEHAVIOR OF RC BEAMS STRENGTHENED WITH CFRP LAMINATES UNDER FIRE -A FINITE ELEMENT SIMULATION

Mohannad Z. Naser, Candidate for the Masters of Science in Civil Engineering

American University of Sharjah, 2011

ABSTRACT

For the last two decades, the use of Fibre Reinforced Polymers (FRP) material has been successfully employed in many civil engineering applications. FRP strengthening systems are mainly used to retrofit existing and deficient structural members. There has been a lot of research on the performance of such strengthened structures at ambient temperatures. However, there is a lack of information on the behavior of RC beams externally strengthened with FRP systems when bonded to structural members when exposed to environmental hazards i.e. fire. In fact, many design codes are seeking further knowledge and data on the behavior of FRP strengthening systems under elevated temperatures, methods of fireproofing, and fire rating of concrete members strengthened with FRP systems [**1**]. For such reasons, code provisions associated with the use of FRP strengthening systems are quite conservative.

Based on the recommendations of ACI 440.2-08: "Guide for the Design and Construction of Externally Bonded FRP Systems for Strengthening Concrete Structures," [**1**] this thesis aims at investigating some of the areas that warrant further research and development of FRP strengthening systems under fire circumstances. Included is a detailed literature review that provides background information and the most important studies in this field. Finite element (FE) models developed and validated against experimental results published in the literature by other researchers. Overall, the developed FE models achieved good correlation with the experimental measured data. The validated FE model was then extended into parametric study to predict the behavior and response of the FRP system when subjected to fire. The parametric study includes different fire curves, different fire scenarios, different sustained live load levels and insulation schemes, types and thickness on the performance of the strengthened RC beams. Hence, the developed FE model could be used as a valid and economical tool to investigate the

performance of strengthened RC beams with FRP systems under elevated temperature as an alternative to expensive and time consuming experimental investigations.

TABLE OF CONTENTS

LIST OF TABLES

LIST OF FIGURES

ACKNOWLEGMENTS

Throughout my time as a graduate student at the American University of Sharjah, I have been surrounded by enormously supportive individuals. I am indebted to their kindness, perception, and friendship and I dedicate this thesis to all of those people who have helped me out along this ruthless way.

First and foremost, I would like to thank my parents and family. A special thanks to my adviser and friend, Dr. Rami Hawileh for his mentorship, patience and friendship over the past four years and for guiding me through opportunities outside my core research that enabled me to think outside the box and grow maturely both as research and instructor. Also, I would like to thank my co-supervisor, Dr. Hayder Rasheed at Kansas State University for his mentorship, ultimate support and help.

I would like also to thank the Faculty, Staff and Graduate Students in the Department of Civil Engineering at the American University of Sharjah for their assistance and support. In particular, I would like to thank Dr. Jamal A. Abdalla, the Head of Civil Engineering Department for his continues support and assist. In addition, I would like to thank Dr. Elias Saqan and Dr. Essam Wahba for being part on the committee. Dr. Ghassan Abu Lebdeh, Dr. Sameh Al Sayegh, Dr. Mousa Attom, Dr. Adil Al-Tamimi, Dr. Sami Tabsh, Eng. Arshi Faridi, Eng. Aqeel Ahmed, Eng. Riyad, Ms. Lenny, Ehab Shaheen, Ade Salman, Hayder Midhat, Ghaith Al Shamsi, Reem Al Humairi, Ahmed Ghdban, Manal Kaakani, Ahmed Hamed, Abdel Waahab Mostafa and Hana'a D. Al Khatib.

CHAPTER 1 INTRODUCTION

1.1 Problem Statement

Reinforced concrete (RC) members are designed to withstand all types of loads, dead, live, snow, rain, wind, earthquake and fire [**1**]. It is well established that FRP materials are very sensitive to temperature variations. In addition, their mechanical properties are known to degrade with elevated temperature. Further research studies are needed to examine the behavior of FRP when used as retrofitting supplements and subjected to thermal loading. Fire could initiate and rapidly develop to reach very high temperature levels; above 1000^{o}C. Such temperatures are sufficient enough to cause great damage to almost any FRP strengthening system and associated bonding materials by dropping its strength, stiffness, and other properties as well.

Any large losses of strength, stiffness of bonding material would likely to cause localized failures that might initiate a progressive collapse that can cause catastrophic disasters; as in loss of both people's lives and structural integrity. Furthermore, burning of FRP or bonding agents tend to spread toxic gases that might cause difficulties when evacuating residents [**2**]. One of the main concerns regarding the external strengthening systems in case of a fire is the lack of concrete cover. The concrete cover would act as a protecting agent and delay the increase of temperature. The absence of protecting material for an externally strengthening system would cause loss of bond, rapid deterioration of mechanical properties and premature failure of the structural member. Due to the limited research in this field, the need for further investigation in this area is required.

This thesis aims at studying the behavior of CFRP-strengthened RC structural members when subjected to environmental hazards; specifically to fire loading scenarios. Computer simulations using the Finite Element method will demonstrate how useful, accurate and important the implementation of such technological advancement in understanding and predicting the behavior of RC structures strengthened with externally bonded FRP systems when exposed to fire. Providing fast, accurate, relatively economical solutions and most of the above, the ability to conduct parametric studies, finite element method is one of the promising

techniques that can be used [**3**]. Parametric studies are useful since researcher can study different parameters and scenarios to draw a better understanding of the behavior of such members.

1.2 Thesis Objectives

The motivation behind this work initialed from the fact that there are limited number of studies on the performance of RC beams strengthened with externally bonded FRP plates and subjected to fire loading. This thesis seeks in depth investigation on the performance of CFRP-strengthened RC structural members, especially beams when exposed to elevated temperatures. Furthermore, this work attempts to narrow down the existing knowledge gap of such complex in nature phenomenon by exploring different numerical and simulation techniques that were rarely explored in earlier studies.

The outcomes of this study would provide a better guidance to engineers, designers and researchers to improve the current existing code provisions and regulations. The primary objectives of this thesis are:

1) Develop Finite Element (FE) models that can accurately predict the behavior of RC beams externally strengthened with Carbon Fibre Reinforced Polymers (CFRP) under elevated temperatures.

2) Validate the performance of the FE models by comparing the predicted and measured experimental data in terms of:

   a) Temperature distribution along the member's cross section

   b) Mid-span deflection

   c) Failure Modes

3) Conduct parametric studies on using:

   a) Different fire curves

   b) Different fire scenarios

   c) Different sustained live load levels

   d) Different insulation techniques:

      i) Installation schemes

      ii) Material types

      iii) Insulation thicknesses

1.3 Scope

The work presented in this thesis engage finite element simulations of different RC beams strengthened with externally bonded FRP systems, insulated and exposed to elevated temperatures. The developed FE models were based on two novel published experimental programs. One of the validated FE model is extended into a parametric study to investigate numerically the effect of different fire curves, different fire scenarios, different sustained live load levels and insulation schemes, types and thickness on the behavior of the strengthened RC beams.

The developed finite element models are 3D in nature and incorporate different nonlinear temperature-dependent material properties that are involved in current FE simulation. Based on the results of the parametric study multiple conclusions, observations, recommendations and charts were developed. The proposed chart would simplify the process of pre-determining the insulation thickness needed to protect the strengthening systems of similar RC beams when exposed to different fire loads and scenarios.

1.4 Structure of the thesis

This document is divided into multiple chapters. Chapter One starts with brief introduction regarding the nature of this work. Chapter Two presents a state of the art literature review of recent studies concerning the behavior of RC structural members subjected to elevated temperatures. It begins with general information concerning FRP materials, production and properties, then shifts to describe the different uses of FRP materials within the civil engineering applications. In addition, sub-sections provide further discussion on the different material properties of concrete, steel, FRP and insulation materials. The chapter highlights some of the very important concepts of structural fire engineering and studies conducted so far.

Chapter Three provides a brief insight on the behavior of fires and fire actions upon occupants and structures. Also, it discusses the different fire protection systems available and implemented so far. Furthermore, it provides key information on the fire endurance philosophy, evaluation process and heat transfer fundamentals. Finally, statistical information is presented to

show the amount of damage on the economy as well as famous incidents that occurred due to different fire scenarios.

Chapter Four shows the process of developing the 3D finite element models. A brief introduction to the ANSYS simulation environment, different element types, meshing and simulation techniques, in addition to loading set-up and boundary conditions. Multiple material constitutive law models and their associated parameters are discussed. Convergence, failure criteria and solution algorithms are also discussed.

Chapter Five provides the results of the validated FE models against their experimental programs. It starts with discussing multiple aspects of the carried simulation against Williams et al. (2008) [**4**] experiment. In addition, it reviews the parametric study's results in terms of the different fire curves and scenarios, sustained load level and insulation's schemes, type and thicknesses, respectively. Then, it discusses the proposed developed chart that can be used to determine the insulation thickness needed to protect the insulated and strengthened RC beams with different protecting materials and exposed to different fire curves. At the end of the chapter, extra validated models of the experimental work conducted by [**5**] Blontrock et al. (2000) is presented to provide better insights and to show the usefulness of FE modeling.

Chapter Six highlights the main outcomes of this thesis. It provides observations, conclusions and recommendations.

1.5 General

The use of Fibre-reinforced polymer (FRP) materials for civil engineering applications has been gaining a great deal of attention from the research community. FRP materials can provide innovative state of the art solutions for constructing new projects and help retrofitting aging structures. FRPs can be used as external tensile strengthening systems for Reinforced Concrete (RC) structural members such as slabs, beams and girders. In addition, they can be used as confinements for RC columns and piers. Furthermore, FRP-made bars are currently being employed to replace conventional steel bars as embedded reinforcement. FRP's unique characteristics; high strength-to-weight ratio, resistance to electro-chemical corrosion accompanied with their ease of installation draws the attention of designers and engineers. Such

materials are highly popular candidates to be used in new challenging/demanding projects i.e. bridges, off shore structures, dams, waste treatment plants and skyscrapers.

The introduction of FRP materials has started in the early 1940's, by the United States (U.S.) Air Force and Navy. Because of their superior properties, many other industries such as airspace and automotive introduced FRPs into their fields too. It was not until 1986, when FRP was introduced to civil engineering applications by manufacturing tendons for a bridge in Germany from Glass FRP material. Following this by the first only made of FRP pedestrian bridge in Scotland in 1992 [**6**]. Since then, many researchers are investigating the FRP materials' capabilities to accommodate its use in many other applications.

The use of FRP as external strengthening systems to rehabilitate old and existing RC structures has showed great performance by maintaining the structural integrity in terms of increasing both their load carrying capacities and life span. Furthermore, the use of FRP can lower the maintenance costs associated with the retrofitting process.

Externally bonded FRP plates, wraps and sheets are some of the ways in which FRP products can be used to retrofit deficient structures. Near Surface Mounted (NSM), an advanced technique has surfaced up among designers. The NSM technique is based on cutting small grooves in the concrete cover and inserting FRP bars and strips. In general, the use of externally bonded strengthening systems would provide additional tensile and confinement capabilities to exterior faces of RC structural members to increase their current capacities.

Starting from the mid 90's, there has been a great deal of attention on the use of FRP as retrofitting materials and systems for aging structures; due to the corrosion of internal steel reinforcements and approaching their capacities and serviceability limits. Hence, aging structures would not be able to maintain their structural integrity, if not repaired properly. The rehabilitation cost of infrastructure in Canada costs $48 billion and the amount is to increase as the rate of deterioration of many aging structures is increasing [**2**]. While in the United States, there are almost 591,707 bridges in the records, 162,869 are classified as deficient, almost 27.5%. Other bridges need retrofitting at a cost of more than $73.8 billion dollars a year for the next 20 years [**7**]. Hence, the large amount of time, maintenance and repair associated with this process, has been referred to as the global infrastructure crisis.

There have been many creative ideas to retrofit aging structures using external steel jacketing and plates that achieved different levels of success. However, steel can easily corrode and due to the complexity of the installation and maintenance, the use of FRP materials seems to be a better choice.

The present state of research has reached high levels that codes and standards on the use of FRP materials are being published. Still, little research has been done on the performance of FRP systems under elevated temperatures. Thus, further investigation is needed. One of the drawbacks of using FRP systems is their sensitivity to high temperatures which would cause a rapid degradation of their mechanical properties. Hence, the major use of FRP was in structures where structural fire safety and design were not major design criteria i.e. bridges.

Fire can be caused by negligence or intentional causes. Also, natural disasters such as earthquakes can initiate fire in buildings and even damage its fire protection systems whether by damaging water pipes used to load sprinklers with water or causing damage in the electrical circuits responsible for alarms. Such incidents would significantly increase the losses of lives and properties. For these reasons, designers should not rely only on active fire protection systems i.e. sprinklers but also, should provide alternative systems; passive systems, to ensure structural stability against such risks; in cases of active systems failure.

CHAPTER 2 LITERATURE REVIEW

2.1 General

The introduction of innovative ideas and materials seemed to provide new solutions to the different civil engineering applications especially, the global infrastructure crisis. Because of their superior mechanical properties, ease of installation and corrosion resistance, the use of the FRP strengthening systems seems to be very promising. Still, the behavior of such material under fire scenarios has not been fully established. This chapter discusses a state of art literature review of the recent studies concerning the behavior of RC structural members subjected to elevated temperatures as well as the concerns regarding the performance of FRP with the increase of temperature.

2.2 Fiber Reinforced Polymer (FRP)

Fiber-reinforced polymers (FRP) are referred to as composites because they are the final product made by at least two different constituent materials. Such process would produce a new material, called composite, that has more efficient properties than its original parents. One constituent is called the fiber while the other is referred to as the matrix phase. The fiber provides strength and the resin matrix acts like a binder to hold the fibers in their positions [**8**]. Overall, the composite material would have high strength and stiffness in the direction of the fibers and relatively lower strength and stiffness in the other direction. The transverse direction will be responsible for providing shear transfer capacities.

The fibres can have many shapes and dimensions. They can be long, short, continuous or discontinuous. Usually the fibers are directed in one direction but they can also be directed into multiple directions depending on the type of application that the FRP system is used for. There are many types of fibers used in the production of FRP like aramid, boron, glass and carbon. Also, metals, epoxies, ceramics, phenolic, nylons, etc. can be used as matrix materials.

During the last century, engineers in Europe used steel bars, and plates to strengthen bridges' decks and girders. Then, researchers in the United States started using steel plates as external tensile reinforcement to reinforced concrete beams. Due to the facts that external

strengthening is exposed to the surrounding environment and that steel can corrode easily, these trails did not gain much interest because of the need for regular maintenance and the corresponding cost. As mentioned earlier, technological advancement allowed scientists to create multiple types of FRP materials. The main types of FRP are bars, sheets and plates with different dimensions and parent materials. Carbon, Glass, Aramid and Basalt are considered the main materials of FRP.

Few years back, one of the main disadvantages of using FRP was their higher costs compared to the conventional steel, mainly because of the complicated process of producing FRP and the limited suppliers. Still, much recent advancement in the production technology and the wide reputation of using such materials in many applications led to improve their performance and lower their cost.

In order to better understand the characteristics of the new composite material, it is advisable to understand the behavior of each parent material individually.

2.2.1 Fibres

In general, FRPs are orthotropic materials that are very stiff in the fibres direction. As mentioned earlier, Carbon, Glass and Aramid are considered as the three main fibres types that are used in the civil engineering applications. Still, the use of carbon fibre reinforced polymers has become the material of choice to strengthen or retrofit existing structures, mainly because of their high tensile strength, low creep and relaxation as well as availability.

Usually, fibres are selected to have consistent length with high strength and stiffness, and uniform diameter [**9**]. Thus, they have a very large length to diameter ratio. According to [**10**], the small diameter associated with the fibres would ensure fewer defects in a volume compared to the defects available in the same volume if the fibres were to have large diameters. Furthermore, in the case of any fibre breaks, the forces will smoothly transfer to the adjacent fibres that would reduce the probability of a total failure in the composite. The forces will transfer through shear stresses built up in the bonding matrix.

2.2.2 Matrix

The matrix acts as a bonding agent that group and protects the FRP fibres. In addition, the matrix would ensure the equal transfer of forces within the longitudinal fibres and aligned those that are not aligned [**9**] [**11**]. Another key aspect that controls the selection of the matrix is its thermal compatibility with the fibres that would minimize the thermally induced stresses resulted from the different thermal properties of each the fibres and matrix. Furthermore, to optimize the weight of the FRP composite, usually matrices with low densities are chosen to reduce the overall weight of the composite.

It is worth mentioning that the matrix materials can be categorized into two different sub-categories i.e. thermoplastic and thermosetting. In general, thermoplastics include polymer compounds such as polyethylene, and polyamides, while thermosetting matrices have epoxies, and vinyl-esters. Both materials are known to have low thermal conductivities [**11**]. According to Blontrock et al. [**12**] thermosetting matrices are used in many structural engineering applications. They have low viscosities, creep and relaxation, thermal stability at service temperatures compared to thermoplastics matrices.

2.2.3 Fibre-Reinforced Polymer

The strength and stiffness of the FRP, mechanical properties of the matrix, fibre's cross sectional area and orientation, fibre-resin volume fraction, parent materials and manufacturing process can all govern the material properties of the FRP composite. Although of their relatively higher costs, Carbon fibres are often used more than Glass fibres because of the their high modulus of elasticity compared to steel material as well as superior corrosion resistance especially to alkaline environments that Glass fibres lack [**13**]. According to [**13**,**14**], the major concerns of the use of Aramid fibers as strengthening materials are their tendency to absorb moisture and susceptibility to creep.

Figure 2.1 shows stress-strain curves for different FRP and steel products available in the markets. It is clear from Fig. 2.1 that the FRP material behaves linear elastically up to failure, they lack a post yield behavior and in some cases they have comparable or even higher elastic modulus compared to steel material. Another observation shown in Fig. 2.1 is that FRP materials

have relatively lower strains at failure in the range of (0.45 to 2.85%) which explains the brittle nature of these composite materials and emphasizes the need to properly detail the to-be strengthened members.

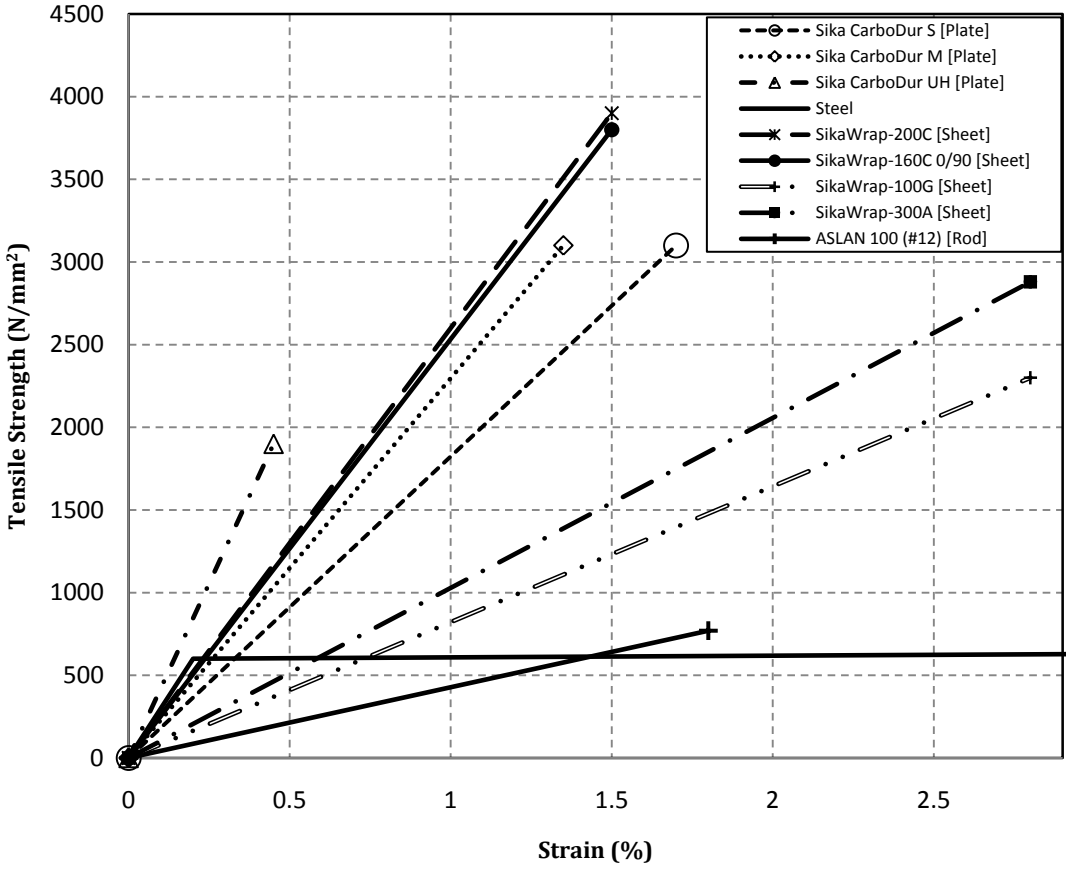

Figure 2.1 Stress-strain curves for different FRP products

On the other hand, Table 2.1 provides qualitative assessment between carbon, glass and aramid FRP based on different criteria.

Table 2.1 Qualitative comparison of different FRP material [**15**]

Criterion	*Carbon*	*Glass*	*Aramid*
Modulus of Elasticity	Very Good	Adequate	Good
Tensile Strength	Very Good	Very Good	Very Good
Fatigue	Excellent	Adequate	Good
Alkaline Resistance	Very Good	Inadequate	Good
Price	Adequate	Very Good	Adequate

2.2.4 The Role of Fibre-Reinforced Polymers in Civil Engineering Application

Concrete material is one of the main choices for civil engineering application because of its long term durability and effectiveness. However, on the long term, reinforced concrete structural members suffer corrosion of internal steel reinforcements. Thus, rehabilitation process must take place to retrofit aging structures; especially those of high importance and long life span i.e. bridges and airports, etc.

The open literature has many successful attempts of using different FRP products to strengthen structural members for example [**6**,**16**,**17**,**18**] and many more. It should be noted that there has been some individual early studies on strengthening of bridges using Near-Surface Mounted steel bars back in the early 1950's by Asplund [**19**].

It appears that most of the researchers conducted so far agree on the following advantages of FRP materials over conventional steel

1. High strength to weight ratio

2. Good fatigue resistance

3. Resistance to electro-chemical corrosion and electro-magnetic neutrality

4. High tensile strength

5. Ease of installation, site corrections

However, the following seem to be the common shortcomings of FRP materials

1. Elastic behavior and lack of a yield zone

2. Inadequate creep and relaxation performance

3. Moisture absorption

4. Low resistance against elevated temperatures which cause severe loss of the mechanical properties such as, stiffness and strength

Many researchers have pointed out the available knowledge gap on the performance of FRP materials under elevated temperatures research area. The ACI Committee 440 [**1**] recommended further investigation on the fire resistance and fireproofing of retrofitted RC structural members using FRP materials. In case of fire, the ACI committee recommends that the additional capacity provided by the FRP system to be completely lost and provided reduced load factors of 1.1 and 0.75 for dead and live loads, respectively. The point of such load factors is to prevent a total collapse of the strengthened structure. Still, it is recognized that such factors seem to be very conservative that makes the use of FRP materials less cost effective [**2**] which draws back designers from using FRP materials.

The main concerns regarding the performance of externally strengthened RC members with FRP materials in case of a fire can be summarized in the following points:

1. Mechanical properties rapid degradation upon reaching temperatures of 300°C as in

    a) Strength

    b) Stiffness

2. Loss of bond between the FRP/Concrete interface due to the low thermal resistance of most adhesive materials except those that are thermally resistant which can reach up to 200°C [**2**]

3. The need for insulation, multiple tests have shown that the use of insulating materials would significantly increase the fire endurance of strengthened members as concluded in [**4**,**12**].

4. Increased concrete spalling in cases of confining RC columns by FRP warps. The justification is mainly related to the fact that the FRP wraps would act as crust that will not allow moisture evaporation to exit the concrete. Thus it would force the moisture vapor to concentrate near the surfaces of concrete cover and generate internal pressure that might cause explosive failure. Although spalling usually occurs in high strength concrete, the presence of FRP wraps might increase its chances.

5. The different thermal properties between the concrete and adjacent FRP material might cause induced thermal stresses to develop at the interface of FRP/Concrete. Hence, designers need to consider sufficient concrete cover to prevent this phenomenon.

2.2.5 Economic Consideration

At the early days of using FRP materials, the carbon fibres for example were very costly almost US $20/lb due to the complex manufacturing process and low demand. By the end of 1999 the cost was reduced to US $6.5/lb because of the high demand and widespread [**20**]. Usually, structures retrofitted with FRP materials have tendency to have longer life span than those reinforced with conventionally steel reinforcements. In addition, they require less costs allocated to maintenance since FRP materials are not susceptible to corrosion. Furthermore, if one is to use advanced monitoring sensing equipments like fibre optic sensor and intelligent remote sensing the long term overall cost will be considerably less [**2**].

2.3 Material Properties under Elevated Temperatures

The different material properties at elevated temperatures should be considered in both, thermal and structural analysis and design of FRP strengthened RC structural members. Figure 2.2 provides a schematic outline of the different thermal and mechanical material properties investigated herein. The material properties that are required for the analysis are divided into two categories, mechanical and thermal. The mechanical properties are composed of elastic modulus, stress-strain behavior, thermal expansion and creep. On the other hand, the thermal properties are density, specific heat, emissivity and thermal conductivity. Those properties apply to all materials involved in this study namely, concrete, steel and FRP. The subsequent sections will discuss each material at elevated temperatures independently.

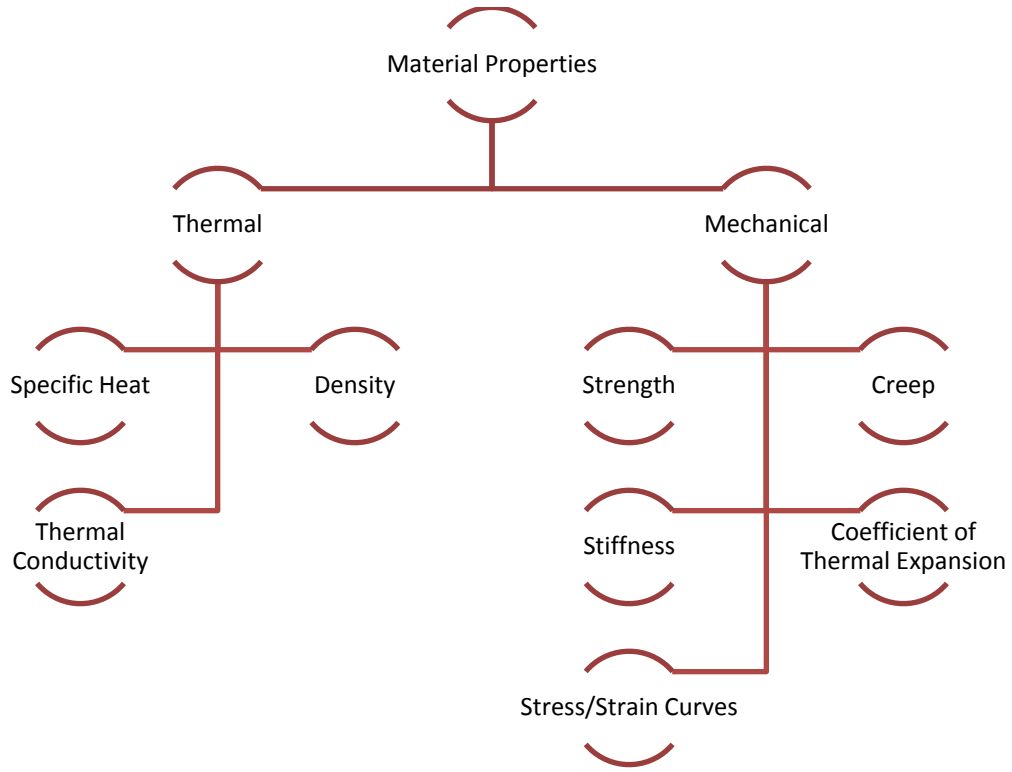

Figure 2.2 Material properties

2.3.1 Concrete

Concrete is a mixture of Portland cement or any other hydraulic cement, fine aggregate, coarse aggregate, and water with or without admixtures [**8**]. Were aggregate refers to as the granular material, such as crushed stone, sand, or blast-furnace slag. Admixtures are chemical agents added to the concrete before or during making the concrete mix. Concrete is known to resist compressive forces; still it is very weak in tension. That is why reinforcing concrete with steel if FRP is a must to ensure structural durability.

Concrete is classified by either its unit weight or its strength as follows,

Unit Weight[1]

Light weight, $90\ pcf \leq \rho \leq 120\ pcf$

Normal weight, $145\ pcf \leq \rho \leq 155\ pcf$

Heavy weight, $200\ pcf \leq \rho \leq 270\ pcf$

[1] Where 1 pcf = 16 Kg/m^3

Compressive Strength[2]

Low strength, $3000 \text{ psi} \leq f'c$

Medium strength, $3000 \text{ psi} \leq f'c < 6000 \text{ psi}$

High strength, $6000 \text{ psi} \leq f'c < 10000 \text{ psi}$

Ultra high strength, $f'c \leq 10000 \text{ psi}$

Discussion the behavior of concrete material has been widely studied and available in the open literature. Lie [**21**] has conducted a detailed comprehensive study on the behavior of concrete material under elevated temperatures. This section will only provide the necessary information related to the behavior of concrete material under elevated temperatures.

2.3.1.1 Mechanical Properties at Elevated Temperature

Strength and Modulus of Elasticity

In physics, the strength of a material is its capability to resist an applied stress without failure while, stiffness is the resistance of an elastic body to deformation by an applied force. Similar to the strength, the type and amount of aggregates generally control the strength of concrete at elevated temperatures. Usually, larger amounts of aggregates provide less venerability of the concrete material to lose its strength when exposed to higher temperatures. However, according to Schneider [**22**] , the room temperature strength, water-cement ratio, type of cement and maximum aggregate size seem to have little effect on the strength and Modulus of Elasticity loss at elevated temperatures as long as temperature gradients are kept below 10°C/mm. Figure 2.3 shows the normalized strength versus temperature of the siliceous and calcareous (carbonate) aggregate concrete, respectively relationships recommended by Eurocode 2 [**23**]. It is clear from Fig. 2.3 that concrete with carbonate aggregate experiences little degradation at elevated temperatures compared to the concrete with siliceous aggregate.

[2] Where 1 MPa = 145 psi

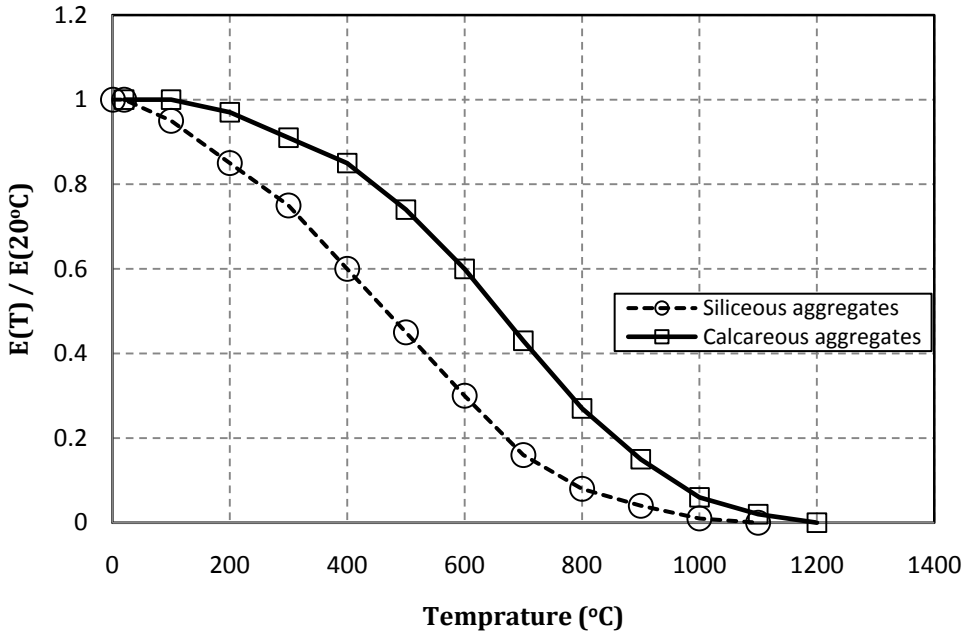

Figure 2.3 Variation of strength of different materials with temperatures

Thermal Expansion

The ability of a substance to alteration in volume in response to a variation in temperature is known as thermal expansion. According to [**21**] it is clear that the aggregate type can affect the magnitude and direction of the thermal expansion because most of concrete materials expand when heated.

Creep

Creep is defined as an increase in strain with time at a constant load level and it is generally caused by a combination of elastic deformation and plastic flow [**24**]. Creep in concrete is very complex and depends on many factors i.e. age, strength, cement and loading. It should be noted at creep effects were not taken into account in the development of the FE models since the fire testing takes a maximum of 2-4 hours.

2.3.1.2 Thermal Properties at Elevated Temperature

The thermal properties of concrete materials vary depending on the minerals involved in the composition of the aggregate and seem to be very dependent on the variation of temperatures.

The main thermal properties involved in the heat transfer phenomena are density, specific heat and thermal conductivity.

Density

The density of a given material is defined by its mass per unit volume. The density of concrete does not rapidly degrade with the increase of temperature until 800°C. According to [**22**], the density of concrete materials made with carbonate aggregate start rapidly degrade due to the mineral degradation within the carbonate minerals.

Thermal Conductivity

The thermal conductivity is a thermal property of materials that measure the ability of different materials to conduct or transfer heat or thermal energy. Concrete materials are known for their relatively low thermal conductivity; hence temperature rises would cause the temperature in the concrete material to rise slowly. Following up with the previous point, during the course of rising temperature, the thermal conductivity of concrete tend to decrease for normal weight concrete while attempts to slightly increase for light weight concrete as shown in Fig. 2.4 for both normal and light weight concrete. One has to keep in mind that the thermal conductivity of concrete at room temperature depends on the type and crystallization of aggregate used as well as moisture content.

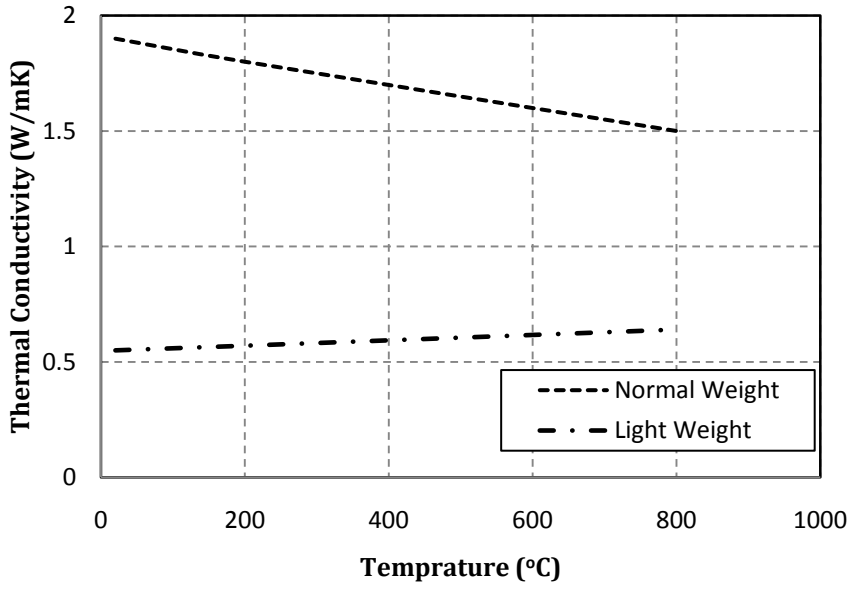

Figure 2.4 Thermal conductivity of normal and light weight concrete [**21**]

Specific Heat

Specific heat measures the amount of heat required to change a specific amount of the material by a unit degree. The specific heat depends on the type of cement and aggregate used in the concrete mix. Moisture content may have a slight influence on the concrete's specific heat in the range of (100°C-115°C) due to moisture evaporation process. The role of aggregate type starts when the temperature of concrete reaches 600°C, then concrete with carbonate aggregates starts to rapidly raise its specific heat due to decarbonazation of carbon particles.

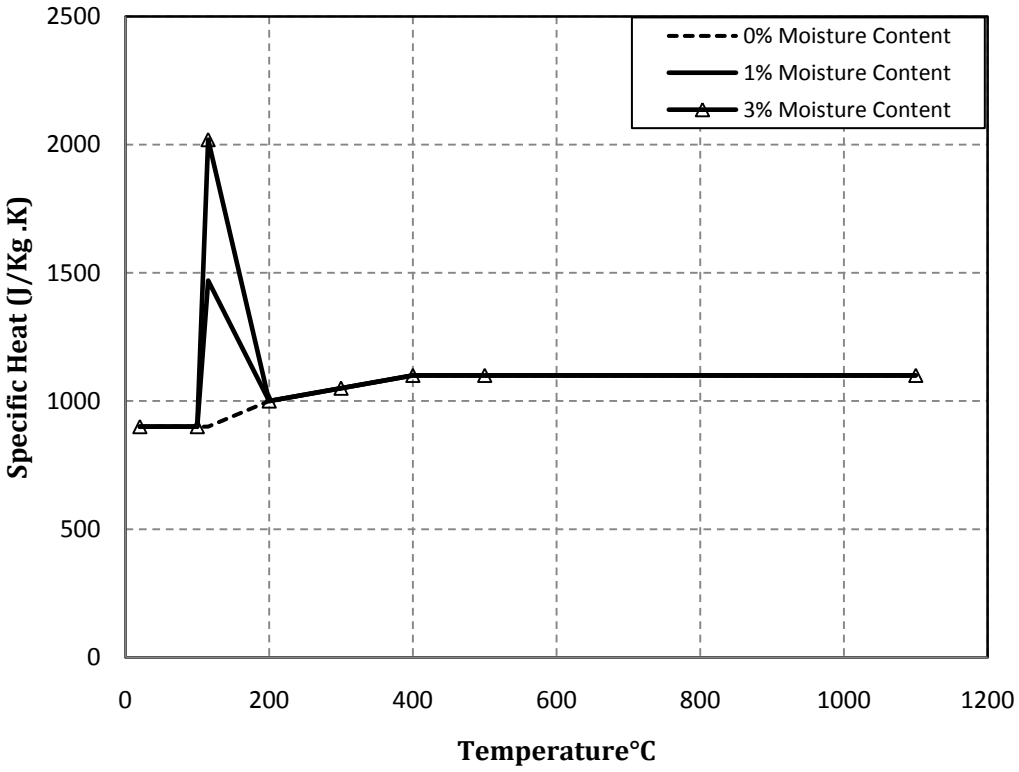

Figure 2.5 Specific heat of concrete with different moisture contents [**23**]

2.3.2 Reinforcing Steel Bars

Because concrete behaves much better in compression than in tension, many designers ignore the concrete's tensile strength. One of the old, most used and enhancements is the steel bars. Steel rebars are used in the tension face of concrete beams to improve concrete beams' resistance to tensile forces and stresses. In addition, they can be used in the compression faces to provide extra resistance to compressive stresses. Steel bars are also used as stirrups to resist shear

and as strips to confine concrete columns. Usually, steel reinforcement has some deformed surfaces to provide more friction and cohesion between the concrete and steel bars themselves.

Usually steel bars are referred to as their yield strength. Such as;

Grade 40 with a yield strength equals 40 ksi

Grade 50 with a yield strength equals 50 ksi

Grade 60 with a yield strength equals 60 ksi

Grade 75 with a yield strength equals 75 ksi

The modulus of elasticity of steel E_s is usually equal to 29000 ksi (200 GPa) at ambient temperatures.

Steel material has some advantages as well. Steel is good in both compression and tension, has better strength to weight ratio than concrete, can be used for longer spans and can be reused and reassembled easily. One of the most advantages of steel is that it is a ductile material. Thus, it can yield before breaking. Such feature is important in terms of design and ductility. However, some of the steel drawbacks are the intensive need for maintenance against corrosion, chemicals and fire.

2.3.2.1 Mechanical Properties at Elevated Temperature

Strength and Modulus of Elasticity

Similar to concrete, steel material's strength and stiffness degrades with the increase of temperature [**25**]. Figure 2.6 shows the strength reduction factors associated with usual steel materials that are used as reinforcements based on Eurocode [**23**]equations. It is clear that steel loses about 50% of its original strength at 500°C. Furthermore, [**21**]showed that the yield plateau of the steel's stress-strain curves observed at ambient temperature disappears at elevated temperatures. Such behavior resembles the softening of the material and reduces its ductility.

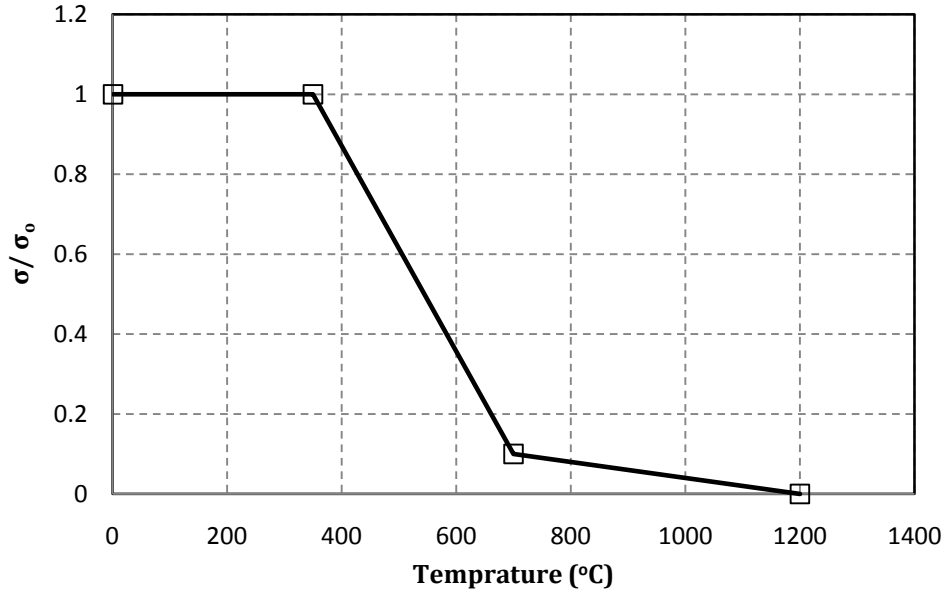

Figure 2.6 Strength reduction factors of reinforcing steel bars at elevated temperature [**23**]

Thermal Expansion

The thermal expansion of reinforcing steel seems to increase with the increase of temperature. Some researchers including Anderberg [**26**] and Purkiss [**27**] believe that the thermal expansion of steel is relatively independent of the type of steel used in the manufacturing process of the steel rebars.

Creep

According to Lie [**21**], creep of steel can be significant at higher temperatures of approximately 450°C. In addition, [**21**]has demonstrated that for practicality, the effects of creep on steel bars can be ignored. Still, one can take into account that there are some published equations that can calculate the effects of creep on structural members as those proposed by Harmathy, [**28**].

2.3.2.2 Thermal Properties at Elevated Temperature

Density

According to Purkiss [**27**] and Buchanan [**29**], designers can use a density of steel at ambient temperature of 7850 kg/m^3 over the whole course of increasing temperature.

Thermal Conductivity

It is known that metals have better conductivity than concrete materials. The thermal conductivity of steel varies with the change in temperature. As shown in Fig. 2.7 the thermal conductivity of steel decreases linearly up to 800°C then stays constant with the increase of temperature.

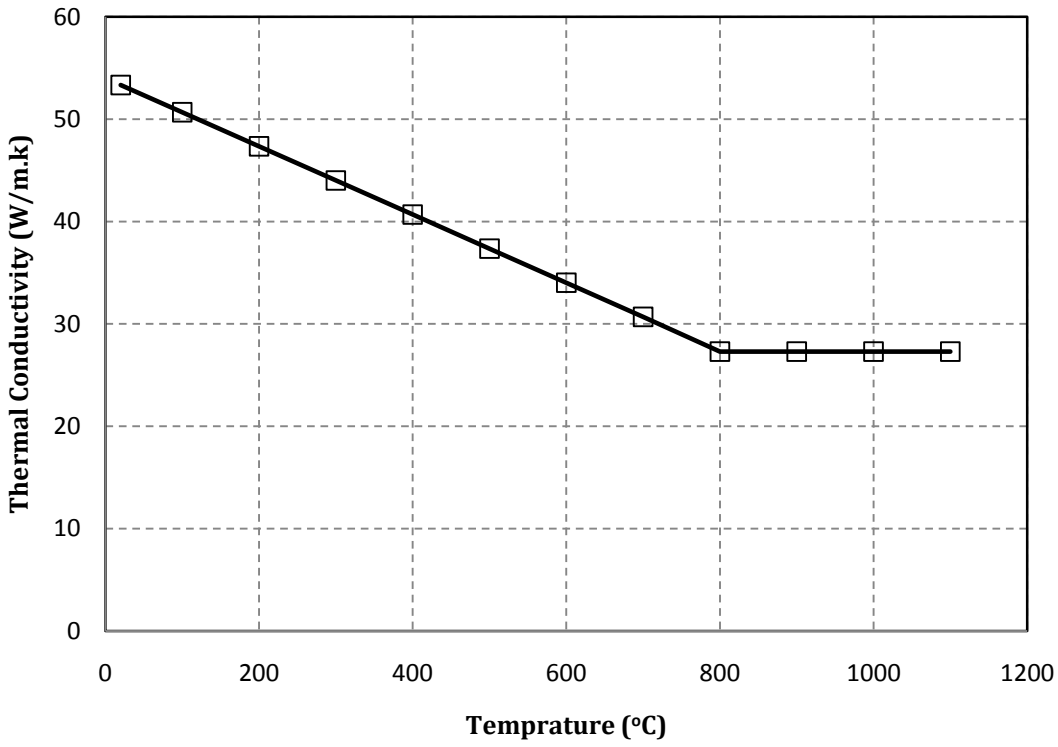

Figure 2.7 Variation of the thermal conductivity of steel materials [**2**]

Specific Heat

The specific heat of steel slightly increase at higher temperatures until temperatures of about 730°C, at which a metallurgical changes occurs that would cause a rapid disturbance in the steel material as shown in Fig. 2.8.

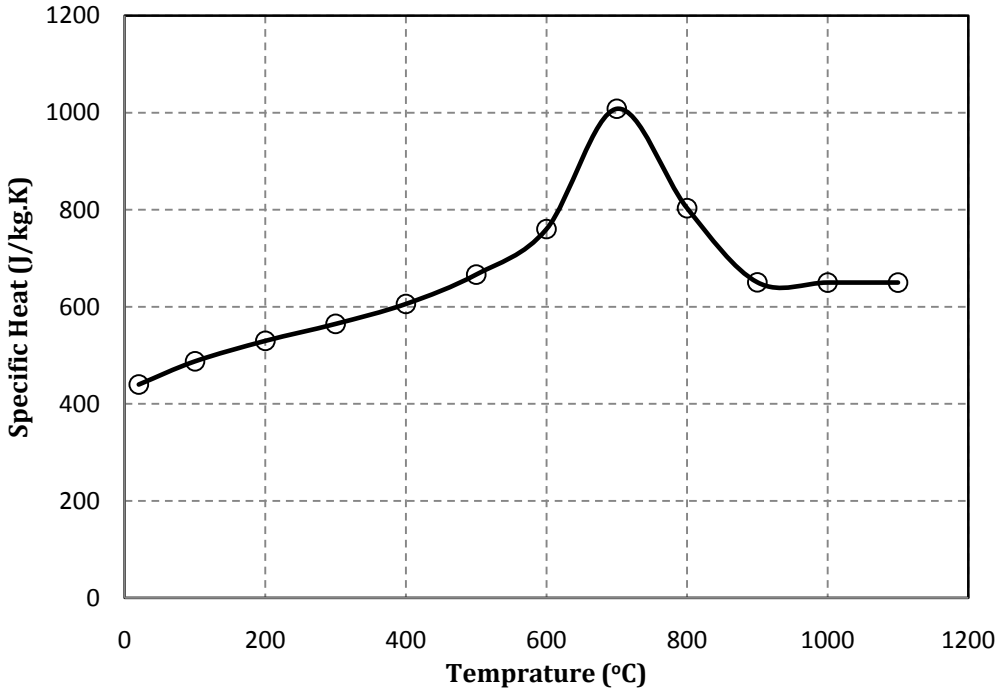

Figure 2.8 Variation of steel specific heat at elevated temperature [**29**]

2.3.3 Fibre-Reinforced Polymers

Fardis and Khalili [**30**] were among the first researchers to recognize the behavior of FRP material when exposed to elevated temperature. Although they recommended the use of flame retardant additives and special fillers to enhance the performance of FRP material against high temperatures, very few studies have investigated the fire resistance of FRP when used in civil engineering structures. Usually FRP composites will quickly burn if subjected to high heats and the resin matrix will contribute to the increase of heat and develop black toxic smokes. Such spread of gases would complicate the process of evacuation and cause some choking cases among residences. Still, once the resin matrix of the first layer burns, the remaining fibres in the layer will act as insulation and protect the rest of the composite for some time.

As mentioned earlier, the main matrix materials are thermosets and thermoplastics. The behavior of thermosets and thermoplastics at high temperature tend to be very different. For example, thermosets usually char and slowly decompose while thermoplastics will soften then melt due to their linear chain molecular structures [**2**,**12**,**31**] have reported a rapid decrease in the elastic and shear modulus of resin matrix materials once the surrounding temperature reaches its

Glass Transition Temperature (GTT). Thus, designers should be aware of the GTT of a given FRP system in order to provide a great deal of attention to such a case. According to Bank [**32**] the GTT is defined as the temperature at which the vague polymeric regions of a FRP material experience a reversible change from solid and brittle to viscous and rubbery. For mostly used resins available in the markets, their GTT is generally below 200°C. On the other hand, the fibres' GTT can reach up to 1000°C; for some materials i.e. carbon fibre. According to [**2**], the maximum service temperatures of general clear epoxies, high performance epoxies, fast cure, and high temperature epoxies are 71, 107, 54 and 204°C, respectively.

2.3.3.1 Mechanical Properties at Elevated Temperature

Strength and Modulus of Elasticity

Figure 2.9 shows a comparison of the strength reduction of different materials based on [**4**]. It can be seen that CFRP and GFRP materials lose 50% of their strength around 300 and 400°C. There have been a good number of experiments on the behavior of FRP materials exposed to elevated temperature i.e. [**33**,**34**,**35**,**36**]. In general, the above researchers agree that FRP materials properties rapidly degrade in case of fire. Some believed that the critical temperature of FRP materials lies between (100 and 200°C) [**33**], while others show that FRP loses almost 85% of its original strength at 300°C [**34**]. On the other hand, [**35**,**36**] illustrated that at 250°C, FRP materials tend to lose 60-75% of their strength provided at room temperature strength. The wide range of temperature is due to the fact that there are many different FRP products available in the market that would make a common generalization conclusion very unlikely. Still, most of the previous studies highlight the roles of insulation in protecting such externally bonded systems.

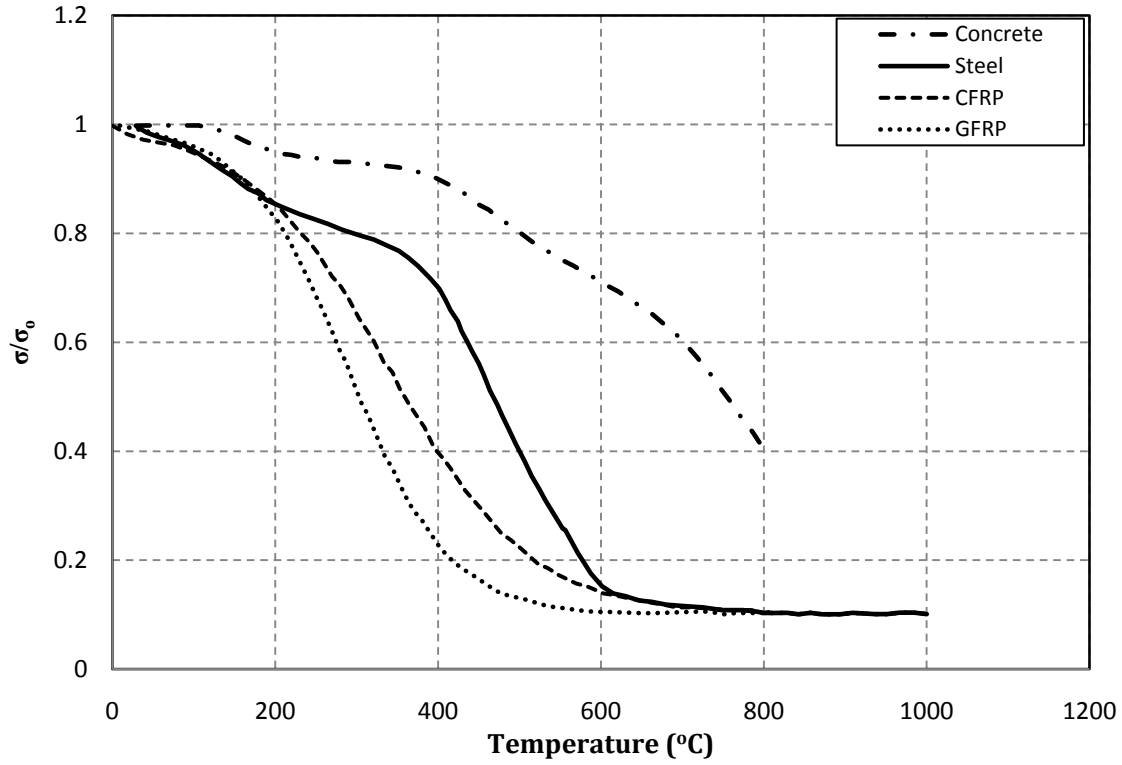

Figure 2.9 Comparison of strength degradation of different material [**4**]

Thermal Expansion

One of the main characteristics of the FRP materials is that they are orthotropic materials. Hence, FRP material has two Coefficients of Thermal Expansion (CTE). In general, the CTE of FRP materials largely depends on the composite material used in the manufacturing process as well as their proportions [**24**]. The CTE of the transverse direction is larger than the CTE of the longitudinal direction because the fibres are concentrated in the longitudinal direction and does not tend to expand a lot. The matrix resins usually have larger CTE compared to the fibres. As mentioned earlier, the thermal compatibility between the FRP and concrete when FRP are used as external strengthening systems may not induce any thermal stresses on the strengthened members at room temperature. Still, the high temperature variation imposed on the strengthened members during fire could be large enough with large magnitude that can cause a significant differential thermal expansion. Such differential thermal expansion might cause concrete spalling, if the concrete cover was not detailed properly or not large enough to withstand the induced thermal stresses.

For comparison purposes, it is worth mentioning that steel, and aluminum are isotropic materials and their CTEs are in the range of ($21.6\text{-}25.2\times10^{-6}$/°C) and ($10.8\text{-}18\times10^{-6}$/°C), respectively. Table 2.2 provides a summary of the longitudinal thermal expansion of different materials at room temperature.

Table 2.2 Summary of the coefficient of thermal expansion of common materials used in civil engineering application [**24**]

Material	***Longitudinal CTE ($\times10^{-6}$/°C)***	***Transverse CTE ($\times10^{-6}$/°C)***
High Modulus Carbon/Epoxy	-0.90	27.0
Ultra High Modulus Carbon/Epoxy	-1.44	30.6
Glass/Epoxy	6.30	19.8
Aramid Epoxy	-3.60	54.0

Creep

It is widely recognized that creep in polymer composite materials is greatly dependent on the matrix of the composite. Also, creep strain of polymer composites increases with the increase in temperature. But, if the direction of the fibres was in the direction of the applied loads, general FRP materials do not exhibit significant increase in creep strain [**24**] and maybe even ignored [**37**].

2.3.3.2 Thermal Properties at Elevated Temperature

Density

The density of FRP material seems to be independent of temperature. The density remains constant up to approximately 550°C then undergoes a slight decrease after which it remains constant until 1000°C. Figure 2.10 shows the variation of density with temperature of a typical FRP material.

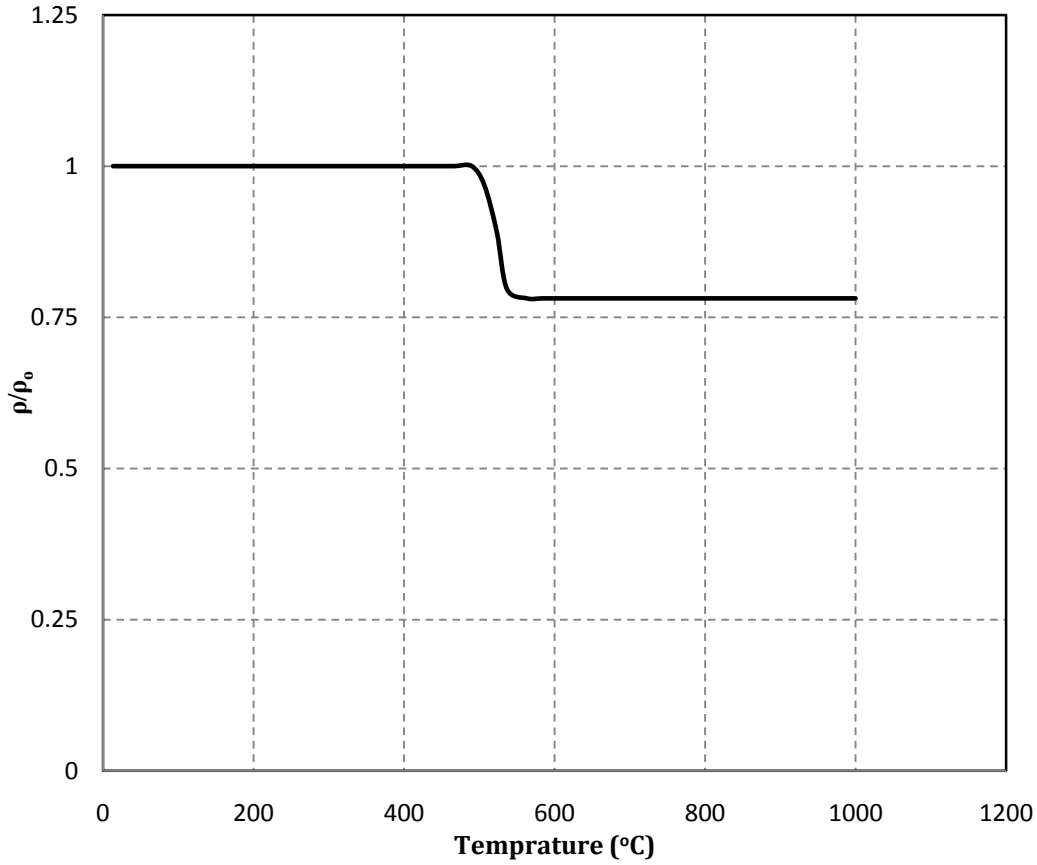

Figure 2.10 Variation of density with temperature of a typical FRP material [**38**]

Thermal Conductivity

Compared to metals, FRP materials have somehow low thermal conductivity. As mentioned earlier, because of the orthotropic nature of FRP materials, the matrix resin material properties and types govern the thermal conductivity of the composite in the transverse direction. Similarly, the high volume and presence of the fibres in the longitudinal direction, governs the thermal conductivity in the longitudinal direction. The thermal conductivity seems to reduce with elevated temperatures. Figure 2.11 shows the variation of both thermal conductivity and specific heat of CFRP materials with the increase of temperature. It must be noted that Fig. 2.11 was reproduced based on the work of [**38**]. Griffis et al., [**38**] studied the thermal properties of CFRP materials by subjecting the specimen to laser radiation up to 3000°C to investigate their performance for potential use in the aerospace industry.

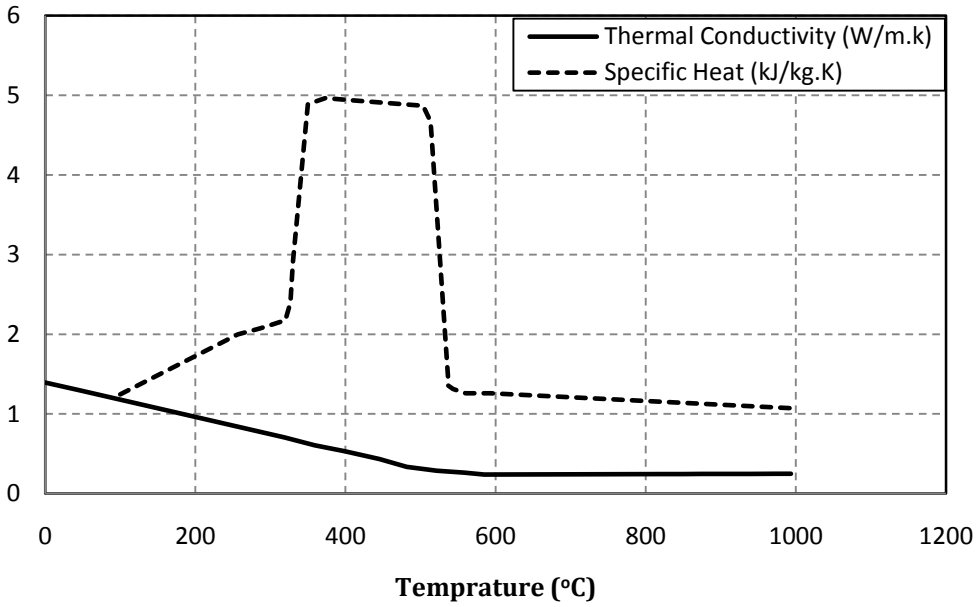

Figure 2.11 Variation of thermal conductivity and specific heat of CFRP materials with the increase of temperature [**38**]

Specific Heat

As shown in Fig. 2.11, the specific heat of FRP materials linearly varies with the increase of temperature. As observed in Fig. 2.11, the complex chemical reactions with the composite are the reason behind the norm of the specific heat of CFRP material shown in Fig. 2.11.

2.3.4 FRP Materials, Smoke Generation and Flame Spread

According to Nelson [**39**], FRP materials tend to ignite toxic gases upon burning. The composite ignition, amount, toxicity and type of smoke depend on the composition of the FRP material. Although there have been many studies on the smoke generation and flame spread of FRP material, few studies are available for the public use since most of the related research was done regarding defense and aerospace industries.

The early use of FRP material as strengthening materials was mainly for bridges. The spread of gases and flames were not a major concern because such strengthening schemes were with relatively small quantities and out in the open air. On the contrary, recent uses of externally strengthening systems are in apartment and buildings. Hence, the spread of gases would cause potential harm to occupants and compromise the fire evacuation process. The higher hydrogen-

to-carbon ratio in the polymers is one of the main causes of the susceptibility of FRP materials to ignite. One should note that other materials i.e. wood have lower ignition temperatures than FRP, which illustrates the beneficial use of FRP [**40**].

To proof that externally bonded FRP systems can achieve better performance when insulated; two sets of tests were conducted by [**41**], the first set was done on unprotected externally bonded systems showed that they achieved a UBC class III. UBC class III rating approves the materials to be used in industrial and factories structures. Then, the same type of specimen in the second test were protected by intumescent latex protective layer have achieved a UBC class I rating. UBC class I rating allow the tested materials to be used in critical areas i.e. exist ways and unsprinkeled stairwells [**41**].

2.3.5 Interface Bond Properties at Elevated Temperature

One of the most important features of the bond between the FRP strengthening systems and concrete surfaces is to form a path at which stresses can transfer from the RC member to the FRP material via shear stresses. At elevated temperatures, degradation of the mechanical properties of the bonding materials can impose some weakness and loss of interaction between the FRP and concrete. Such loss would compromise the state of structural member and initiate a localized failure.

To study the effect of high temperatures on the FRP/Concrete interface, some studies have been conducted lately. Several researchers have studied the performance of FRP rebars embedded in concrete at high temperature. Katz and Berman [**42**], studied the effect of six different texture of GFRP bars on their behavior at temperatures up to 250°C. The bond was found to degrade rapidly at temperatures in the range of 200-220°C. On the other hand, the loss in bond at 100°C was equivalent to the loss of steel bars at the same temperature.

Similarly, Sumida et al. [**43**] tested the bond of carbon and aramid bars at elevated temperatures and recommended that the temperature of the bars should be kept below 100°C. Furthermore, the authors recommended the use of high temperature resistant epoxies.

2.3.6 Insulation Materials

In the building construction industry, insulation systems have been historically used to protect structural steel and timber members. On the other hand, concrete members did not require

insulation due to the good thermal properties of concrete material. Recently, insulation materials have been used to protect concrete structures against extreme fires i.e. tunnels incidents. The insulation materials available nowadays can be best categorized into the following categories insulation mats and plates, insulation boards, Spray-applied insulation materials and Intumescent coatings.

There are different insulation mats and plates that have embedded fibres such as Rockwool® insulation materials. Rockwool® protection materials are made of mineral (rock) fibres and a phenolic binder. Such combination provides low thermal conductivity up to 0.044 W/m.K [**44**] and high melting temperature of fibres (almost 1000°C). Similarly, Fiberfrax® is a ceramic fibre insulation that is made of ceramic fibres. Fiberfrax® also has a low thermal conductivity (0.057 W/m.k) and a very high melting temperature of fibres (1750°C) [**45**].

Spray applied insulation materials are usually combined with Portland cement or Gypsum binder and water, and then the mixture is sprayed on the structural members i.e. columns, beams and slabs. The use of water is to reduce the heat transfer associated with the elevated temperature via evaporation of water particles. Spray applied insulation materials tend to have very low thermal conductivity in the range of 0.043 to 0.078W/m.K [**46**].

Finally, Intumescent coatings protect the insulated structural members via two methods. Once they reach a critical temperature; known as activation temperature, the thin coated layer (0.13-13mm) swells up to 15-30 times its original thickness [**4**]. Such expansion would provide a thicker layer that works as a barrier against any elevated temperatures. Not only this, once the coated layer expands it will create a char layer that will fall off exposing a new Intumescent coated layer and the process repeats itself [**47**].

2.4 Experimental and Numerical Studies

In the last 35 years, several research studies took place to investigate the performance of RC structural members under elevated temperatures. Such studies founded the basic needed information that led to the development of design codes in this field. Some of the key parameters were distinguished to be the concrete cover, size of the member, concrete compressive strength and aggregate type.

The introduction of FRP materials into the civil engineering application introduced a lack of understanding on the performance of FRP strengthening systems under elevated temperatures. Hence, further testing is required. Although there have been very limited experimental testing that made drawing conclusions very hard and not applicable to different type of assemblies or strengthening systems [**2**].

There is not much research on the performance of RC structures strengthened with FRP when exposed to fire. One of the very first studies was conducted by Deuring [**48**] He performed tests on six concrete beams were some were externally strengthened but all exposed to the ISO-834 standard fire curve. The first beam was unstrengthened, while another one was strengthened with an adhesive bonded steel plate. Finally, four were strengthened with CFRP plates. Two of the FRP plated beams were tested without insulation and two were protected with insulating plates of different thickness. It was observed that the unprotected FRP-strengthened beam achieved a fire endurance of 81 minutes. On the other hand, an identical insulated beam with the FRP protected with 40 mm calcium/silicate insulation achieved a fire endurance of 146 minutes. Deuring [**48**] experimental program showed the need for protection systems since the bond action between the CFRP and concrete was lost within the first few minutes for the unprotected specimens.

Similarly, Blontrock et al. [**5**] tested, in a different fire test matrix program, a series of 10 RC beams strengthened with CFRP plates and protected with different insulation boards. In his experimental study, the beams were 200×300mm and spanned 3.15m subjected to the maximum service loads as calculated according to the Eurocode 2 and tested under four point bending. The experimental matrix was composed of two monotonically tested beams up to failure. The two beams served control beams in which the first was unstrengthened virgin beam while the other was strengthened in flexure with a CFRP plate. Then, 2 unprotected and unstrengthened beams and 6 strengthened and protected beams were loaded to full service load and tested under the ISO834 fire exposure.

Blontrock et al. [**5**] investigated several insulation factors i.e. insulation board thickness, location, length and attachment method. The used insulation was mainly consisting of rock wool and/or gypsum board layers (Promat-H and Promotec 100). It was observed that the best fire endurance can be achieved if the U-shaped fire protection insulation is applied to the soffit and

sides of the beams. In addition, the loss of bond between the CFRP and concrete occurred when the temperature in the CFRP/concrete interface reached between 66 and 81°C. A maximum fire endurance of 38min was achieved with this insulation scheme, which is less than the fire endurance ratings required by North American standards in typical building applications.

One of the few studies was conducted by Williams et al. [**4**]. The authors conducted two full size experiments on T-beams strengthened with CFRP plates attached to the soffit of the beams under service loads and exposed to the ASTM E119 [**49**] fire curve. The beams were insulated using U-wrap Vermiculite/Gypsum (VG) insulation with 25mm thickness for the first beam and 38mm for the second. The objective of their study was to evaluate the performance of the strengthened beams and show that CFRP strengthening system can maintain their structural integrity if provided sufficient insulation system. The beams were able to stand the fire up to 4 hours because the insulation system kept the temperature of the strengthening system below the critical temperature.

Another study conducted by Bisby et al. [**50**] on RC slabs strengthened with NSM CFRP bars and subjected to temperatures close and exceeds the transient temperatures of the resin used to bond the NSM bars to the slabs' grooves. A total of 13 slabs were studied with different type of bonding materials; resins and cementitious. The results showed that using cementitious adhesive instead of resins would achieve better results than resins due to the fact that cementitious adhesives have a higher glass temperature than resins. Also, the results showed that NSM bonded by cementitious adhesives were able to withstand fire up to 4 hours while NSM bonded with resins managed to withstand fire to only 44 minutes.

In addition, Yaqub and Bailey [**51**] tested a series of short RC columns under elevated temperatures. They investigated the axial capacity of post-heated circular RC columns repaired with glass and carbon FRP systems. The matrix program was composed of columns that were unheated, post-heated, post-heated and seriously spalled then repaired with mortar, post-heated and wrapped with either glass or carbon fibre reinforced polymer, and finally post-heated and seriously spalled and repaired with both mortar and either glass or carbon FRP. Their study showed that the properly repaired post-heated columns can restore their original capacities or greater.

On the other hand, Raut and Kodur [**52**] tested the performance of high strength concrete columns but under design fire exposure curves. The columns were 3350mm long with a 203×203mm square cross section. Two columns were exposed to the ASTM E119 fire curve while the other four columns were tested under two different design fire curves. The design fire curves differ than the standard curve by having a decay portion that simulates the absence or finish of the burning materials usually available in the apartments. The columns achieved a fire rating between 61 and 221min depending on their compressive strength and fire scenario. On the other hand, 2 columns did not experience any failure due to the recovery of the RC column during the decay phase (burn-out phase). The authors concluded that the current state of rating concrete members based on standard fire curves might be very conservative compared to design fire curve; since burn-out (decaying phase) often occurs in the real fire scenarios.

It is widely known that full scale fire testing is very expensive and requires a lot of preparation and facilitations. Thus, numerical models were extensively improved and used to overcome the difficulties associated with the experimental testing. Williams et al. [**53**] performed numerical study on the behavior of circular RC columns under elevated temperatures. Furthermore, Ahmed and Kodur [**37**] presented a numerical technique based on a macroscopic finite element model that can predict the bond degradation of FRP strengthened RC beams exposed to high temperatures.

Lamont et al. [**54**] developed a 2D heat transfer FE model using HADAPT software. The model was used to simulate the heat transfer across a composite steel beam supporting a RC concrete slab at the Cardington frame fire tests. The heat transfer model was able to simulate the moisture evaporation process in the concrete slab. Although the model was restricted to 2D thermal analysis, good correlation was observed between the predicted and measured results.

Rafi et al. [**55**] modeled the effect of elevated temperature on RC beams reinforced with steel and CFRP bars. The authors used nonlinear temperature dependent material properties to model the different materials used in the RC beams. Modified constitutive material models for the different materials were used. Good correlation was obtained between the FE and experimental results. It was concluded that the FE modeling techniques can be a powerful tool to predict the performance of conventional and strengthened RC beams under elevated temperatures.

In order to study the performance of FRP reinforced concrete structural members i.e. slabs, panels, pre-stress and regular beams. Several key studies were conducted by [**35**,**56**,**57**], Abbasi and Hogg [**58**], respectively.

2.5 Summary

Based on the presented literature review herein, it can be seen that almost all FRP materials used currently in civil engineering applications experience rapid reduction in both strength and stiffness when exposed to elevated temperatures. In addition, FRP materials generally go through large transverse thermal expansion that might cause cracking and spalling of the adjacent concrete cover. Furthermore, if not properly protected by insulating materials, FRP systems will ignite and spread toxic gases after a short period of fire exposure. It is clear that the current literature lacks a lot of information on the performance of strengthened RC structural members when exposed to fire. Thus, the aim of this study is to add more observations, techniques and further explore the performance of such strengthened systems under fire loading. Such information is very important in order to establish relevant design codes.

CHAPTER 3 Fire Phenomenon

3.1 General

The evolution of fire in buildings is a very complex event [**59**]. Yet it can be best described as shown in Fig. 3.1. According to Buchanan [**29**], there are four periods that the development of fire can be described with namely *Incipient*, *Growth*, *Burning* and *Decay*. In the incipient period, heating of available, potential fuel takes place. The transition of stages from Incipient to growth starts by the ignition of fuel. At this point, the spread of fire is generally slowly and extends to the surfaces of combustible materials. Then, more rapidly the fire will grow igniting large flames, hot gases which would spread throughout the entire room and as the temperature of the surroundings increase, the potential of igniting more material increases. Once a good amount of fire plumes develops, they will create a flow of hot gases towards the ceiling and compartment walls. Then, a layer of hot smoke develops under the ceiling that will radiate heat back towards the rest of the room causing more surfaces to ignite [**54**]. The rate of burning in the growth period is mainly controlled by the amount of fuel available. If the initiation of a fire was inspected and extinguished before it reaches flashover or the amount of fuel and ventilation were not sufficient to start a large fire, then the fire would cause some localized damage.

When the burning rate increases, the transition from growth to burning periods completes. Such transition is referred to as flashover. Because the flashover is the transition from a local fire into a larger one, it is a key stage that must be delayed as possible to delay the burning period. Such delay would provide extra time for occupants to leave the damaged area and firefighters to reach the building. This can be done by the aid of smoke detectors and water sprinkler systems. In the burning period, the fire is fully developed that all available materials and surface are burning and the rate of burning is controlled by the ventilation presence. At this stage, the structural members are vulnerable to failure as the fire is very severe and any absence of insulating systems or water sprinklers would even damage the available structural system. Finally, when all available fuel is consumed, and temperatures drop by almost 80% of its maximum value, the decay period takes place. In the decay period, the burning rate is a function

of the fuel itself rather than the available ventilation. The decay period also depends on the shape and material of the fuel, thermal properties of the materials available in the room and opening size.

Fuel controlled fires have sufficient supply of air that it is controlled by the amount and type of the fuel itself. Whereas, ventilation controlled fires tend to have insufficient air supply that the burning process depend on the presence of air at each moment.

It should be noted that the human behavior also differs in each of the four stages of the fire development process. For example, in the incipient period, humans try to prevent the ignition of the materials usually by inspection. On the other hand, the role of regular humans i.e. residences extend to trying to extinguish the initiation of fire in the growth period and if the attempts were not successful, they will escape as the spread of fire rapidly increases. Finally, fire fighters would have to use special equipment to extinguish the fully developed fire in the burning phase.

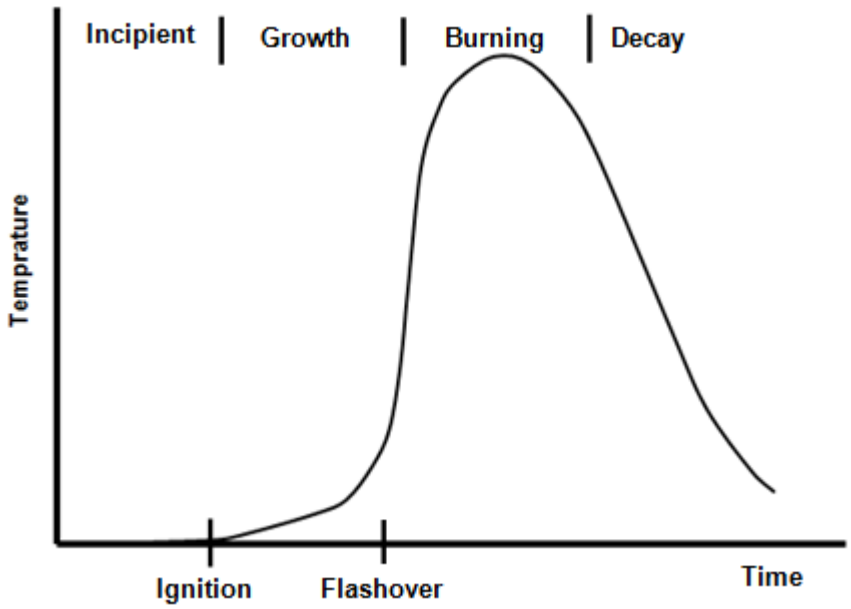

Figure 3.1 Typical Temperature-Time curve for the development of fire [**29**]

Both, the duration and severity of a given fire sound to be a function of the

1. Available mass of fuel

2. Nature of the fuel

3. Degree of ventilation

4. Thermal inertia

3.2 Active and Passive Fire Protection Systems

Humans can detect the very early stage of fire development by sight or smell. Nowadays, sensitive equipments can also be used to detect the ignition of fire. Although such equipment are mainly used in important facilities i.e. museums, still humans are the main way the initiation of fire can be detected in early manner. However, after fire initiation and ignition, a growing fire can still be detected by residents or smoke and heat detectors. Thus, there are two main different systems used to control any incidence of a fire i.e. active and passive protection systems [**29**].

3.2.1 Active Protection Systems

Active protection systems are defined as those systems that can control the spread of fire by action taken persons or other automatic systems. Smoke protection active systems have been introduced lately [**29**,**60**]. Such systems are still new and need complicated design, testing and installation to ensure that the fanned smoke and toxic gases are removed to pre-defined pressurized staircases. Furthermore, fire alarms and activated water sprinklers are considered one of the most used automatic protection systems. As the fire alarm will notify occupants and fire fighters, water sprinklers will delay the growth of fire. Water sprinkler systems if designed and installed correctly, will extinguish burned items in local areas; below the installed sprinklers, and prevent the spread of fire to large areas. One of the drawbacks of using sprinkler systems is that they are dependent on a limited size water supply system that may not be able to extinguish large fire or be operating for a long time. In addition, sprinklers' water supply system can be damaged in case of an earthquake or lack of maintenance.

3.2.2 Passive Protection Systems

On the other hand, passive protection systems are defined as the components built within the structure. They are always present and do not activate in case of a fire. Technically, they can be in forms of insulating materials, poor conductors and special barriers. The passive protection systems tend to be very effective against fire and cost efficient.

3.3 Fire Endurance Philosophy

The purpose of fire engineering is to protect life and property [**21**]. In addition, the fire engineering discipline is meant to prevent the ignition of fires, help preventing fires from spreading across a given structure and impounding fires to allow for safe evacuation of available residences.

As mentioned earlier, at elevated temperatures, the different materials used in the civil engineering applications tend to lose much of their strength and stiffness. Such losses would jeopardize the performance of the individual structural members which would compromise the structural integrity of the available structural systems. The design for fire safety is a complex process and involves different parameters i.e. choice of construction materials, insulation systems, sprinklers, smoke detectors, exits and escapes routes.

One of the commonly used ways of evaluating the fire behavior of a given structural member or structure is by the duration a structure or member (rather than a material) can withstand the exposure to a standard fire curve without losing its load bearing capacity or fire separating function [**59**]. Such duration is called Fire Endurance. Fire Endurance requirements for buildings are provided by different building codes i.e. International Building Code [**61**] International Fire Code [**62**] and the National Building Code of Canada [**63**]. The ASTM E119 standard states that the fire endurance of a flexural assembly is the time during at which the structural member is capable of withstanding its applied loads, the reinforcing steel in the concrete maintains temperatures less than 593°C and the average unexposed surface temperature does not rise more than 140°C, and no individual temperature on the unexposed face rises more than 180°C above room temperature [**64**]. The Fire Endurance requirements are given in terms of allowable times. Such required times are based on the building occupancy and size, member size, dimensions, applied load, end supports conditions, materials involved and fire intensity [**2**]. Such required times are developed for traditional materials i.e. concrete, steel and timber. But still, further work is required for the use of innovative materials and structural systems.

The fire endurance of typical RC members i.e. columns, slabs and beams differs greatly from one to another. Columns are considered the main load bearing members, thus they have the highest required fire endurance; usually up to 4 hours. On the other hand, slabs and beams tend

to have relatively lower fire endurance, typically 1 or 2 hours [**21**]. The reason behind this is that a failure in a slab or beam is considered as a local failure while a failure in a column could trigger a progressive collapse. According to Kodur [**65**], there are three main failure criteria for the different RC members, namely; loss of bearing capacity, loss of insulating capacity and loss of integrity/separating capacity.

The loss of bearing capacity occurs whenever the structural members cannot withstand its applied loads and collapse. On the other hand, the loss of insulating capacity refers to the walls and floor that serve as separators within a building with a maximum temperature rise at the unexposed face of the specimen shall not exceed 181°C, and that the average temperature rise at the exposed face shall not exceed 139°C. Loss of integrity refers to wall, floors assemblies and roofs such that no holes should be formed during a course of a fire.

Concrete is known to have low thermal conductivity. Perhaps this was one of the main reasons why RC members succeeded to achieve good fire rating without externally applied insulation systems. The lower thermal conductivity of the concrete would act as insulation to the embedded steel reinforcements against high temperatures if provided with sufficient concrete cover. The use of enough concrete cover will ensure that the temperature of the steel and prestressing reinforcement remain below their critical temperatures. According to [**65**], the critical temperature is defined as the temperature at which the reinforcement loses up to 50% of its original strength provided at room temperature. The critical temperature of steel and prestressing reinforcement is well established as 593°C and 426°C [**65**]. Unfortunately, critical temperature limits have not been fully developed for most of the FRP materials used so far by the civil engineering industry. There have been few attempts to qualify the critical temperature of GFRP bars [**36**,**66**]. In which the [**36**] presented a detailed literature review and suggested 250°C as a temperature of for the internally used GFRP bars. The use of concrete cover is beneficial for the internally used FRP materials, still for externally bonded FRP system; the concrete cover does not exist.

3.4 Evaluation of Fire Endurance

The main method of measuring the fire endurance of a given structural member or assembly was to experimentally test it against a given standard fire curve [**21**]. The fire endurance testing was formulated in the first quarter of the last century. Still, some fire testing has been recorded and took place when insurance companies needed a comparative evaluation of

different construction types [**54**]. The early fire test recorded so far was conducted by The Associated Architects in the UK. The test was conducted on a floor assembly in the 1790's. Then, a column and another floor assembly were tested by The Technical High School in Munich in 1884 and Denver Equitable Building in the USA in 1890, respectively [**54**].

Although fire tests seem to be the best choice to measure the fire endurance of different elements, one should keep in mind that such tests have been criticized over the years. For example, consistency between different furnaces is hard to achieve since different lining materials, fuel used (oil or gas) and loading rigs differs greatly [**67**]. In addition, the rate of convection and radiation within a given furnace depends upon the degree of turbulence; that is controlled by the geometry of the furnace, and linings materials that contribute to the radiation rate absorbed by the tested specimen, respectively. Drysdale [**68**] commented that the same fire exposure will not be the same in two different furnaces. Figure 3.2 shows different types of the available fire furnaces.

(a) Structural Fire Testing Furnace (Large scale, for Walls) at the Center for Fire Science and Technology in Tokyo, Japan

(b) Fire-Testing Facility at Lawrence Technological University

Figure 3.2 Different fire furnaces

As mentioned earlier, standard fire curves do not represent a decay period which real fires have once the burning stage ends and the fuel is used. Furthermore, the main criticism of standard fire testing is that they test isolated or small assemblies of structural members. In real fire, the rest of the structure would restrain the heated members from expanding; thus imposing additional stresses that might be beneficial in some ways. This was observed by Lie, [**21**] who noted that the fire endurance of a member in an assembly is more than its endurance when tested alone. In addition, although different codes recommend that restraint end conditions should represent those met in practice [**54**]. Still, specimens are often tested unrestrained, since applying boundary conditions is difficult and they might change during the course of the test.

Due to the mentioned reasons above and the fact that experimental testing is a very costly and time consuming process, more attention is being employed towards the use of numerical techniques that uses advanced algorithms, constitutive material models and nonlinear material properties. Such techniques have the potential of reducing the amount of time and computation needed to evaluate the fire endurance. Below is a brief discussion of both procedures.

3.4.1 Experimental Procedures to Evaluate Fire Endurance

The experimental procedure often used to evaluate the fire endurance of a given structural member/assembly is based on full scale testing of that member or assembly in special testing facility (fire furnace) under full and sustained unfactored service loads and subjected to a

given standard fire. The fire curve is defined by a time-temperature curve developed specially for fire tests. The standard fire curve is designed to represent a severe fire incident in a building. Typical standard fire curves used in buildings donated as ASTM E119, ISO834 are shown in Fig. 3.3. Figure 3.3 also shows different fire curves used world widely to test the fire endurance of structures other than buildings i.e. tunnels and oil rigs.

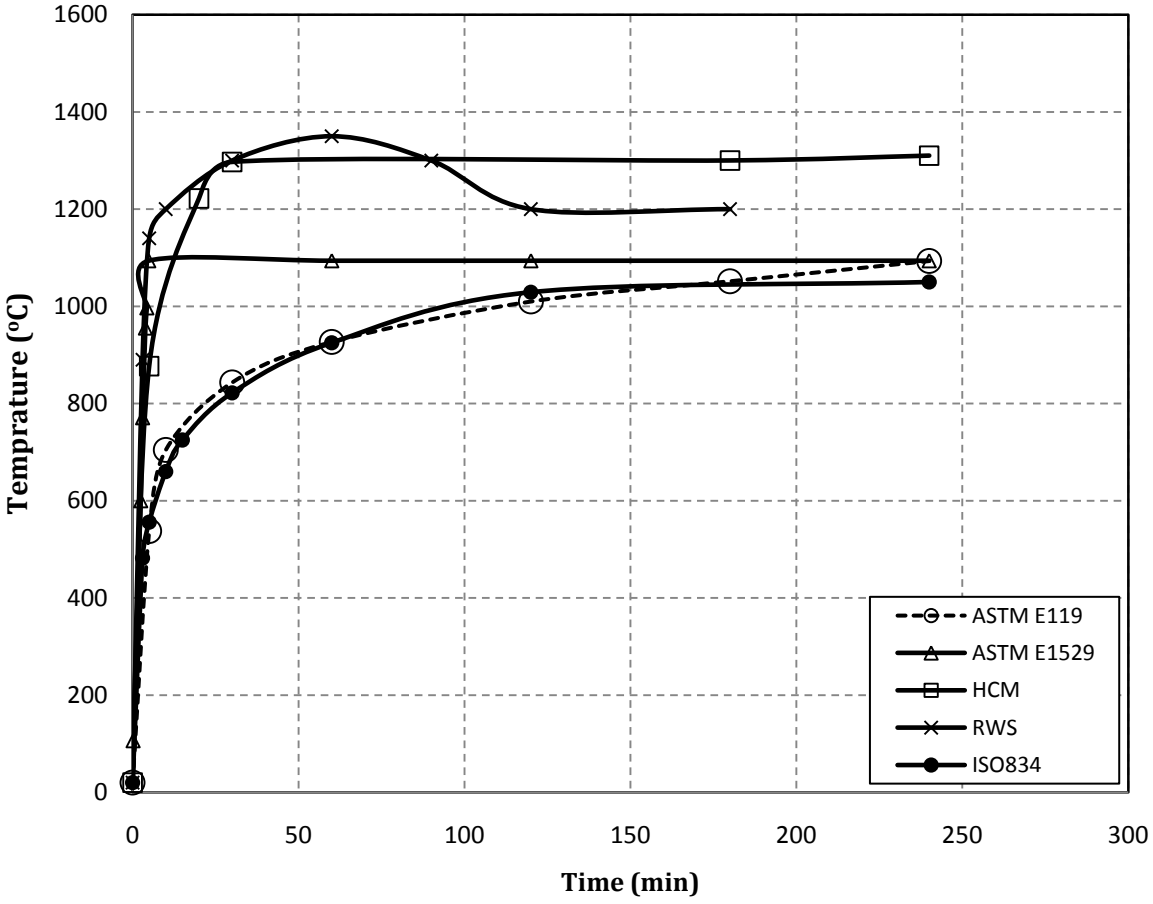

Figure 3.3 Typical Temperature-Time curves (Fire Curves)

Here are some of the definitions and uses of the standard fire curves shown in Fig. 3.3

ISO834 was defined by the International Standards Organization (ISO) in 1932. ISO834 represents a typical fire in which the fuel is made of materials found in general building materials i.e. wood, paper, fabric etc. Temperature increases from 20 to 842°C after the first 5 min and will reach 1,000°C over a period of 120 min [**69**]. The ISO834 curve is mostly used in the design of buildings and apartments. The ISO834 is similar to some European Standards (BS 476part 20, DIN 4102, AS 1530).

ASTM E119 is an American version of the ISO834 standard fire curve for building construction and materials and variety of structural components. Previously called C19 and was established in 1918. According to [**21**], the standard ASTM E119 [**64**] fire curve is similar to the ISO834, UL 263, NFPA 251 and UBC 7-1 fire curves.

ASTM E1529 is another standard fire curve that simulates the effects of large hydrocarbon pool fires on structural members and assemblies. The E1529 was first issued in the early 1990's. It all started when the petroleum industry in the late 1980's needed to develop a new fire testing curve as a result of multiple failures of fire-proofed structural steel members exposed to petroleum spill fires. The ASTM E1529 was designed to apply a sudden and intense shock by instantaneously applying a 158 kW/m^2 on the tested element (FEMA, 2004). The ASTM E1529 has at least a rise of 815°C after the first 3min of fire and 1,010°C and 1,180°C at all times after 5min in exposure.

Hydro-Carbon Modified (HCM) Analogue to the "Hydrocarbon" fire curve, the French Standard defines a fire characteristic curve with a maximum temperature of 1300°C as opposed to the 1100°C used in the old Hydrocarbon fire curve [**69**]. Both the "Hydrocarbon" and the "Hydrocarbon Modified" fire curves initiated within the pet-chemical industries then used in the civil engineering applications. As shown in Fig. 3.3, the HCM is more severe than the ASTM E1529 fire curve. The fuel used in the HCM is based on large amounts of benzene and gasoline around the fire, especially in road tunnels [**69**]. The extreme temperature gradient in the first few minutes would cause a thermal shock to the surrounding materials and possibly causing concrete spalling [**70**].

RWS, RijksWaterStaat It was established by the Ministry of Transport in the Netherlands in 1979 for the evaluation of protecting materials in tunnels which represents the most severe hydro-carbon fire curve. It rapidly reaches 1,200°C and peaks at 1,350°C after 60min, at which concrete materials usually melt, then falling down to 1,200°C after 120min [**70**]. RWS shows the highest temperature of all the curves shown in Fig. 3.3. It describes a scenario of an accident in a road tunnel of which a $50m^3$ gasoline carrying tanker explodes. As a consequence, 300MJ of energy progresses in 180minutes.

It should be noted that the standard fire curves presented in Fig. 3.3 do not include a final decay stage, whereas in a real situations the temperature eventually decreases once most of the

combustible materials have been burnt or extinguished. On the other hand, Fig. 3.4 shows a comparison between the ISO834 standard fire curve and several time-temperature curves that might occur in buildings. Figure 3.4 clearly shows that the standard fire curve might not be able to accurately represent the course of fire in a building from either duration or temperature wise.

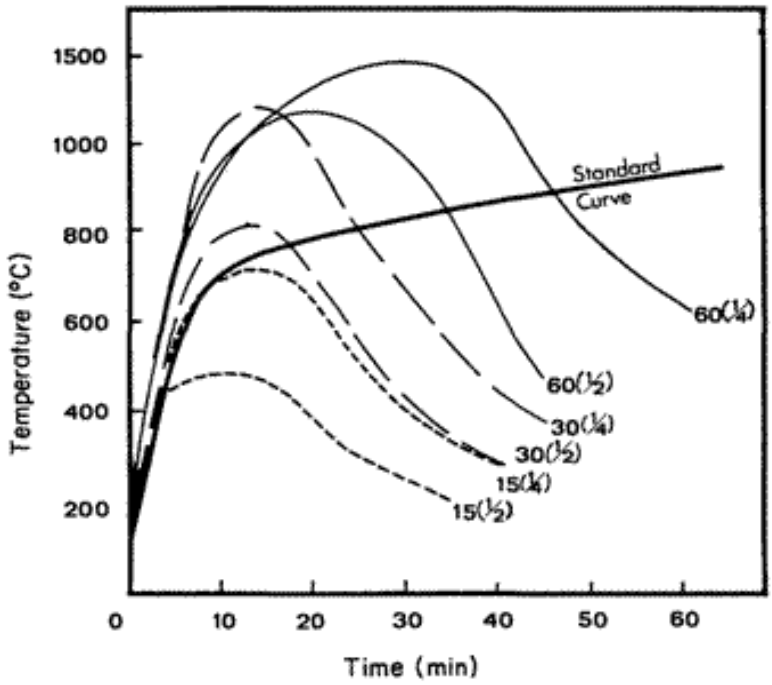

Figure 3.4 Typical time-temperature curves of compartment test fires compared to the ISO standard fire test curve [**71**]

In order to over counter the problem that standard fire curves do not represent real fire scenarios, Ingberg [**72**] presented the concept of Equal Area Concept. The Equal Area Concept can relate any temperature-time curve to the standard fire curve if the areas under the two fire curves were equal above a temperature of 300°C. This concept was the conclusion of different fire tests, in which the fire load was an important factor of measuring the Fire Severity.

The fire severity is a measure of the destructive impact force, in terms of forces and temperatures, of a given fire on a structure [**29**]. Another approach of relating the fire exposure in a real fire to that in a standard fire test was the Time Equivalent Concept. The Time Equivalent Concept uses the fire, fuel load and ventilation of a given room in a real fire to produce a time that would produce the same heating effect of the standard fire curve. Another way developed by Law [**73**] and Pettersson et al. [**74**] is the Maximum Temperature Concept. The Maximum Temperature Concept defines the time of exposure to the standard fire curve that

would result in the same maximum temperature in a protected steel member exposed to a compartment fire as the fire severity. The Minimum Load Capacity Concept is defined as the fire severity as the time of exposure to the standard fire curve that would result in the same load bearing capacity as the minimum that would happen in the real fire scenario [**29**]. So far, the Minimum Load Capacity Concept seems to be the more realistic method of measuring the fire severity.

Lately, The Natural Fire Method has been introduced. The Natural Fire Method incorporates energy and mass balance formulas for different materials available in buildings. In addition, it uses the provided fire load, ventilation presence and compartments geometry to capture the actual fire history and duration [**54**]. Unlike the previously mentioned concepts, this method cannot be related to the standard fire curves.

The results of the experimental tests conducted so far have been used to provide guidelines for minimum concrete cover dimensions needed to keep the temperature of the reinforcements below their critical temperatures. Then, out of these minimum dimensions, fire ratings were evaluated for different elements and assemblies then published in tables [**65**]. But, little experimental programs have been conducted on FRP strengthened RC members that the available data so far cannot be used to generate tables that cover the standard structural elements.

3.4.2 Numerical Procedures to Evaluate Fire Endurance

The use of advanced computational techniques has been extensively used in the area of fire engineering. Different numerical models based on numerical techniques such as finite difference method, finite element method… etc. have been published not long ago by (Lie and Denham, [**75**]; Lie and Irwin, [**76**]; Lie and Kodur, [**77**]). So far, the developed models were based on explicit finite-difference heat transfer, coupled in some cases with a stress-strain or equilibrium analysis [**2**]. Lately, the use of nonlinear 3D finite element has been employed in coupled thermal-stress analysis. The 3D FE models take into account the nonlinear behavior of the different materials used in the analysis. Temperature dependent material properties and full field of results are currently available in some of elite FE software i.e. ANSYS, ABAQUS.

3.5 Heat Transfer

Heat transfers via three ways, namely; Conduction, Convection and Radiation and depending on the conditions, they can occur simultaneously or separately. Figure 3.5 shows the different means of transferring heat. In addition, a brief discussion of each phenomenon is presented herein.

3.5.1 Conduction

The way in which heat transfers within solids is called, conduction. Good heat conductors' transfer heat by the interaction of the free electrons available. In general, good electrical conductors are also considered good heat conductors. On the other hand, poor heat conductors' transfer heat via vibration of molecular lattice [**29**]. Conduction is the main reason solid materials ignite and temperature increases within the structural members and associated insulation systems. Density (ρ), specific heat (C_b) and thermal conductivity (k) are all needed to calculate the heat transfer in solids. Another two derived material properties are needed, Thermal Diffusivity (α) and Thermal Inertia ($k\rho C_b$).

Equations 3.1 and 3.2 show the governing equations for the one dimension of steady state transient heat conduction. The same concept can be extended into two and three dimensions as needed.

$$q'' = k\, dT/dx \tag{3.1}$$

$$d^2T/dx^2 = \frac{\mathbf{1}}{\boldsymbol{\alpha}}\, dT/dt \tag{3.2}$$

where,

q'' is the heat flow per unit area (W/m^2)

According to [**29**], if the structural elements are linear or planar in geometry, then the use of 2D heat transfer procedure is sufficient for almost all fire engineering applications. Still, one has to assume that there is not any thermal gradient within the cross section of the element, on the basis that the temperature of the surrounding environment is uniform. Such basis might be inaccurate for fires occurring in areas with large spaces. Furthermore, performing such 2 and 3D

analysis in finite element software might be time efficient, still such FE packages may not be able to accurately model both mass and vapor transport within permeable materials. Mass and vapor transport can affect the heat transfer phenomena as shown by [**78**].

3.5.2 Convection

Convection is defined as the heat transfer by the movement of fluids i.e. liquids or gases [**29**]. In summary, when the liquid or gas is heated, it expands and becomes less dense then rises upwards. Then, a cooler, denser layer takes place and the phenomenon continues in cycles. Convection is the main factor in both flame spread and raising the heat and smoke layers upward as what is known to be the stack effect [**79**]. The stack effect is defined to be the natural movement of air that resulted in pressure differences between two areas. The pressure difference by itself is the outcome of temperature differences within the layers or floors of a building. Convection usually evolves heat transfer between a fluid and a solid surface. The fluid would either heat or cool the surrounding solid. It is the velocity of the fluid that determines the convection rate. Equation 3.3 shows governing equation of convection.

$$q'' = h\,\Delta T \tag{3.3}$$

where,

h is the convective heat transfer coefficient in (W/m^2K), typical vale is $25W/m^2K$

ΔT is the temperature difference between the solid surface and fluid in (°C or K)

3.5.3 Radiation

The transfer of energy by electromagnetic waves through a vacuum or transparent solid or liquid is called radiation [**29**]. Radiation is considered as the main mechanism of heat transfer between burning flames and available fuel. Not only this, but also from burning rooms and buildings to adjacent rooms or buildings. It is evident from Eq. 3.4 that the radiation is linearly proportional to the fourth degree of the emitting surface temperature.

$$q'' = \Phi \boldsymbol{\varepsilon_t} \sigma \boldsymbol{T_e^4} \tag{3.4}$$

where,

Φ is a configuration or view factor depends on the area (A) of the emitting surface and distance (r) to the receiving surface. $\Phi = A/\pi r^2$

$\boldsymbol{\varepsilon_t}$ is the emissivity factor, ranged from 0-1.0

σ is the Stefan-Boltzmann constant taken as (5.67×10^{-8} W/m^{2}K^4)

T_e is the absolute temperature of the emitting surface (K)

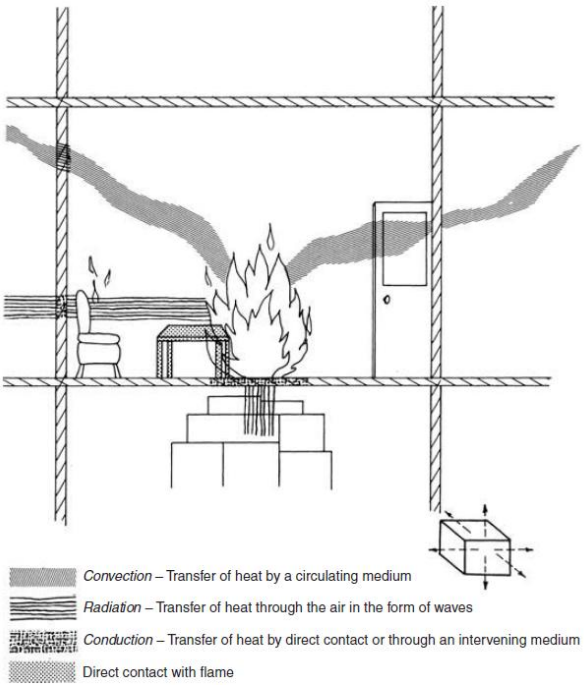

Figure 3.5 Different heat transfer means **[60]**

Further discussion on the heat transfer equation will be presented in subsequent sections.

3.6 Traditional and Performance Based Design Methods

Traditional design methods for fire engineering have been out there for many years now [**29**,**54**]. In general, traditional (perspective) methods state how the building should be constructed from A to Z. This gives little room for designers to make judgments and use innovate tools to analyze and design new structural system or challenging projects. In addition, the use of perspective methods can be easier to use and checked by construction offices and building officials. On the other hand, performance based design methods state how structures should perform under the different applied loads. Such methods are quite flexible when it comes

to designing new challenging systems. Performance based guidelines leave it to the engineers and designers to come up with the best suited strategy to design a structural system.

The main reason why perspective guidelines are still in use is because the performance based design methods have not reached a mature level of understanding and practice yet. The requirements are often descriptive than quantitative that makes it sometimes difficult to quantify and be checked. However, the implementation of performance based methods can lead to innovate and cost effective designs. There is high demand on shifting to performance based methods in the area of fire engineering. Custer and Meacham [**80**] have shown that by 1996 there were almost 13 countries including the United States, Canada, Francs and the United Kingdom that implemented the performance based method [**80**] and the number has numerously increased by now.

One has to keep in mind that the designer should use the available tools i.e. numerical, approved hand calculation… etc. in order to achieve the needed performance requirements. The performance requirements will ensure that the main functional objectives i.e. maintaining structural integrity will not fail during the action of applied loads i.e. fire actions. Once the functional objectives are met, the main goals of the performance based methods i.e. protect life and property will be achieved. Figure 3.6 shows a typical schematic of the fire engineering performance based design methods implemented so far.

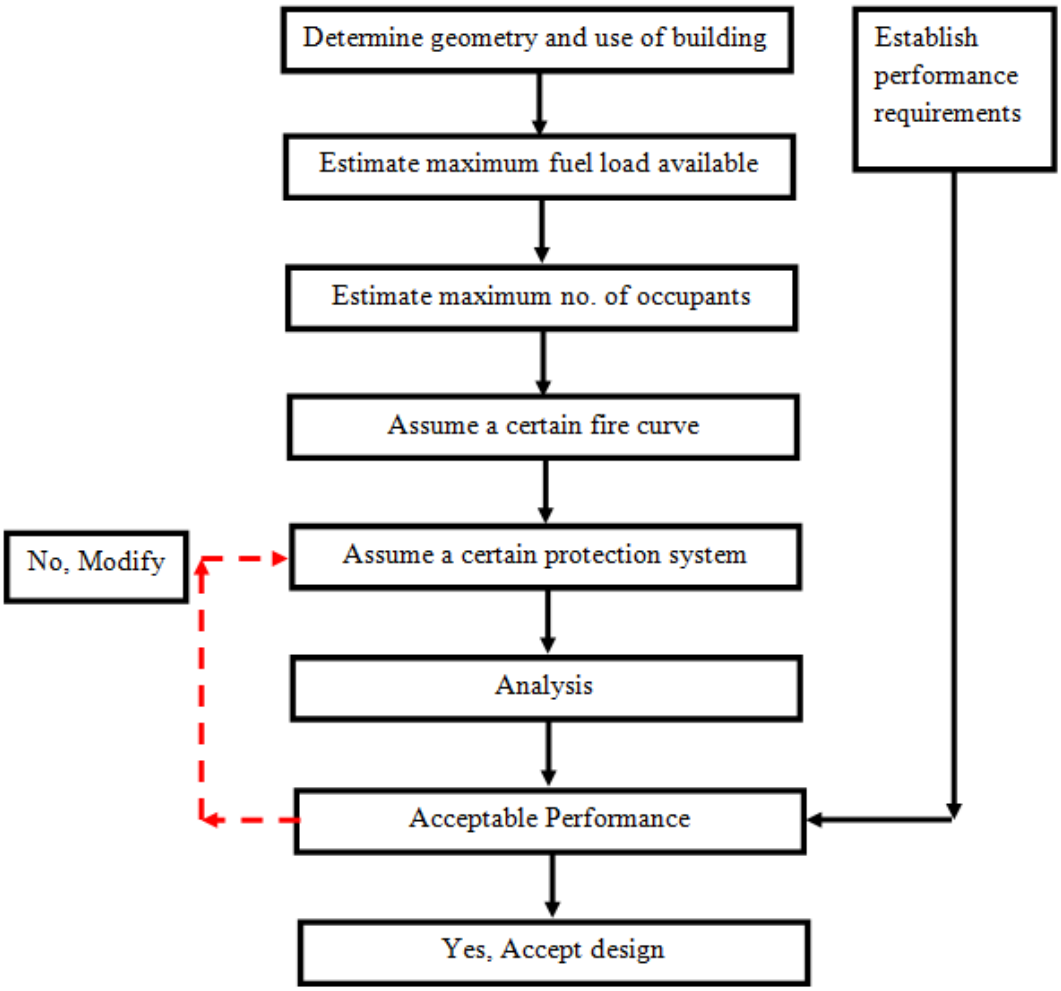

Figure 3.6 Typical schematic of the fire engineering performance based design method [**54**]

3.7 Statistics and Famous Fire Incidents

According to the National Fire Protection Association published report in 2010 [**81**], in the United States alone, there were an estimated of 1,348,500 fires. The casualties of these fires resulted in 3,010 injuries and 17050 civilian fire fatalities, as well as an estimated direct property loss of $12,531,000,000. In addition, there was a civilian fire death every 175 minutes and a civilian fire injury every 31 minutes. Similarly, Council of Canadian Fire Marshals and Fire Commissioners [**82**] stated in 2002 that the population was 31,485,263 and estimated loss of $1,489,012,263 which approximately $47 for individual.

This thesis aims to investigate of the performance of strengthened RC structural members via external FRP systems under fire actions. Since buildings have multiple flooring systems with hundreds of occupants and materials susceptible to fire. The occurrence of fire in buildings can take place at any time. History shows how fire can be a very destructive force. Some of the famous historic incidents known so far and listed in Table 3.1, in addition, Fig. 3.7-3.8 show some pictures of selected buildings under fire.

Figure 3.7 The Great Fire of Rome in 1666 [**29**]

(a) Before Fire (b) During Fire (c) After Fire

Figure 3.8 Television Cultural Center of China [**83**]

Table 3.1 Famous fire incidents [84**]**

Location	***Date***	***Remarks***
Alexandria, Egypt	50 BC	The burn of the library of Alexandria
Rome	64	The Great Fire of Rome
Edo, Japan	1657	30,000 -100,000 fatalities, 60-70 if the city was destroyed
London	1666	Destruction of 13,200 houses and 87 churches
Peshtigo, Wisconsin	1871	Resulted in most deaths by a single fire event in U.S. history
Chicago	1871	Destruction of 17,000 buildings
Chicago	1903	The deadliest single building fire in Iroquois Theater, 602 fatalities
Stalingrad	1942	955 fatalities because of the German bombardment
San Juanico, Mexico	1984	500-600 fatalities and 5000-7000 injuries in fire explosion of a liquid petroleum gas tank

Bradford, England	1985	Bradford City stadium fire with 52 fatalities
New York City	2001	September 11 attacks
Asunción, Paraguay	2004	Ycuá Bolaños supermarket fire, 400 fatalities
Beijing, China	2009	Television Cultural Center fire

CHAPTER 4 Development of The FE Models

4.1 General

This chapter presents the development of the nonlinear 3D Finite Element (FE) models presented in this thesis and used to simulate the behavior of FRP strengthened RC beams exposed to elevated temperatures. As mentioned earlier, the development of a numerical model representing the behavior of strengthened or non-strengthened RC members should take into account both thermal and mechanical response of those members when subjected to elevated temperatures. The main reason behind the development of such FE models is because once they validated against experimental results, the validated models can aid researchers through experimenting different scenarios and parameters that would reduce the dependency on costly, time consuming full scale experimental programs. The FE simulation environment was based on the ANSYS 11.0 FE package. This chapter focuses on the development of the FE models in terms of geometry, element types, meshing techniques, material properties and different constitutive laws at elevated temperature, as well as boundary and loading conditions. In addition, convergence criteria and solution algorithms are discussed herein.

The developed FE models present the experimental work of Williams et al. [**4**] and Blontrock et al. [**5**]. Williams et al. [**53**] tested 2 RC T-beams strengthened with externally bonded CFRP plate and insulated with vermiculite/gypsum (VG) insulation system. The beams were loaded and exposed to the ASTM E119 fire curve during the tests.

Blontrock et al. [**5**] experimental program consisted of ten RC beams varied in the strengthening and protection schemes. The experimental matrix was composed of two loaded and unstrengthened beams and on six loaded and strengthened beams. The fire testing was conducted on the six loaded and strengthened beams under the ISO834 fire exposure. It should be noted that the beams were loaded in a four-point bending set-up. Further information will be discussed in the subsequent sections.

4.2 Mathematical Modeling

In general, the thermal analysis is based on the 3D transient heat flow governing equation that is given by Eq. 4.1, which is derived from the Law of Conservation of Energy. The Law of Conservation of Energy states that the total inflow of heat in a unit time across a certain body must be equal to the total outflow per unit time for the same body [**55**].

$$\rho c \frac{\partial T}{\partial t} = k \frac{\partial^2 T}{\partial x^2} + k \frac{\partial^2 T}{\partial y^2} + k \frac{\partial^2 T}{\partial z^2} + Q \quad (4.1)$$

where:

ρ is the density

c is the specific heat

k is the conductivity

Q is the is the internally generated heat on unit volume per unit time

T is the temperature gradient

t is time

Furthermore, the solution of Eq. 4.1 can be determined if both an initial and boundary conditions on a division or all the boundary of the body in question (domain). Basically, the initial condition defines the temperature distribution over the whole body (domain) at the initiation of heat transfer i.e. $t = 0$. The initial and boundary conditions can be given by Eqs. 4.2 and 4.3, respectively:

$$T(x, y, z, 0) = T_0(x, y, z, 0) \quad (4.2)$$

$$- k \frac{\partial T}{\partial n} = h_c \left(T_s - T_f\right) + h_r \left(T_s - T_f\right) \quad (4.3)$$

where,

n is the direction of heat

h_c is the heat transfer coefficient of solid surface

T_s is the temperature of solid surface

T_f is the temperature of fluid

h_r is the radiation heat transfer coefficient given by Eq. 4.4

$$h_r = \sigma \varepsilon_s \left(T_s^2 + T_f^2\right)\left(T_s + T_f\right) \quad (4.4)$$

where,

ε_s is the emissivity of surface with a range from (0 - 1) 1 being the darkest color

σ is the Stefan-Boltzmann constant 5.669×10^{-8} W/m^2.K^4

The FE formulation is based on the Galerkin weighted residual method where each element is discritized yielding the first order differential equation, Eq. 4.5

$$[k]\{T_n\} + [c]\{T_n\} = \{F_n\} \quad (4.5)$$

where,

$[k]$ is the element heat conduction and convection matrix

$[c]$ is the element heat capacity matrix

T_n is the element nodal temperature vector

F_n is the element nodal heat input vector

Then, the global system is summed up to collect the individual elements yielding the global system shown in Eq. 4.6.

$$[K]\{T\} + [C]\{T\} = \{F\} \quad (4.6)$$

On the other hand, the stiffness matrix [*D*] used in the structural simulations is based on Eq. 4.7. Equation 4.7 tends to relate stresses with mechanical and thermal strains.

$$\{\sigma\} = [\mathrm{D}]\{\varepsilon - \varepsilon_T\}$$

where,

$\{\sigma\}$ is the stress vector

$\{\varepsilon\}$ is the strain vector

$\{\varepsilon_T\}$ is the temperature related total strain

This chapter will introduce the element types used in the FE simulations, then will discuss the geometry, material properties, loading and boundary conditions, convergence criteria and solution techniques for each experimental program individually.

4.3 The Developed FE models of Williams et al. (2008)

4.3.1 Geometry

The RC T-beams were designed with typical dimensions as those used in regular buildings to represent actual fire scenarios. In addition, the beams were loaded up to their service load conditions while exposed to the ASTM E119 fire curve. The beams were identical to each other and had a depth, width of the flange and web thickness of 400, 1220 and 300mm, respectively. Furthermore, the beams were 3900mm long. It should be noted that the length of the members were chosen to satisfy the ASTM E119 standard, which states that the length of the member should be more than 3660mm. In addition, the length of the members was limited to this size due to the limitation of the fire furnace located in the National Research of Canada (NRC), where the tests took place. The main steel reinforcement was two 20mm diameter bars. On the other hand, shear stirrups was 10mm diameter bars spaced at 150mm centre to centre. The main steel reinforcement were two 20mm diameter bars that have a yield and ultimate strength of 500 and 650MPa, respectively [**53**]. Similarly, the 10mm diameter bars have a yield and ultimate strength of 429 and 611MPa, respectively [**4**]. Clear concrete cover to the stirrups was 40mm. Figure 4.1 shows a cross-sectional view of the T-beams. Different cross sectional views of the full and quarter model FE model (FE Beam 1) are shown in Figures 4.2-4.5.

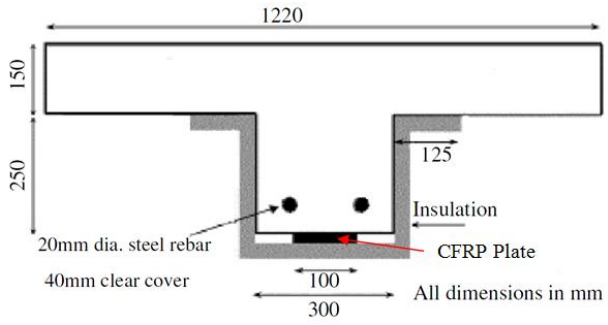

Figure 4.1 Cross-sectional view of the T-beams [**4**]

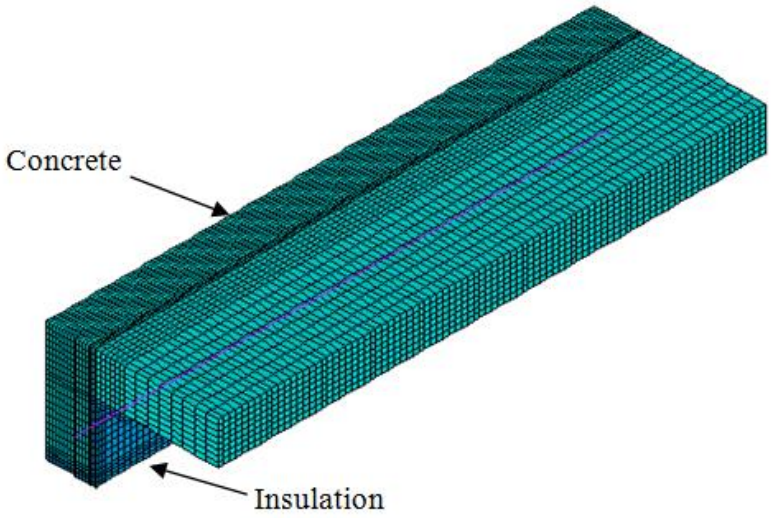

Figure 4.2 Isoparametric view of the Quarter model (FE Beam 1)

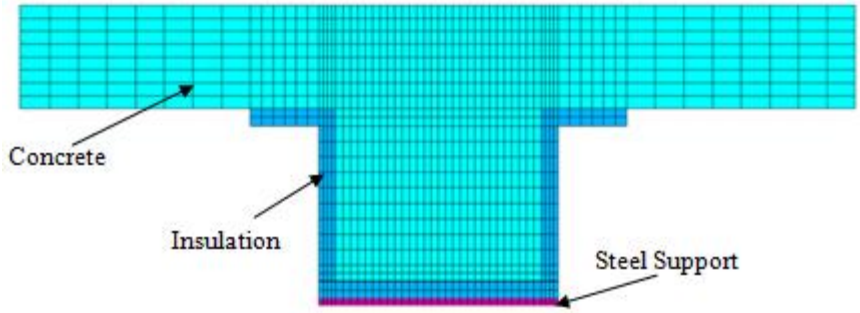

(a) Full model

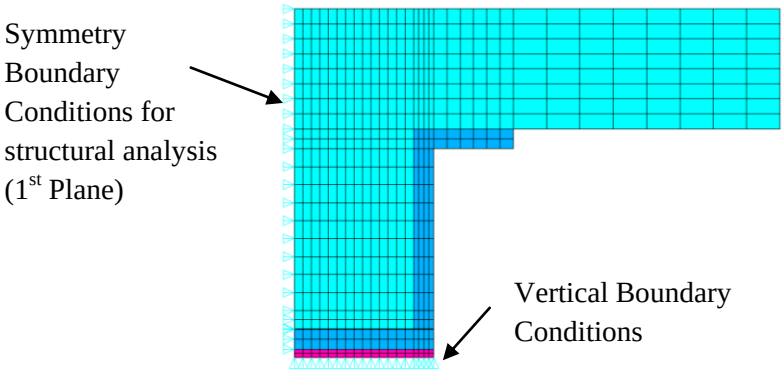

(b) Quarter model

Figure 4.3 Cross-sectional view of the Quarter model (FE Beam 1)

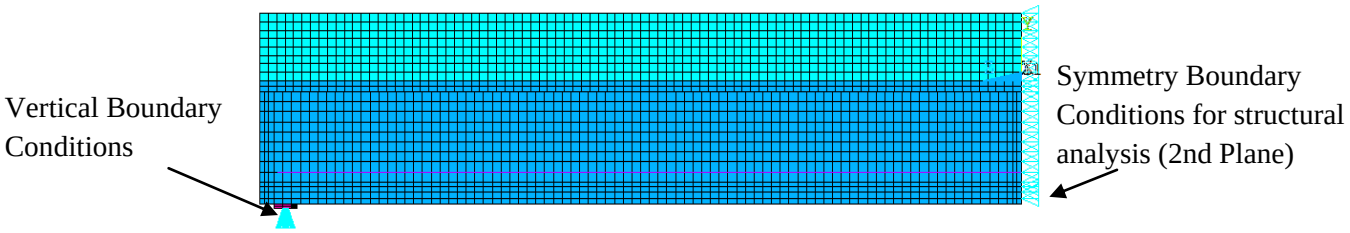

(a) Side view of the Quarter model

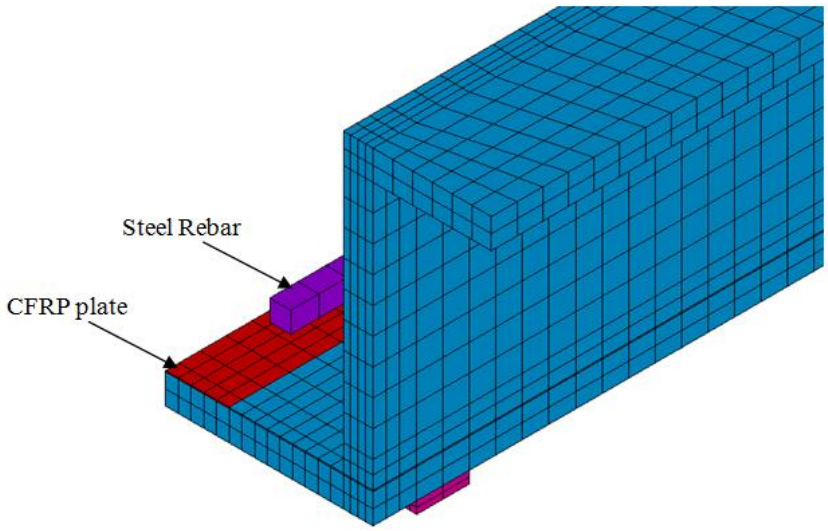

(b) Different materials used in the Quarter model

Figure 4.4 Different views of the Quarter model (FE Beam 1)

4.3.1.1 Mesh Sensitivity Analysis

Mesh sensitivity analysis was performed to obtain the optimum element size in this numerical investigation. Four different mesh sizes were developed and analyzed. The results of the mesh sensitivity analysis are provided in section 5.3.1. Figure 4.5 shows the four different meshes used in the mesh sensitivity analysis. Table 4.1 shows the number of elements in each of the different meshes used in the mesh sensitivity analysis. Furthermore, it should be noted that the thermal analysis for both the full and quarter model shown in Figs. 4.3a and 4.3b are conducted to confirm the validity of the quarter model in the analysis of this study.

Table 4.1 Number of elements used in the mesh sensitivity analysis

Models	*Number of elements*
Mesh 1	9000
Mesh 2	16650
Mesh 3	30000
Mesh 4	51000

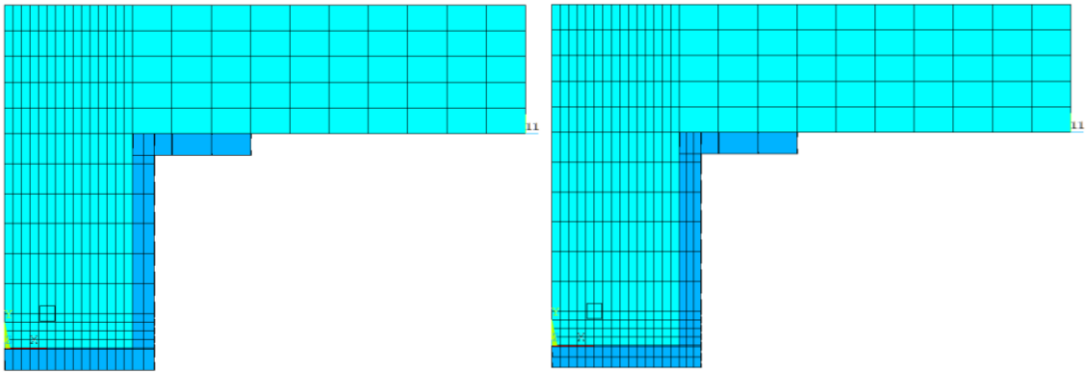

(a) Mesh 1 (b) Mesh 2

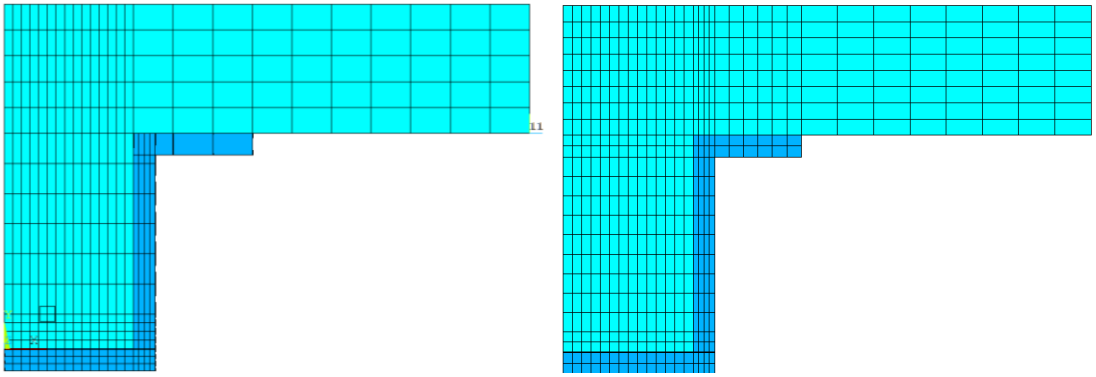

(c) Mesh 3 (d) Mesh 4

Figure 4.5 Different meshes used in the mesh sensitivity analysis

4.3.2 Elements Types used in FE simulation of Williams et al. (2008)

The developed FE simulations were divided into two main categories; thermal and structural. Each kind had its own different associated element types. For example, there were

seven main types of elements used to develop the FE models presented in this thesis. Four kinds of 3D solid elements, two kinds of 3D spar elements and 3D interface elements. Out of the four kinds of the 3D solid elements, one was used in the thermal simulation while the other three were used in the structural simulation. On the other hand, one of the two 3D spar elements was used in thermal analysis while the other was used in the structural simulation. It must be noted that the interface elements were used specifically in the structural simulation. Description of each element type will be presented.

4.3.2.1 Thermal Element Types

SOLID70

SOLID70 has a 3-D thermal conduction capability. The element has eight nodes with a single degree of freedom defined as temperature at each node. The element is applicable to carry on a 3-D, steady-state or transient thermal analysis. The element also can compensate for mass transport heat flow from a constant velocity field [**85**]. Figure 4.6 shows the geometry of SOLID70. SOLID70 has 2×2×2 integration scheme for both conductivity and specific heat matrices.

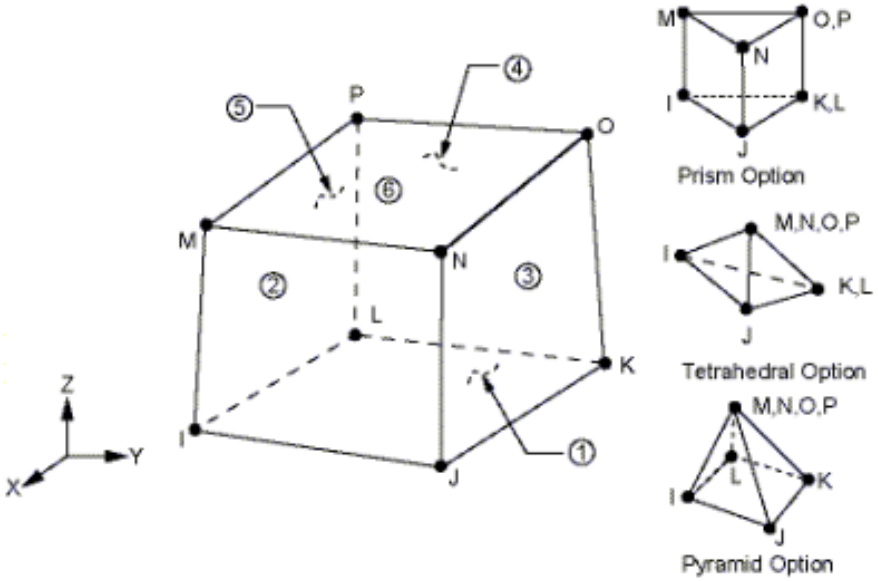

Figure 4.6 3-D SOLID70 [**85**]

Limitations and restrictions of SOLID70

 Zero volume elements are not allowed.

 The specific heat and enthalpy are evaluated at each integration point to allow for abrupt changes

LINK33

LINK33 is a uniaxial element with the ability to conduct heat between its nodes. The element has a single degree of freedom, temperature, at each node point. The conducting bar is applicable to a steady-state or transient thermal analysis [**85**]. Figure 4.7 shows the Geometry of LINK33.

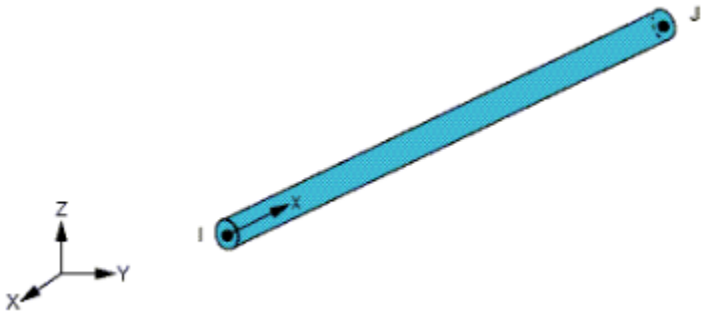

Figure 4.7 3-D LINK33 Conduction Bar [**85**]

Limitations and restrictions of LINK33

 Heat is assumed to flow only in the longitudinal element direction.

 The element must not have a zero length

4.3.2.2 Structural Element Types

SOLID65

SOLID65 is used for three-dimensional modeling of solids with or without reinforcing bars (rebars). SOLID65 is capable of cracking in tension and crushing in compression. In the different applications that require a nonlinear definition of the behavior of concrete materials, for example, the solid capability of the element may be used to model the concrete while the rebar capability is available for modeling reinforcement behavior. SOLID65 follows William and

Warnke, [**85**] constitutive model for modeling concrete material i.e. is capable of cracking (in three orthogonal directions), crushing, plastic deformation, and creep. Other applications would be reinforced composites and geological materials. The element is defined by eight nodes having three degrees of freedom at each node translations in the nodal x, y, and z directions and up to three different rebar specifications may be defined [**85**]. The element geometry, node locations, and the coordinate system are shown in Figure 4.8. Additional concrete material properties, such as the shear transfer coefficients, tensile stress, and compressive stress are inputs in the concrete data table. Typical shear transfer coefficients range from 0.0 to 1.0, with 0.0 representing a smooth crack (complete loss of shear transfer) and 1.0 representing a rough crack (no loss of shear transfer). This specification may be made for both the closed and open crack [**85**]. SOLID65 has 2×2×2 integration scheme for both stiffness matrix and thermal load vector.

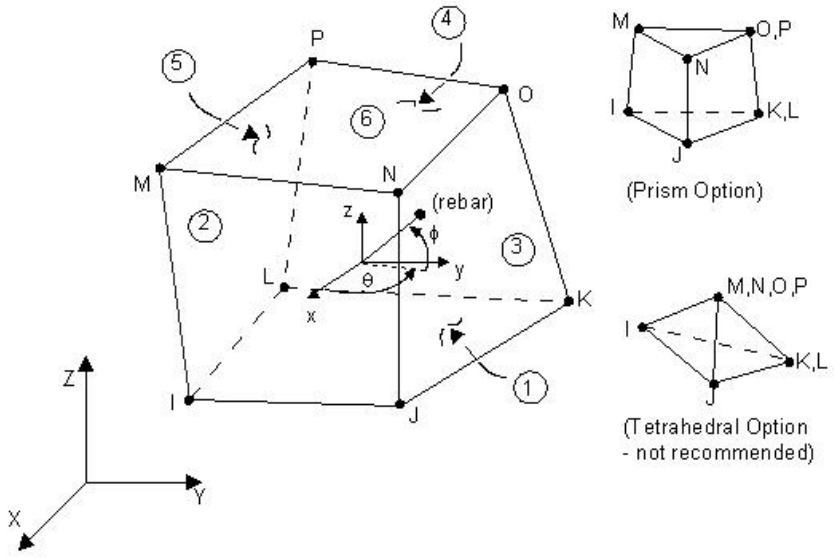

Figure 4.8 SOLID65 3-D Reinforced Concrete Solid [**85**]

Limitations and restrictions of SOLID65

 Zero volume elements are not allowed.

 All elements must have eight nodes.

 Whenever the rebar capability of the element is used, the rebar is assumed to be "smeared" throughout the element. The sum of the volume ratios for all rebar must not be greater than 1.0.

 The element must have isotropic material properties

SOLID45

SOLID45 is used for the 3-D modeling of solid structures. The element is defined by eight nodes having three degrees of freedom at each node translations in the nodal x, y, and z directions. The element has different capabilities i.e. plasticity, creep, swelling, stress stiffening, large deflection, and large strain. A reduced integration option with hourglass control is available. Figure 4.9 shows the geometry of SOLID45. SOLID45 has 2×2×2 integration scheme for both stiffness matrix and thermal load vector.

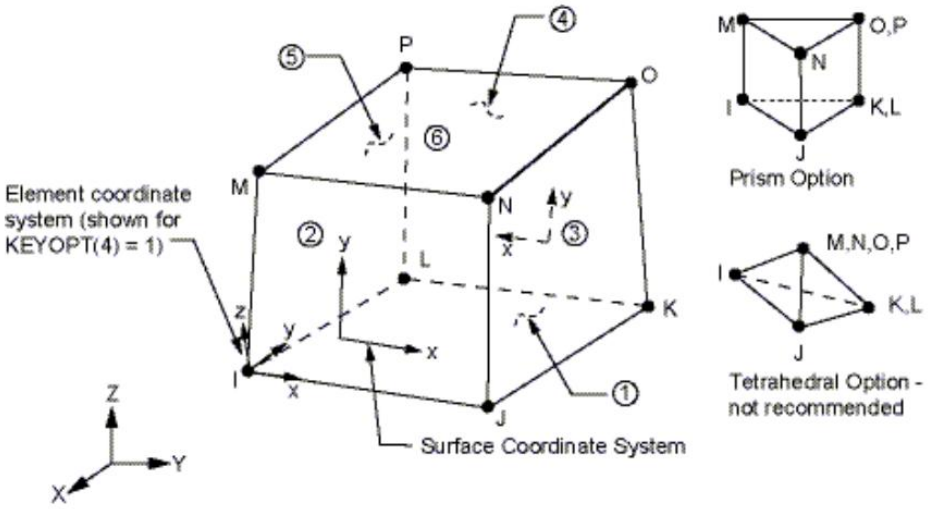

Figure 4.9 SOLID45 3-D solid element [**85**]

Limitations and restrictions of SOLID45

 Zero volume elements are not allowed.

 The element may not be twisted such that the element has two separate volumes.

SOLID46

SOLID46 is a layered version of the 8-node structural solid (SOLID45) designed to model layered thick shells or solids. The element allows up to 250 different material layers. The element has three degrees of freedom at each node translations in the nodal x, y, and z directions. The geometry, node locations, and the coordinate system for this element are shown in Figure 4.10. The element is defined by eight nodes, layer thicknesses, layer material direction angles, and orthotropic material properties. The orthotropic shear modules GXZ and GYZ must be within a factor of 10,000 of each other [**85**]. SOLID46 has 2×2×2 integration scheme for both stiffness matrix and thermal load vector.

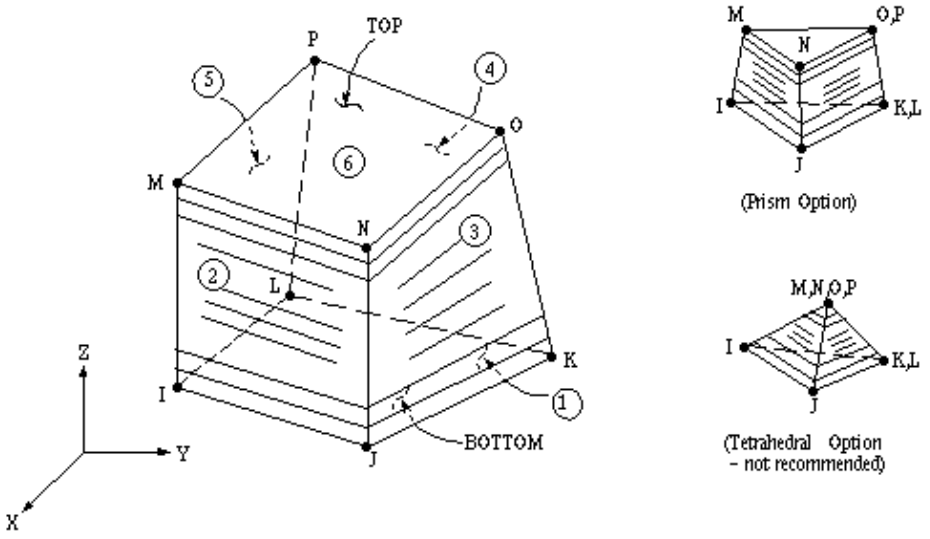

Figure 4.10 SOLID46 3-D Layered Structural Solid [**85**]

Limitations and restrictions of SOLID46

- Zero volume elements are not allowed.
- Zero thickness layers or layers tapering down to a zero thickness at any corner are not allowed
- No slippage is assumed between the element layers
- All material orientations are parallel to the reference plane.

LINK8

LINK8 is a 3D two node uniaxial tension-compression spar element with three degrees of freedom at each node translations in the nodal x, y, and z directions. This element is used to model the internal reinforcement for RC beams and columns. It is capable of plasticity, creep, swelling, stress stiffening, and large deflection but no bending of the element is considered. The geometry, node locations, and the coordinate system for this element are shown in Figure 4.11 below. The element is defined by two nodes, the cross-sectional area, an initial strain, and the material properties [**85**].

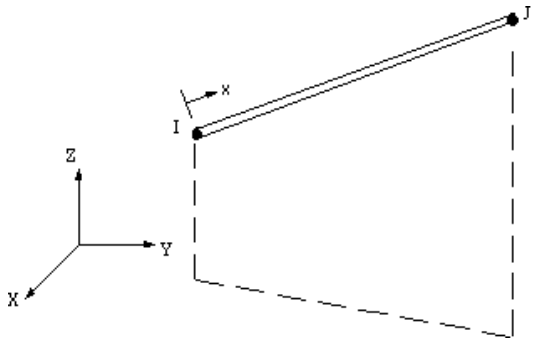

Figure 4.11 LINK8 geometry [**85**]

4.3.3 Material Properties at Elevated Temperature

The developed FE model takes into account the different nonlinear material properties of the materials included in the FE models. The nonlinearity is mainly due to the natural compositions of such materials and the changes they experience when exposed to elevated temperature. Such material properties are needed as inputs to conduct the thermal-stress analysis in order to obtain a full field of results i.e. thermal and mechanical wise. Table 4.1 provides lists the mechanical and thermal properties for concrete, steel, CFRP, and insulation materials at room temperature. On the other hand, the normalized stiffness (modulus of elasticity), variation of concrete compressive strength, steel reinforcement strength, thermal conductivity, and specific heat with increasing temperature for the different materials needed for the FEs simulation are shown in Fig. 4.12-4.16.

As mentioned in Chapter 2, there has been a lot of research on the mechanical and thermal properties of both concrete and steel. The behavior of the concrete and steel materials

was assumed to follow the proposed equations and charts provided in the [**23**]. Still, little research have been published on the mechanical and thermal properties of FRP materials, thus the use of the suggestions of several other researchers [**86**,**87**] is implemented. Furthermore, Griffis et al. [**88**] performed tests on a carbon/epoxy FRP used in aerospace applications while Park et al. [**89**] studied the thermal and mechanical properties of gypsum board at high temperature.

Table 4.2 Mechanical and thermal material properties at room temperature [**90**,**91**]

Property / ***Material***	E_x ***(MPa)***	E_y ***(MPa)***	E_z ***(MPa)***	***K*** ***(W/mm.K)***	***C*** ***(J/kg.K)***	μ_x	$\mu_{y,z}$	α_x	ρ (Kg/mm^3)
Concrete	30200	-	-	2.7×10^{-3}	722.8	0.20	-	6.08×10^{-6}	2.40×10^{-6}
Steel bars	210000	-	-	5.2×10^{-2}	452.2	0.30	-	6.00×10^{-6}	7.86×10^{-6}
CFRP	228000	10000	10000	1.3×10^{-3}	1310	0.28	0.0122	-0.90×10^{-6}	1.60×10^{-6}
VG Insulation	2100	-	-	2.5×10^{-4}	1654	0.30	-	1.70×10^{-5}	2.69×10^{-7}

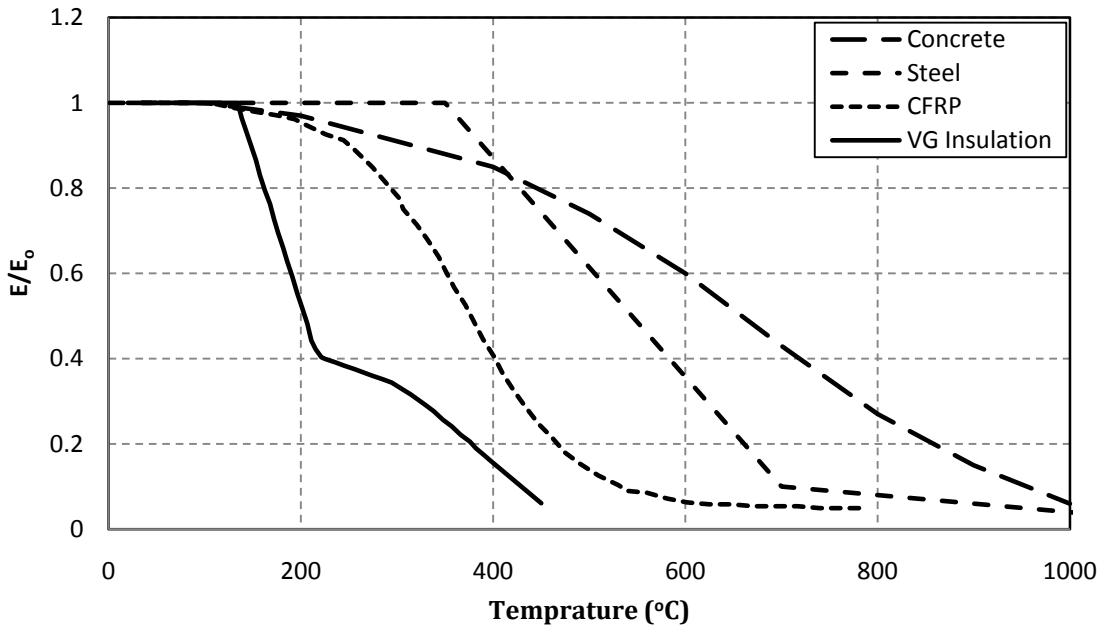

Figure 4.12 Variation of stiffness of different materials with temperature [**4**]

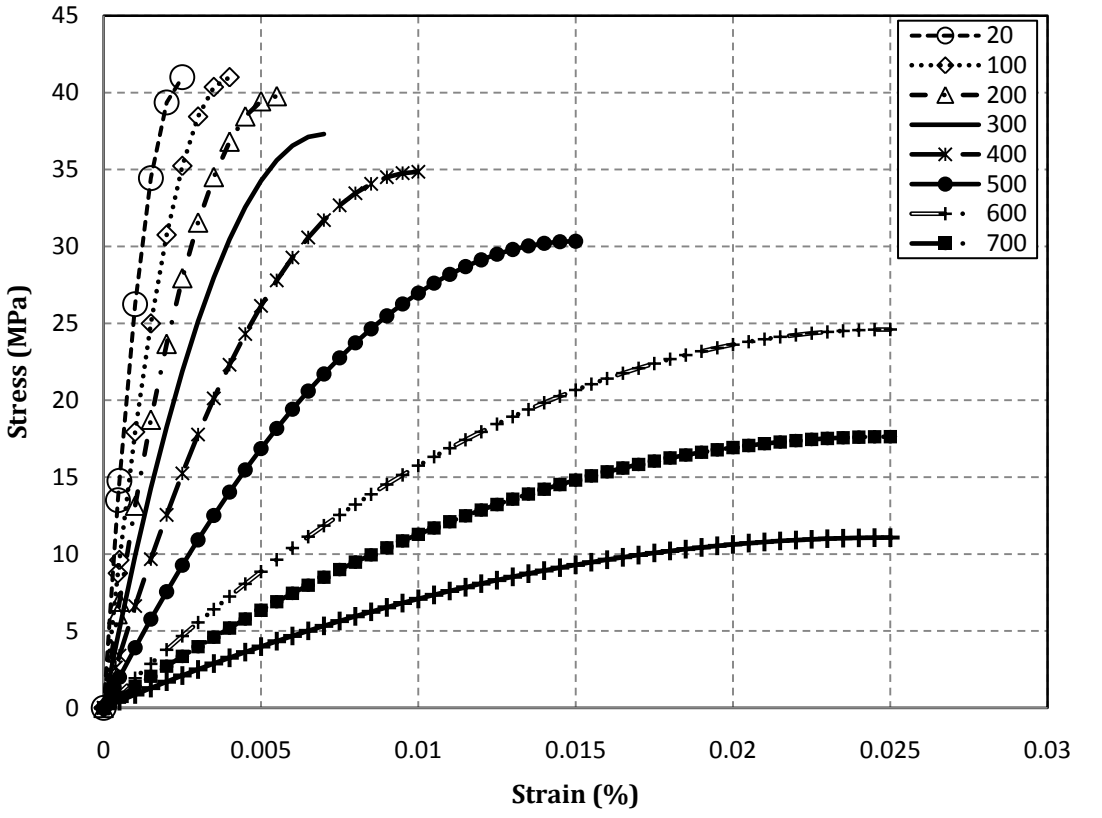

Figure 4.13 Variation of concrete compressive strength with temperature [**23**]

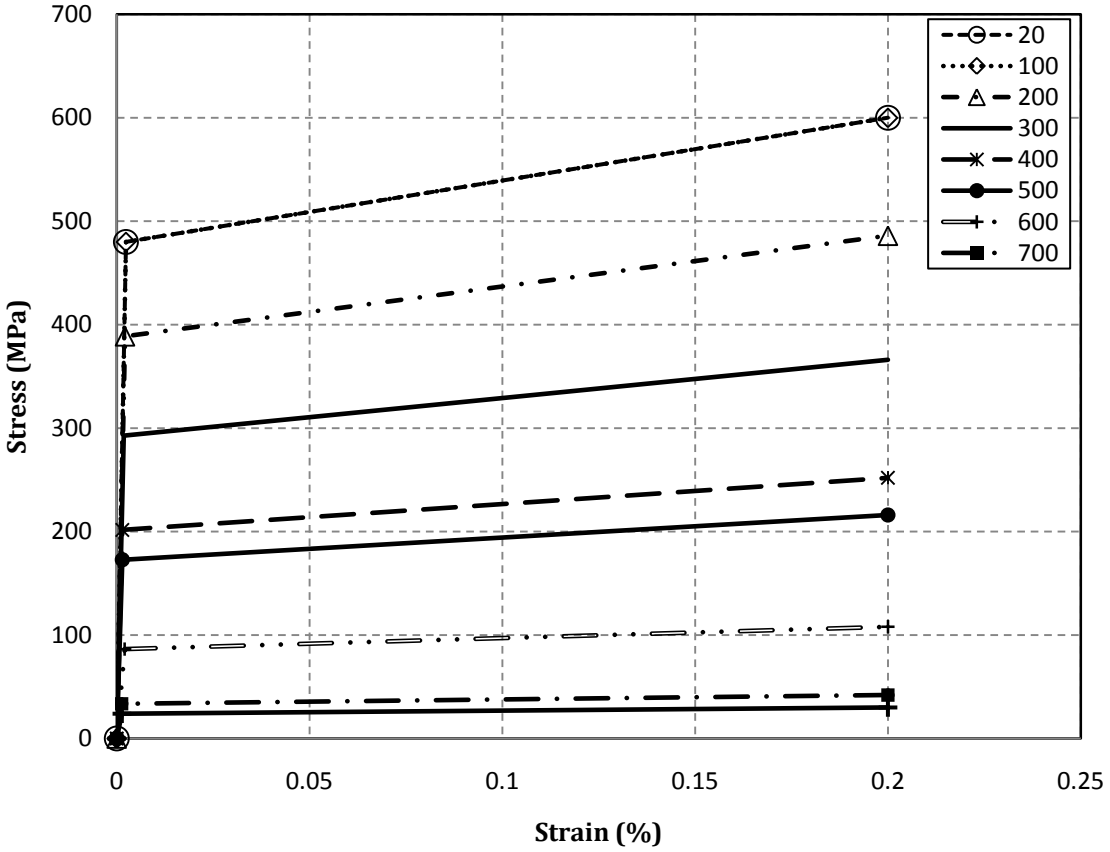

Figure 4.14 Variation of steel reinforcement strength with temperature [**23**]

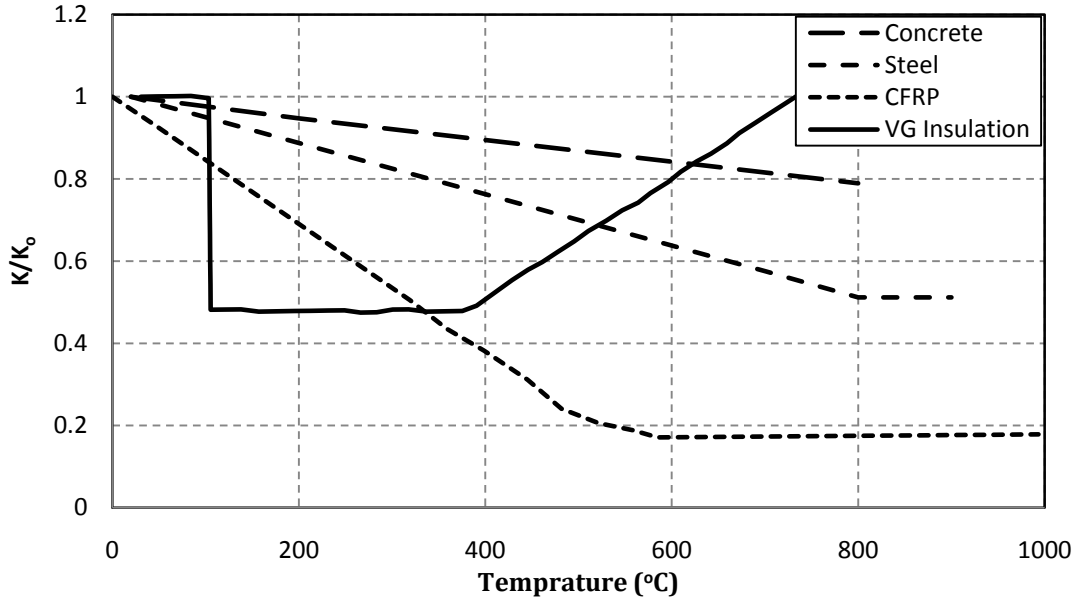

(a) Thermal conductivity

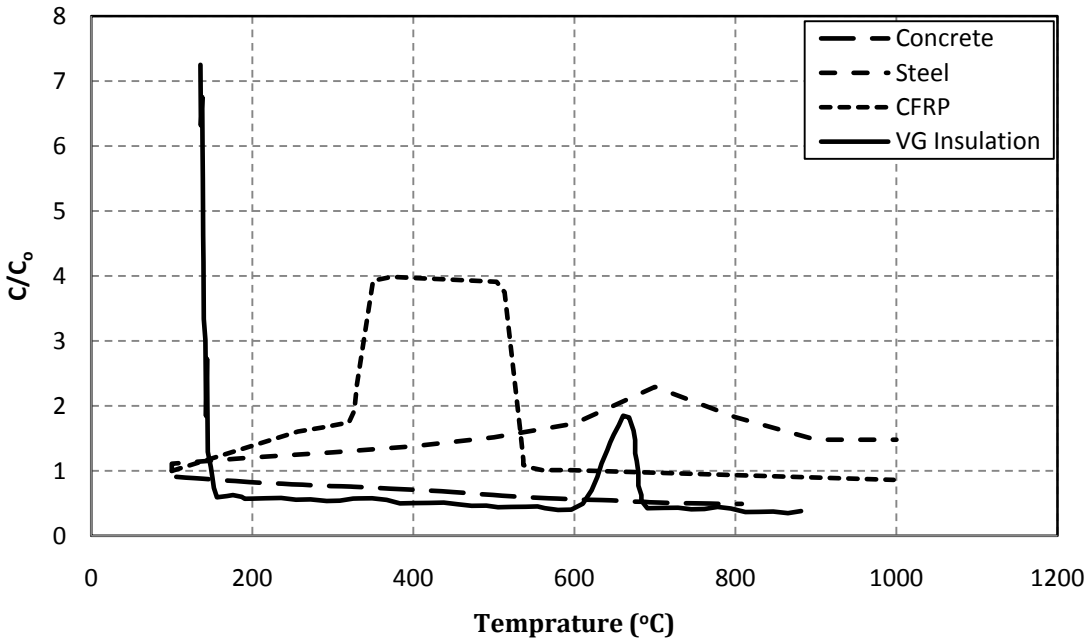

(b) Specific heat

Figure 4.15 Variation of thermal conductivity and specific heat with temperature [**2**]

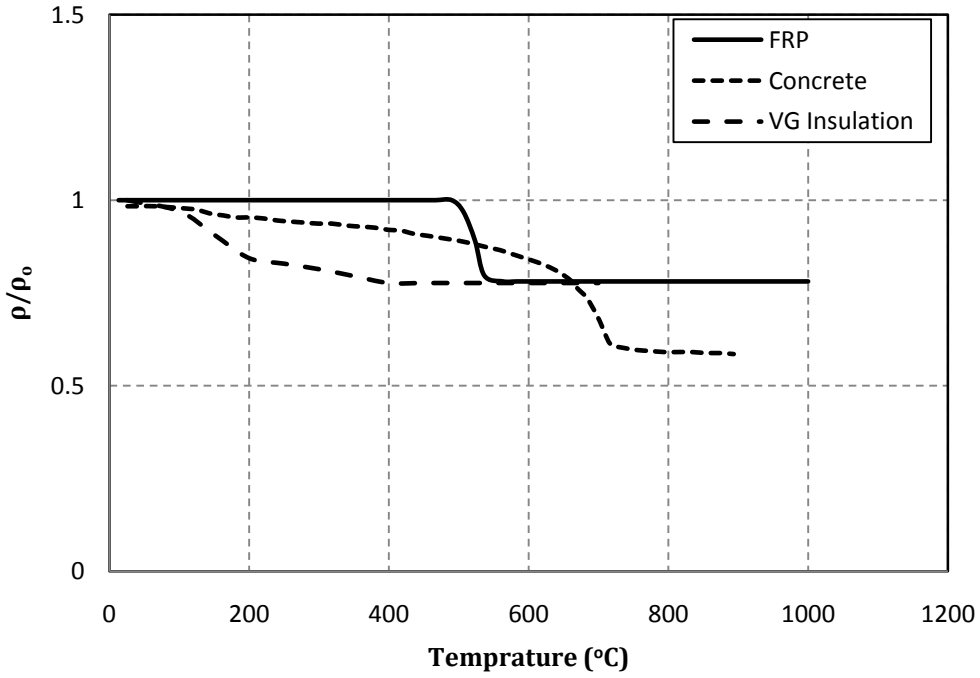

Figure 4.16 Variation of density with temperature [**2**]

4.3.4 Fire Test of the Experimental Program of Williams et al. (2008)

The experimental program took place at the Canadian Institute for Research in Construction's (IRC); Fire Risk Management laboratory. The beams were exposed to the ASTM E119 fire curve in a full scale furnace; the furnace and beams are shown in Fig. 4.17. The fire furnace can expose large specimens that have a size up to 4.87m x 3.96m and apply sustained load through 30 distributed hydraulic jacks spreading the load over three main circular paddings [**59**].

Furthermore, the fire chamber contains 30 propane burners divided equally into two longitudinal banks. The capacity of the chamber is 4700kW of energy. To enable the control system of monitoring the temperature of the burning gas inside the chamber to follow the standard curves, the inside temperature is monitored by nine thermocouples distributed within the furnace [**59**].

Figure 4.17 Furnace and beams specimens [**59**]

4.3.5 Loading and Boundary Conditions

The thermal simulation was carried out by applying the ASTM E119 temperature-time curve into the nodes of the bottom and sides of the RC T-beam. Figure 4.18 shows a comparison between the ASTM E119 and ISO834 fire curves. The main heat transfer phenomena in the fire furnace are radiation and convection. However, in the FE simulation the temperatures were

applied directly to the nodes of the elements. The use of this technique might seem conservative; still it showed a great correlation with the experimental program, as will be discussed in Chapter 5. The temperature points were applied in a sequence of temperature steps at several time loads. Then, each load step is then divided into equal number of sub steps.

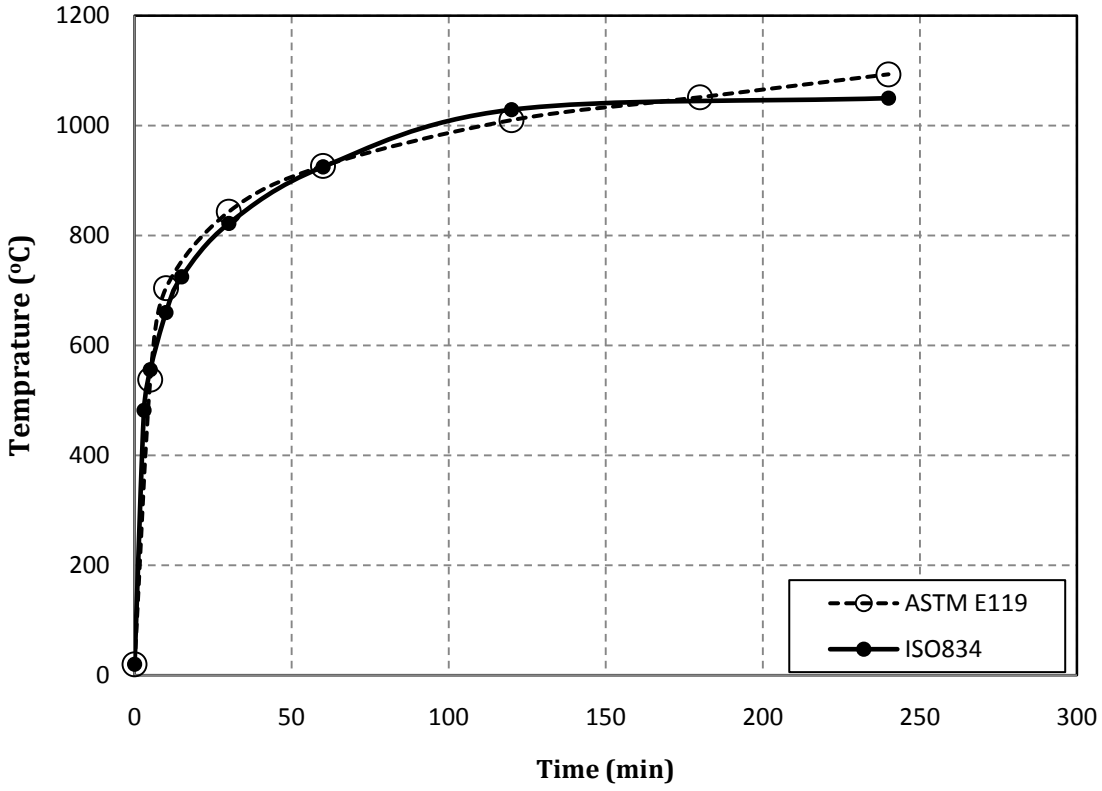

Figure 4.18 Comparison between the ASTM E119 and ISO834

The researchers meant to satisfy both Canadian (CAN/ULC) [**92**] and American (ASTM) [**64**] standards; the RC assemblies were simply supported and subjected to the ASTM E119 fire exposure from below. A sustained uniformly distributed load of 34kN/m was applied during the test that was calculated through back substitution [**53**].

4.3.6 Analytical Methodology

The general methodology of the model development and transient thermal-stress analysis follows the following procedure:

1. Building a 3D FE model of the corresponding beam. The model incorporates the exact geometry, materials properties, and boundary conditions. There are two FE models i.e. thermal and structural elements, to enable the thermal and structural analysis.

2. Applying the temperature (thermal loads) to the bottom and sides of the insulated beam simulating the furnace transient fire (in the form of transient temperatures versus time)

3. Validate the finite element model by comparing the predicted and measured temperature at key points within the cross section of the beam.

4. Applying structural loadings i.e. sustained uniformly distributed load at the top face of the beam or point loads, to simulate the applied loading of Williams et al. [**4**] and Blontrock et al. [**5**] during fire. In addition, apply the thermal loads (nodal temperature) at several time points (load steps and sub-steps). It should be noted that the deformation due to the applied gravity load at the first load step is used to verify the correct behavior of the model.

4.3.7 Convergence and Solution

In this study, automatic time stepping option is turned on to predict and control load step sizes. At the end of each load step, convergence is achieved by the Newton-Raphson equilibrium iterations. Only when the temperature difference at each node from each iteration to another is less than 0.5 degree, the solution converges. As for the structural simulations, the solution is converged when the Newton-Raphson equilibrium iterations, the force convergence tolerance limit value was 0.1 (typical range 0.05 to 0.2) to achieve convergence of the solution.

4.4 The Developed FE models of Blontrock et al. (2000)

4.4.1 Geometry

Blontrock et al. [**5**] tested a series of ten RC beams strengthened with CFRP plates and protected with different insulation boards. In the experimental study, the beams had rectangular cross section of 200×300mm and spanned 3.15m subjected to the maximum service loads as calculated according to the Eurocode 2 and tested under four point bending test. The main steel reinforcement was two bars that have 16mm diameter. On the other hand, the compression reinforcement consists of 2 bars of 10mm diameter. Closed 8 mm stirrups were used as shear

reinforcement spaced at 100mm centre to centre except the maximum moment region were the spacing increased to 150mm. The concrete cover was 25 mm.

The experimental program was composed of ten RC beams. Two beams were tested monotonically up to failure. The two beams served as reference beams in which one of them was conventional beam while the other was strengthened with a CFRP plate attached at the soffit of the beam. Then, 2 unprotected and unstrengthened beams as well as 6 strengthened and protected beams were loaded to full service load and tested under fire the ISO834 exposure. The ISO834 is shown in Fig. 4.18.

In addition, Blontrock et al. [**5**] investigated the effects of several insulation parameters i.e. insulation board materials, thickness, location, length and attachment method. The used insulation was mainly consisting of rock wool and/or gypsum board layers (Promat H and Promotec 100). It was observed that the best fire endurance can be achieved if the U-shaped fire protection insulation is applied to the soffit and sides of the beams. Loss of bond between the CFRP and concrete happened to occur whenever the temperature at the CFRP/concrete interface reached between 66 and 81°C; the glass transient of the epoxy/resin used to attach the CFRP plate to the RC beam. A maximum fire endurance of 39min was achieved with this insulation scheme, which is less than the fire endurance ratings required by North American standards in typical building applications. Figure 4.19 shows a schematic of the different RC beams used in the experimental program. On the other hand, Figs. 4.20-4.21 show the different views of the developed FE model that was based on Beams 1 and 8, respectively.

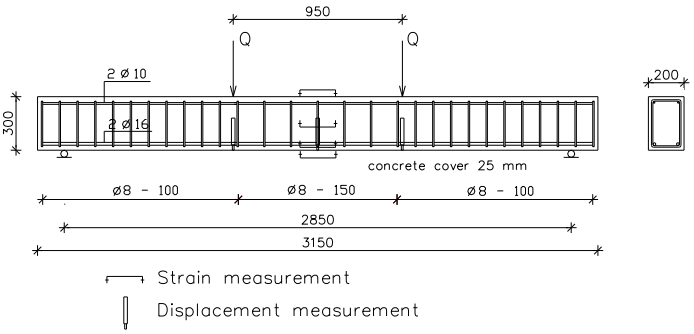
950
Q
Q
2 ø 10
2 ø 16
300
200
concrete cover 25 mm
ø8 - 100
ø8 - 150
ø8 - 100
2850
3150
Strain measurement
Displacement measurement

Beam 1

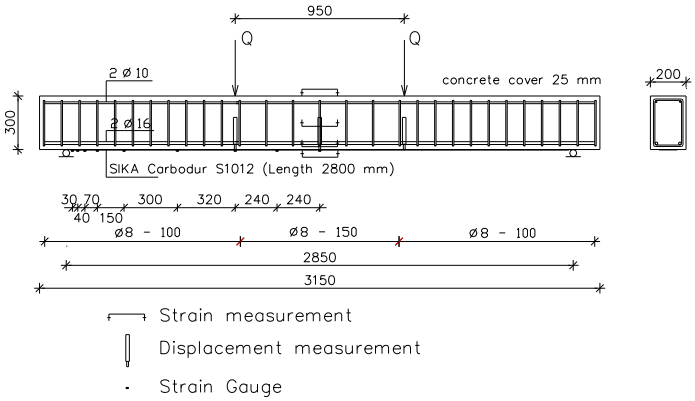
950
Q
Q
2 ø 10
2 ø 16
300
concrete cover 25 mm
200
SIKA Carbodur S1012 (Length 2800 mm)
30 70
40 150
300
320
240
240
ø8 - 100
ø8 - 150
ø8 - 100
2850
3150
Strain measurement
Displacement measurement
Strain Gauge

Beam 2

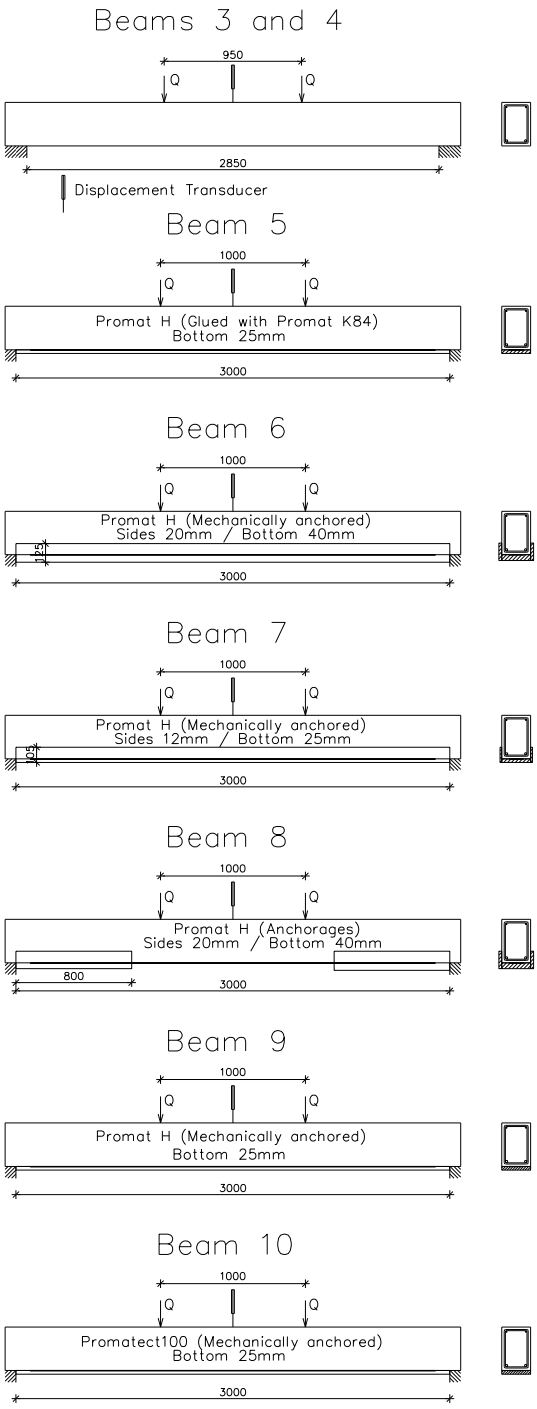

Figure 4.19 Blontrock et al. [**5**] experimental program

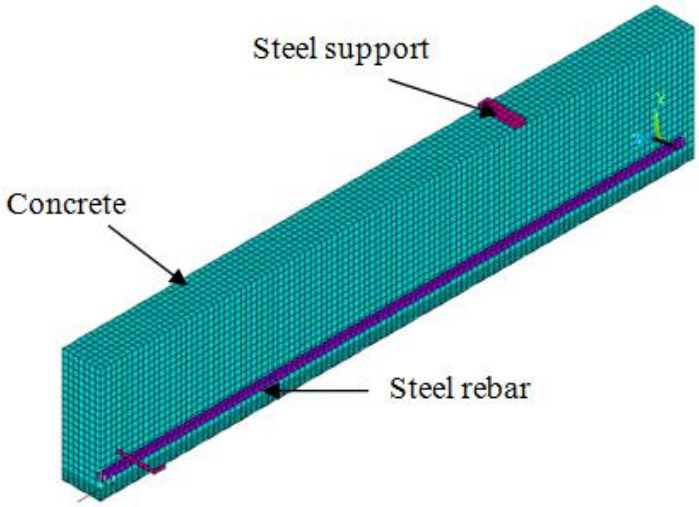

Figure 4.20 Isoparametric view of the Quarter model

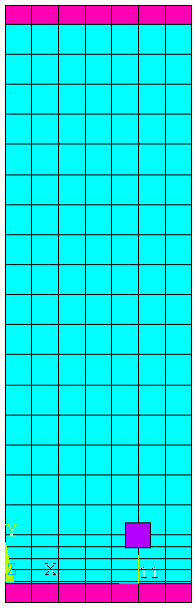

Figure 4.21 Cross-sectional view of the Quarter model

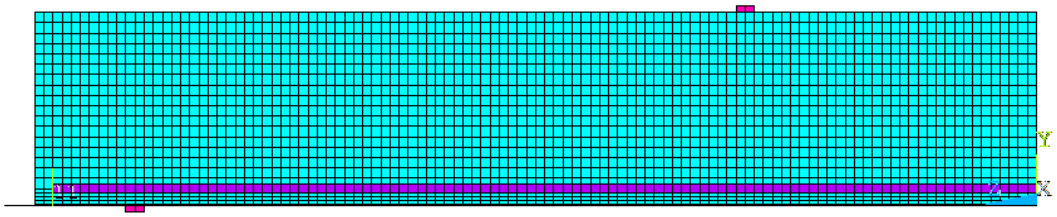

Figure 4.22 Side view of the Quarter model

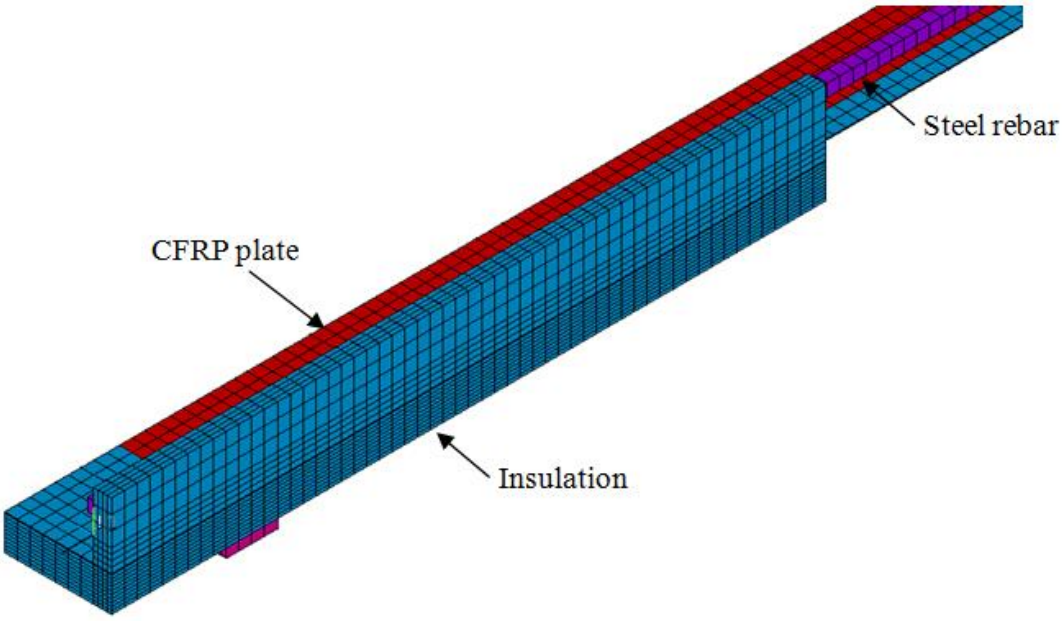

Figure 4.23 Different materials used in the Quarter model

On the other hand, Fig. 4.24 shows a sample of the different FE models associated with the matrix experimented by Blontrock et al. [**5**].

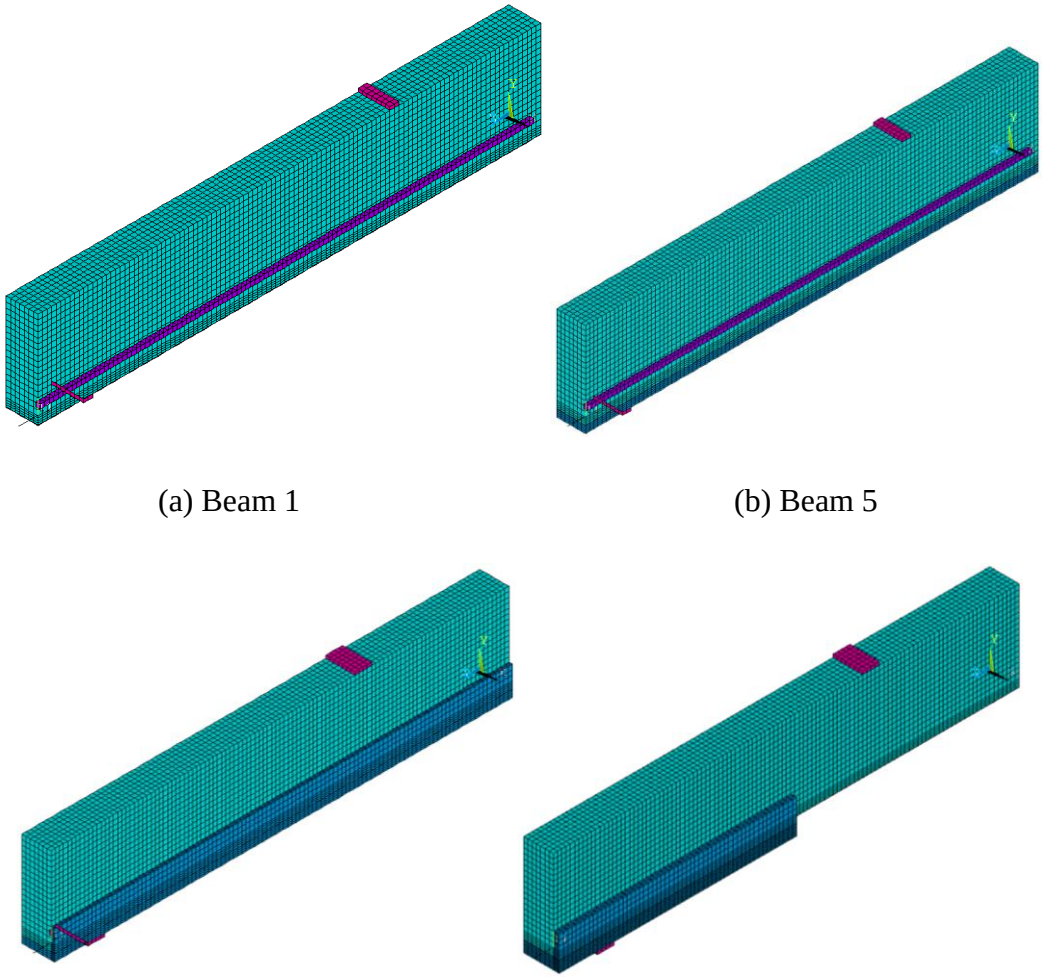

(a) Beam 1 (b) Beam 5

(c) Beam 6 (d) Beam 8

Figure 4.24 Sample of the developed FE models

4.4.2 Elements Types used in FE simulation of Blontrock et al. (2000)

The same element types used in the developed FE models of Williams et al. [**4**] were used herein namely, SOLID70, LINK33, SOLID65, SOLID45 and LINK8. In addition, INTER205 was used to simulate the cohesive element. The cohesive elements are capable to modeling the debonding failure mechanism. More on this is provided in subsequent sections.

INTER205

INTER205 is a 3-D 8-node linear interface element. INTER205 can simulate an interface between two surfaces and the subsequent delamination process, where the separation is represented by an increasing displacement between nodes, within the interface element itself.

The nodes are initially coincident. It is defined by eight nodes having three degrees of freedom at each node translations in the nodal x, y, and z directions. Figure 4.25 shows the geometry of INTER205. INTER205 has 2×2 integration scheme for the stiffness matrix. It should be noted that debonding was not reported in the experimental program of Williams et al. [**4**], hence the cohesive elements were only used in the simulation of Blontrock et al. [**5**] validation models.

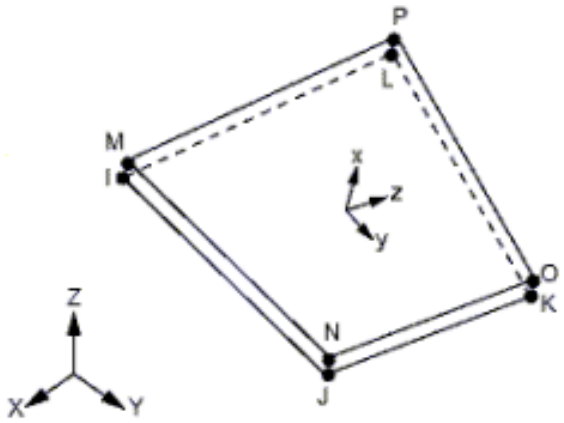

Figure 4.25 INTER205 geometry [**85**]

Limitations and restrictions of INTER205

 This element is not supported for initial stress.

 Pressure as a type of surface load on element faces is not supported by this element.

 This element is based on the local coordinate system.

4.4.3 Material Properties at Elevated Temperature

The average concrete compressive strength for the tested specimen was 57MPa while the average concrete tensile strength was 4MPa. The steel reinforcement had a yield and ultimate strength of 591 and 699MPa, respectively. The steel reinforcement modulus of elasticity is taken as 200GPa. Furthermore, the CFRP plate Sika Carbodur S1012 had a tensile and modulus of elasticity of 2.8 and 165GPa, respectively. The concrete, steel and CFRP materials properties variation at elevated temperatures were assumed to behave in a similar manner (same reduction

factors were used) to the data presented in Figs. 4.12-4.16. The variation of the insulation materials was taken directly from the manufacturer datasheets and is shown in Table 4.2.

Table 4.3 Insulation material properties

Property	***PROMATECT®-H***	***PROMATECT®-100***
Density (Kg/m^3)	870	850/875*
Thermal Conductivity (W/m.K)	@ 20°C => 0.17 @ 100°C => 0.19 @ 200°C => 0.21	@ 25°C => 0.285* @ 40°C => 0.164
Specific heat (kJ/Kg.K)	0.92	0.92
Modulus of elasticity (MPa)	4200	4200
Coefficient of expansion (1/K)	-6.4 x 10^{-6}	-16.0 x 10^{-6}

*Blontrock et al. 2000

4.4.4 Bond-Slip Model

Blontrock et al. [**5**] have reported several debonding cases in the strengthened and protected tested beams. Hence, bond-slip at the CFRP/Concrete interface was modeled in this study using the cohesive elements presented in Chapter 4. In order to accurately model the bond-slip behavior, ultimate shear stress (τ_{max}) and its corresponding slip (displacement) (s_u) must be determined first. There have been good amounts of published data on the bond-slip phenomena between FRP plates and concrete (Lu et al., [**93**] Nabaka et al., [**94**]; De Lorenzis, [**16**]). Figure 4.26 draw a comparison between the normalized Nabaka et al. and Lu et al. models.

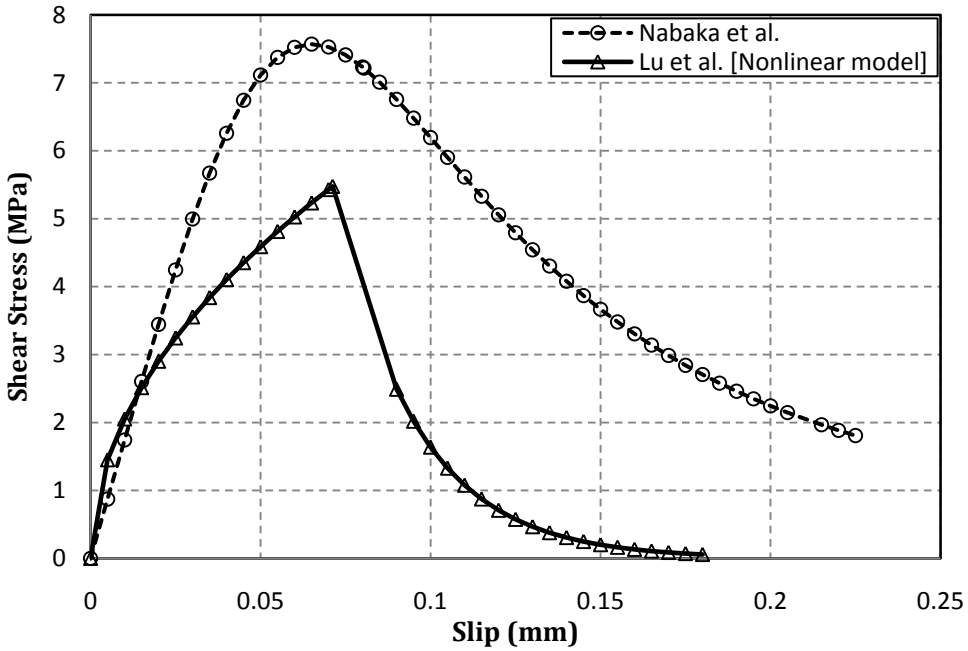

Figure 4.26 Different bond-slip models

The calculation of the ultimate shear stress (τ_{max}) and slip (s_u) was based on Lu et al. [**93**] model. Lu et al. [**93**] model is based on a single equation that represents the bond-slip curve. Equation 4.7 shows Lu et al. model

$$\tau = \begin{cases} \tau_{max}\sqrt{\dfrac{s}{s_0}} & when\ s \le s_0 \\ \tau_{max} e^{-\alpha\left(\frac{s}{s_0}-1\right)} & when\ s > s_0 \end{cases} \tag{4.7}$$

where,

$s_0 = 0.0195\beta_w^2 f_t$,

$\alpha = \dfrac{1/G_f}{\tau_{max} s_0} - \dfrac{2}{3}$,

$G_f = 0.308\beta_w^2 \sqrt{f_t}$,

$\beta_w = \sqrt{\left(2.25 - \dfrac{w_f}{S_f}\right) / \left(1.25 + \dfrac{w_f}{S_f}\right)}$

$\tau_{\max} = 1.5\beta_w \, \mathrm{f_t}$

s is the slip between the concrete and CFRP interfaces

Hence, the ultimate shear stress (τ_{max}) and corresponding slip (s_u) were 5.4MPa and 0.07mm, respectively. It must be noted that the degradation of the bond-slip at the CFRP/Concrete interface was also taken into account as shown in Fig. 4.27. Due to the limited number of experiments in this field, an assumption was taken. The assumption was based on the experimental program of Leone et al. [**95**] in which they showed bond-slip curves for tested CFRP strengthened concrete prisms at different temperatures i.e. 25, 50 and 80°C. Thus, the degradation of bond-slip of the current study was assumed to behave the same as the tested prisms of the experimental program of Leone et al. [**95**].

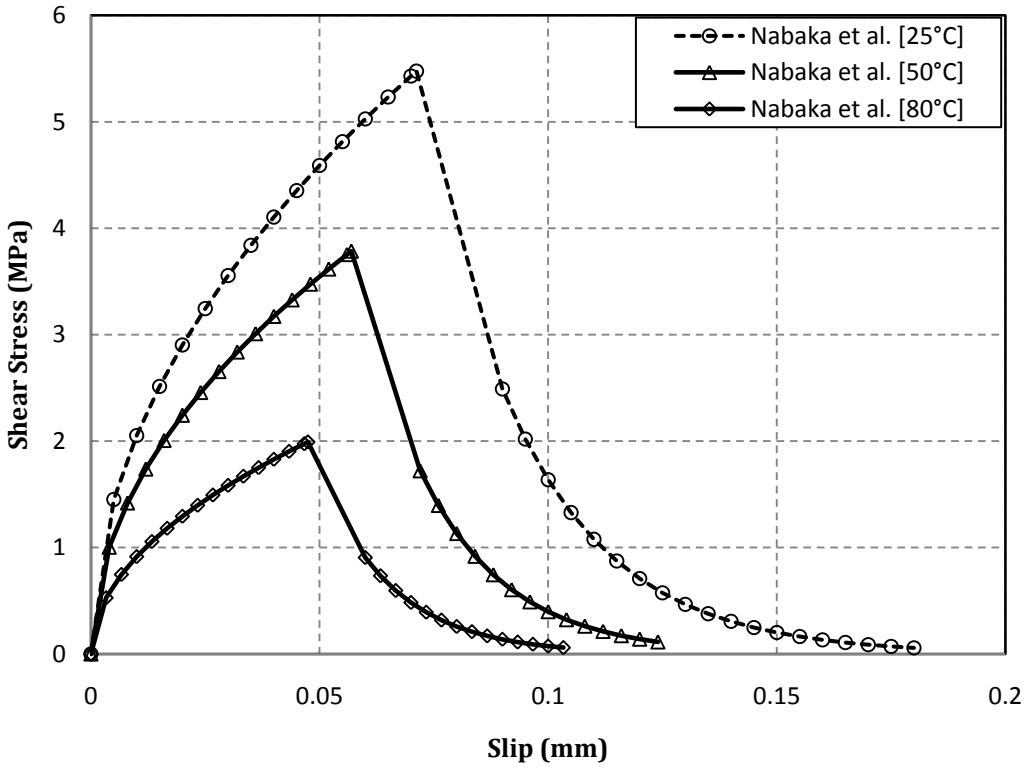

Figure 4.27 Degradation of Bond-slip model with elevated temperature

The FE model solves this cohesive problem using Xu and Needleman [**96**]exponential cohesive zone material model. This model has two segments, an increasing segment up to the ultimate shear stress (τ_{max}) and corresponding slip (s_u), and then descends with a softening response up to the slip at failure (s_f) which assumed to be equal to four times (s_u).The interface elements were placed along the interface of the CFRP/Concrete; in the longitudinal direction of the beam's x-axis.

4.4.5 Fire Test of the Experimental Program of Blontrock et al. (2000)

The beams were exposed to the ISO834 fire curve in a full scale furnace; at the Magnel Laboratory for concrete research, Ghent University. The fire furnace can expose large specimens that have a size up to 3m x 6m and apply sustained load through a large reaction frame. The reaction frame loads the beams via two hydraulic jacks. The ISO834 fire curve was prescribed through the following equation:

$$T_g = T_0 + 345log_{10}(8t + 1) \quad (4.8)$$

Where,

T_g is the temperature of the combustion gases (°C)

T_o is the initial temperature, taken as 12 and 16°C

t Time in minutes

4.4.6 Loading and Boundary Conditions

The thermal simulation was carried out by applying the ISO834 temperature-time curve into the nodes of the bottom and sides of the RC beam. The same technique used in the modeling of the thermal analysis of Williams et al. [**4**] experiment was also used herein. The next chapter will discuss the results obtained in details.

As mentioned in the previous section, the beams were tested under four point bending test. A 2×30.6kN and 2×40.6kN force was chosen to be constantly applied during the fire tests of the unstrengthened and strengthened beams, respectively.

4.4.7 Convergence and Solution

The same convergence criteria used in the modeling of Williams et al. [**4**] study was used herein.

CHAPTER 5 Results and Discussion

5.1 General

This chapter presents the results and outcomes of the analysis of the developed FE models in terms of model validation and parametric study. The developed FE models were validated with those measured full scale tested beams in the experimental programs by Williams et al. [**4**] and Blontrock et al. [**5**]. The validation process is mainly divided into two stages. The first stage is based on the transient thermal analysis, in which the temperature response with time at key locations across the beam's cross section compared to that measured by the thermocouples during the course of fire. The second stage is based on the structural (stress analysis) simulation in which the mid-span deflection response history of the developed FE models is compared against the measured mid-span response of the tested specimens.

In addition, the temperature endurance, strength, failure modes and debonding were also compared against the observed experimental data. Furthermore, one of the validated models is extended into a parametric study to investigate and predict the behavior and response of the FRP system when subjected to fire. The parametric study includes different fire curves, different fire scenarios, different sustained live load levels and insulation schemes, types and thickness on the performance of the strengthened RC beams.

5.2 Fire Endurance Criteria

The fire endurance criteria used by Williams et al. [**4**] was based on the ASTM E119 standard. The ASTM E119 standard uses a pre-defined fire curve known as the ASTM E119 fire curve as a temperature-time fire scenario applied to the structural member or assembly. The ASTM E119 fire curve can reach a 1000°C within two hours of exposure. The fire endurance is defined as the amount of time that a structure or member withstands exposure to the fire without losing its load bearing capacity or fire separating capacity [**64**]. According to the ASTM E119 standard [**64**], the following three major criteria must be met during a fire exposure:

1. The structural member is able to withstand its applied loads.

2. The temperature of the reinforcing steel does not exceed 593°C.

3. The average temperature increase at the unexposed face must be less than 140 º C and no individual point temperature on the unexposed side reach 180°C above the room temperature.

In addition, Williams et al. [**4**] and Williams [**59**] assumes a total loss of the FRP strengthening system once the temperature of the FRP/epoxy matrix reaches its glass temperature. The glass temperature for the tested FRP system was determined by [**4**] to be 93°C. The glass temperature is defined as the temperature at which the material undergoes changes from hard, brittle state into molten, softer state [**97**], It should be noted that this criterion is very conservative [**4**,**59**].

5.3 Model Validation of Williams et al. (2008) Experimental Program

In order to examine the validity of the developed FE models, a validation against the experimental program conducted by Williams et al. [**4**] is performed. The temperature variation and mid-span deflection are compared at the time of failure with the obtained experimental data.

5.3.1 Thermal Validation

The experimental program used multiple number of thermocouples distributed along the cross section of the tested beams. The key locations were:

1. At the exterior face of the VG insulation

2. At the interface of the VG insulation and CFRP plate

3. At the interface of the FRP/ Concrete

4. At the tension steel reinforcement

Figure 5.1 shows a schematic of the thermocouples within the section at mid-span of the beam. To simulate the exact heating scenario in the fire furnace, the ASTM E119 fire shown in Fig. 4.19 is applied to the nodes as transient nodal temperature loading.

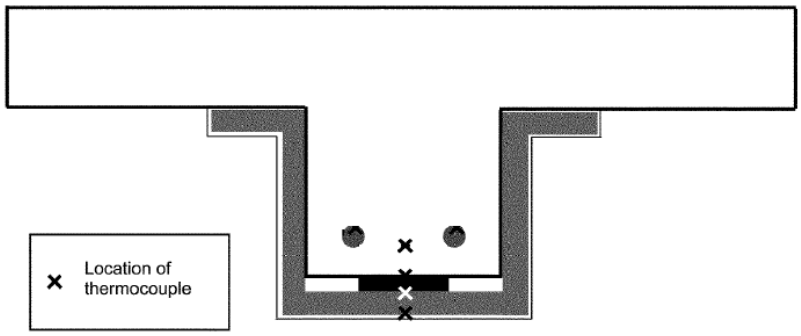

Figure 5.1 Thermocouple locations [**4**]

Figure 5.2 shows a comparison between the different size meshes for the predicted temperature at the CFRP/Concrete interface described earlier in Chapter 4. It is clear from Fig. 5.2 that the converged results of mesh 3 are very close to mesh 4. Thus, mesh 4 that has 51000 elements is adopted in the analysis of the structural element. Stability is shown whenever the results of the different meshes converge and get closer, as shown in meshes 1, 2 and 4. This shows that the used Mesh 1 is accurate enough, thus was used to model both the validation and parametric cases.

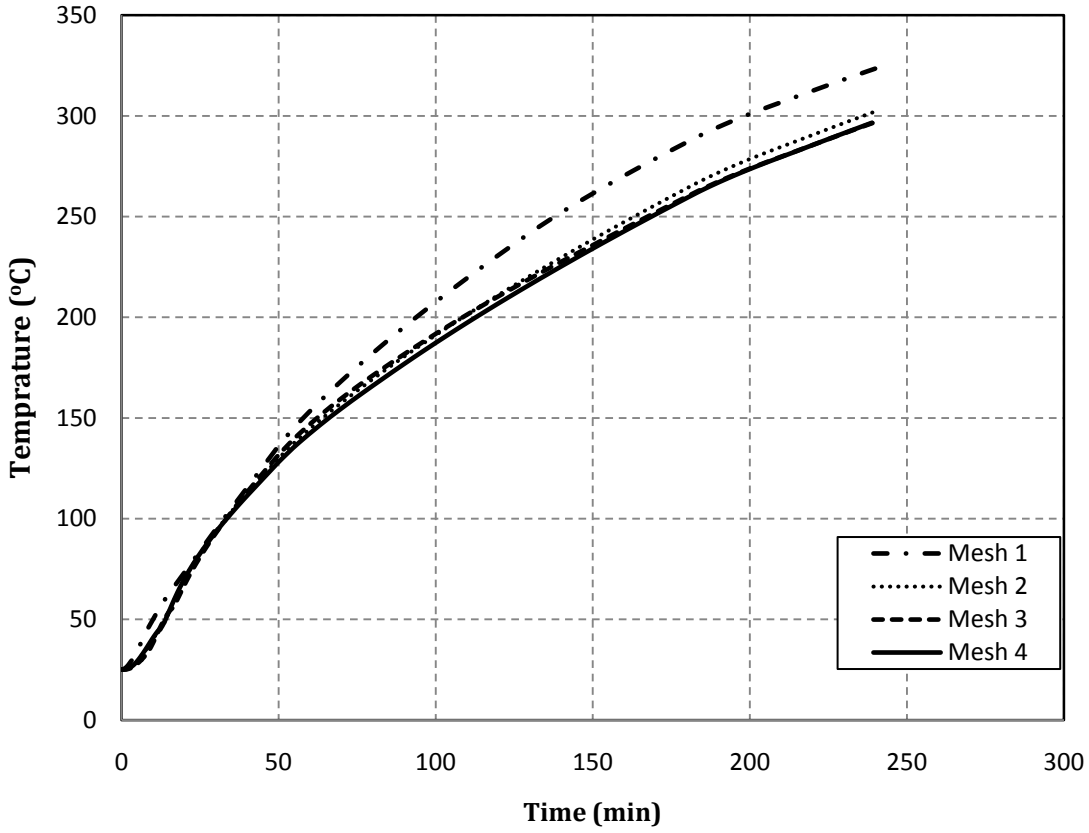

Figure 5.2 Mesh sensitivity analysis results at the CFRP/Concrete interface

Figure 5.3 shows a comparison between the measured and predicted FE temperatures at the different locations within the cross section of the tested T-beams. It is shown that there is a good agreement between the measured and predicted results. Also, it can be seen that the FE results underestimates the temperature at the VG/CFRP interface for both beams. This is due to the fact that there were multiple cracks in the VG insulation cracks after the spraying of the VG insulation took place. So, another VG layer was sprayed to fix the initiated cracks for the Beam 1. Furthermore, when the T-beam was installed into the furnace, more cracks were developed because of the installation process. Upon heating the specimen, it was seen that the new layer of the VG insulation starts to fall at 76min [**4**] due to the uncured bonding between the new and old VG installed layers. When small chunks of the insulation fell down, the thermocouple located at that location was exposed to the fire, hence relatively higher temperatures beyond this point in time was recorded. The temperature at the interface of VG/Concrete was approximately 200°C after 2 hours of fire exposure and 400°C after 4 hours of heating.

As for Beam 2, the FE predicted results agree well with the measured temperatures across the different interfaces. However, the measured temperature at the VG/CFRP interface seems to significantly increase after 75min. The deviation between the predicted and measured temperature at the VG/CFRP interface can be explained by either a slight movement of the thermocouple or an initiation of some major cracks in the VG insulation near the embedded thermocouple. Those cracks allowed the fire to penetrate near that location.

Furthermore, it is noticed from Fig. 5.3 that the temperature at the VG/CFRP interface faced some disturbance in the first hour of the fire exposure. This is due to the evaporation of water moisture from the VG insulation because of increase of thermal energy provided from the fire. Such phenomena may not be accurately simulated in the available FE packages due to its highly nonlinear characteristics and limitation of the elements capabilities. Further research has been taken to enhance the rule of FE into modeling of such phenomena.

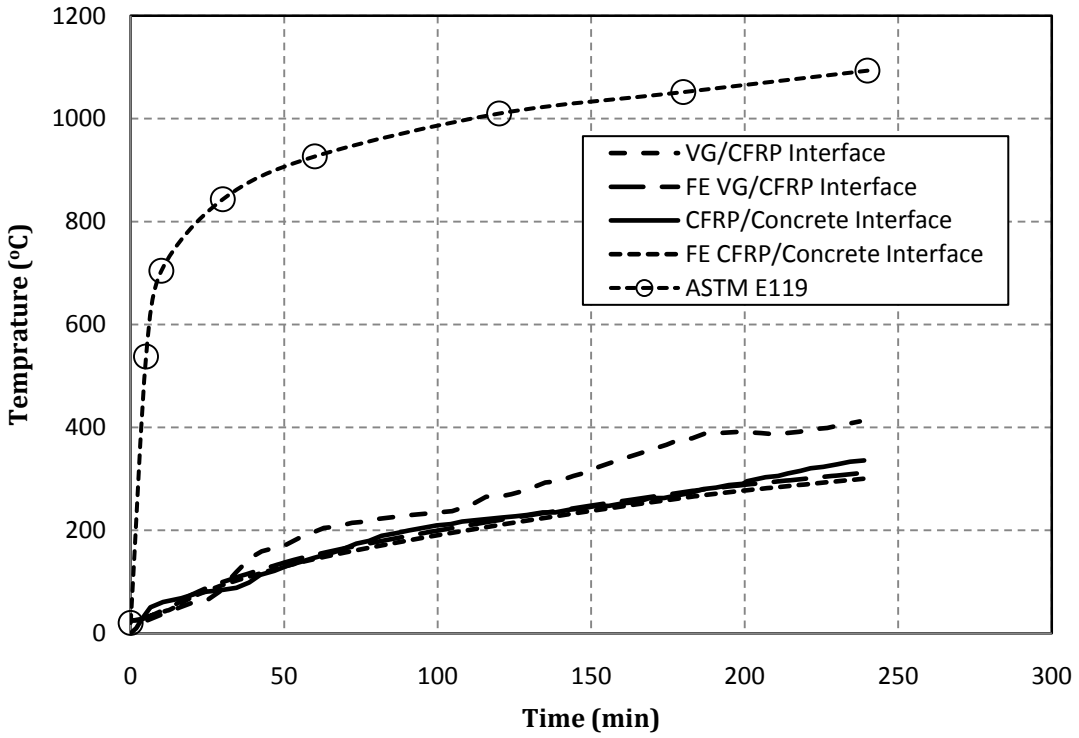

(a) Beam 1

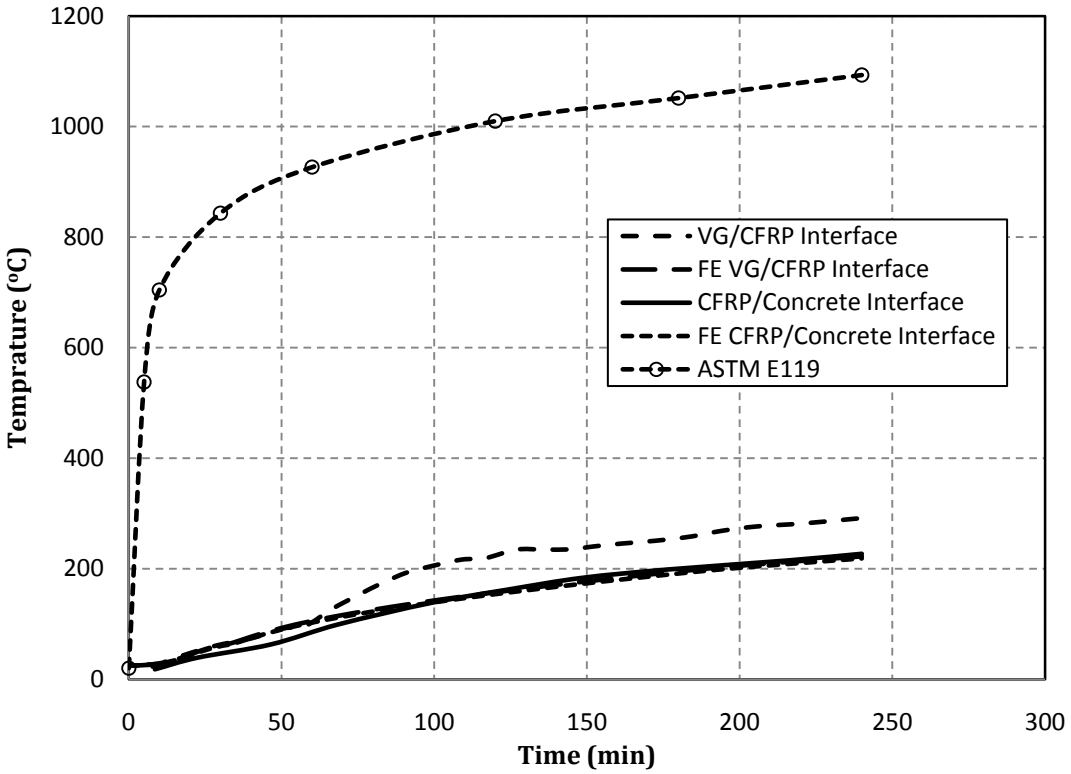

(b) Beam 2

Figure 5.3 Comparison of the FE and measured temperatures

Figure 5.4 shows that the temperature of the steel rebars was kept below the threshold determined by the ASTM E119 standard (593°C), thus passing the second fire endurance criteria related to the temperature of the tension reinforcement. Furthermore, it can be seen that the temperature at the steel rebars increased in a linear fashion up to the end of the test. The temperature at 2 and 4 hours of heating was 127 and 230°C for Beam 1 and 100 and 160°C for Beam 2, respectively. This implies that the temperature of the top fibers of the RC tested beam was below 140ºC with no individual point temperature on the unexposed side reach 180°C above the room temperature, hence the third criteria is also met. Therefore, this concludes the validation of the FE model in the thermal analysis.

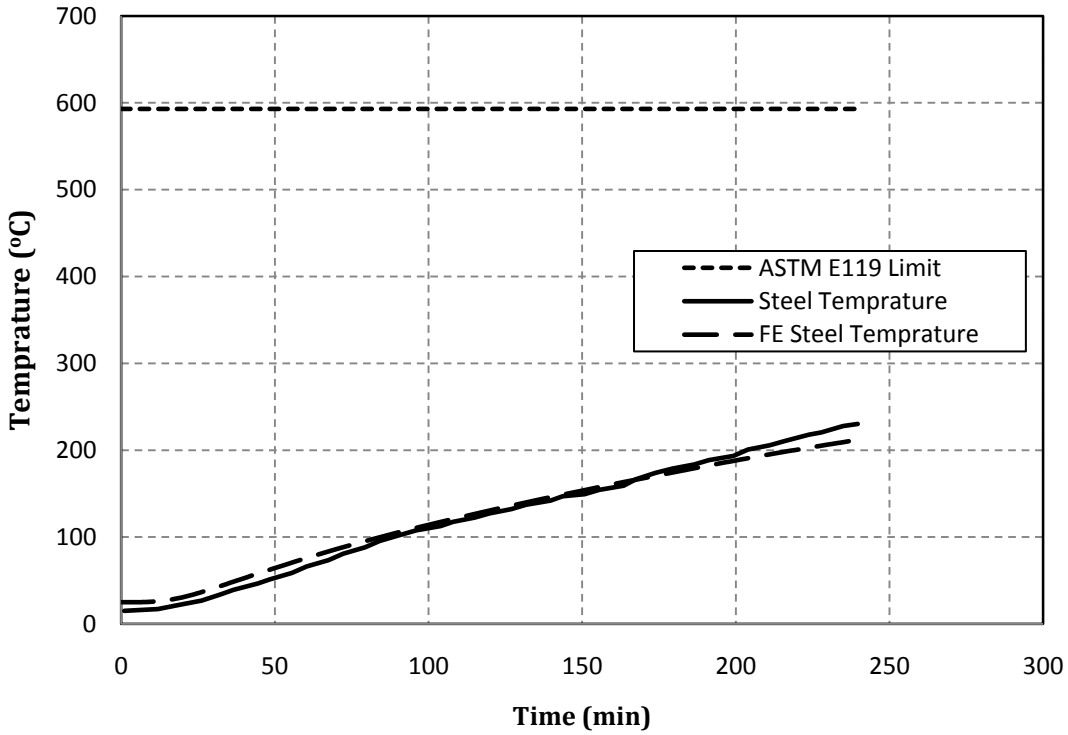

(a) Beam 1

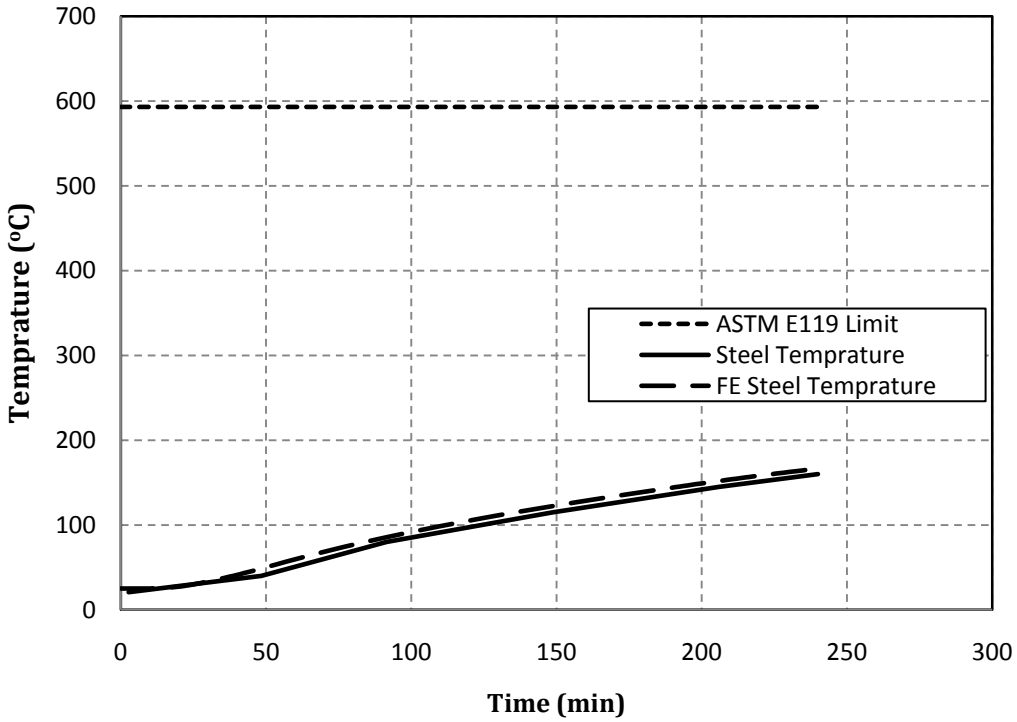

(b) Beam 2

Figure 5.4 Comparison of the FE and measured temperatures at the steel rebars

5.3.2 Thermal Response

Figure 5.5 shows the evolution of temperature with time within the T-beam's cross-section for the full and quarter models. It is clear from Fig. 5.5 that the results of the quarter model are identical to that of the quarter model. Thus, the quarter model can be used to investigate the fire performance of the RC T beam. Furthermore, it can be noted that the initiation of the starts from the edges of the beam, namely the edges of the VG insulation, and propagates diagonally into the cross-section. Furthermore, the corner surrounded by the VG insulation seems to have the largest increase of temperature since the temperature at that spot is bounded by an increase in temperature from two axes (horizontally and vertically). In addition, it is clear that the temperature distribution changes depending on the different materials properties used. Also, an advantage of the FE modeling over the experimental program is its ability to provide results along any point within the developed FE model rather than certain location at which thermocouples were installed.

Figure 5.5 can be used to determine the temperature at any point (node) during the entire fire exposure. After the good correlation shown in Figs. 5.3 and 5.4, the use of Fig. 5.5 can be used with great confidence. Similar temperature contour plots based on earlier fire tests were produced by the ASCE standard [**98**] for conventional RC beams cross sections exposed to the E119 fire scenario.

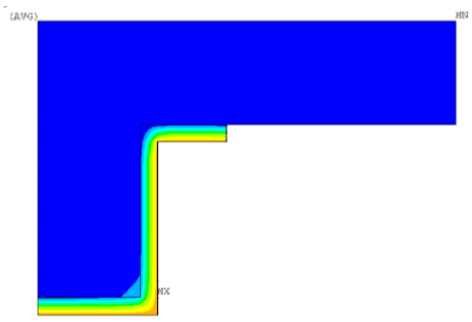

30min

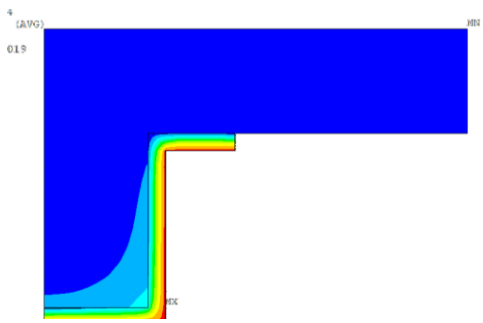

60min

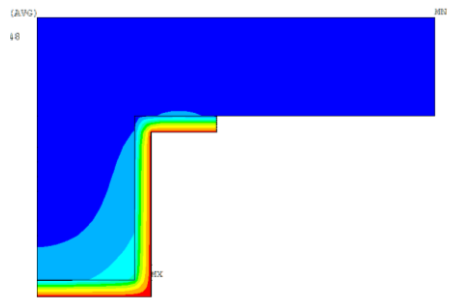

90min

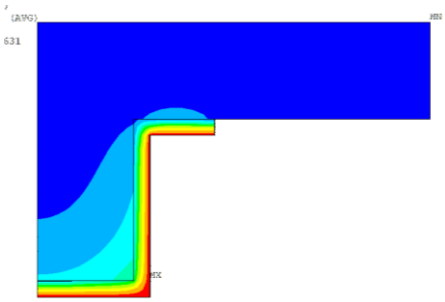

120min

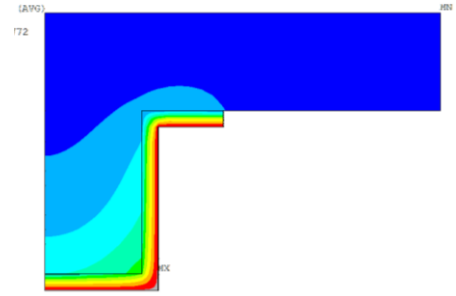

180min

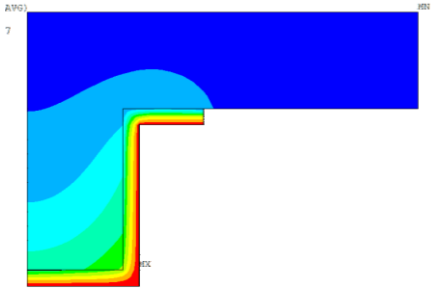

240min

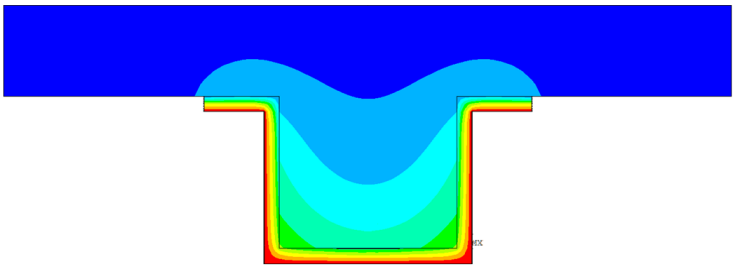

Temperature distribution in the full scale model after 240min

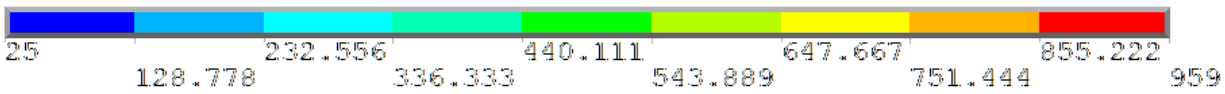

Figure 5.5 Temperature evolutions at different time of exposures (Beam 1)

Another advantage of using the FE simulation is the ability to define several parameters and extract detailed results. For example, Fig. 5.6 shows two path lines defined at the center-line of Beam 1 and across the bottom surface of the flange towards the center-line of the beam.

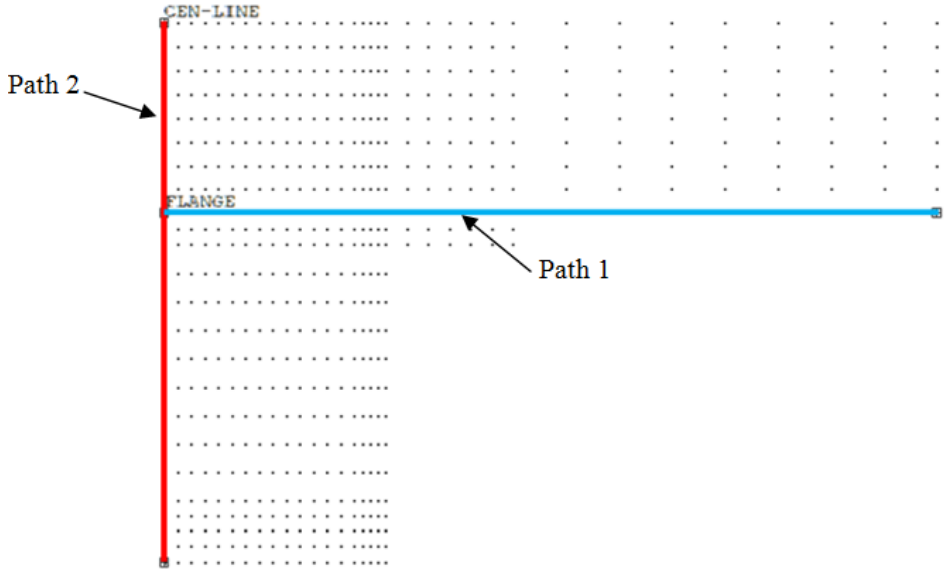

Figure 5.6 Path lines defined in the FE modeling for Beam 1

The path lines defined in Fig. 5.6 were used to extract the temperature distribution along them. Figure 5.7 and 5.8 show the variation of temperature along the predefined path lines. Figure 5.7 shows the variation of temperature along the bottom surface of the flange. A closer look will show that the peak temperatures around 400mm are associated with the increase of temperature at the edges of the VG insulation. Since the horizontal and vertical sides of the VG insulation meet at 400mm from the center-line, thus the location of 400mm experiences the most increase of temperature along this path line. In addition, the core of the T-beam seems to have the lowest temperature recorded due to the large amount of the available concrete material and presence of insulation materials.

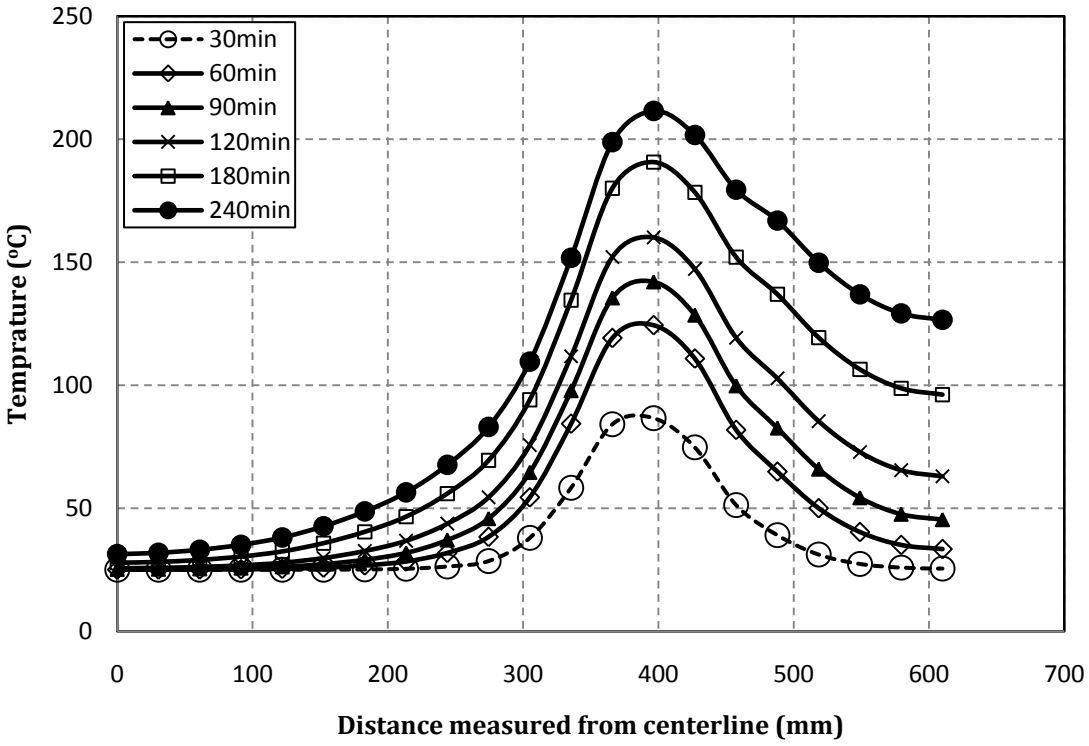

Figure 5.7 Temperature evolutions in path 1 at different exposure times

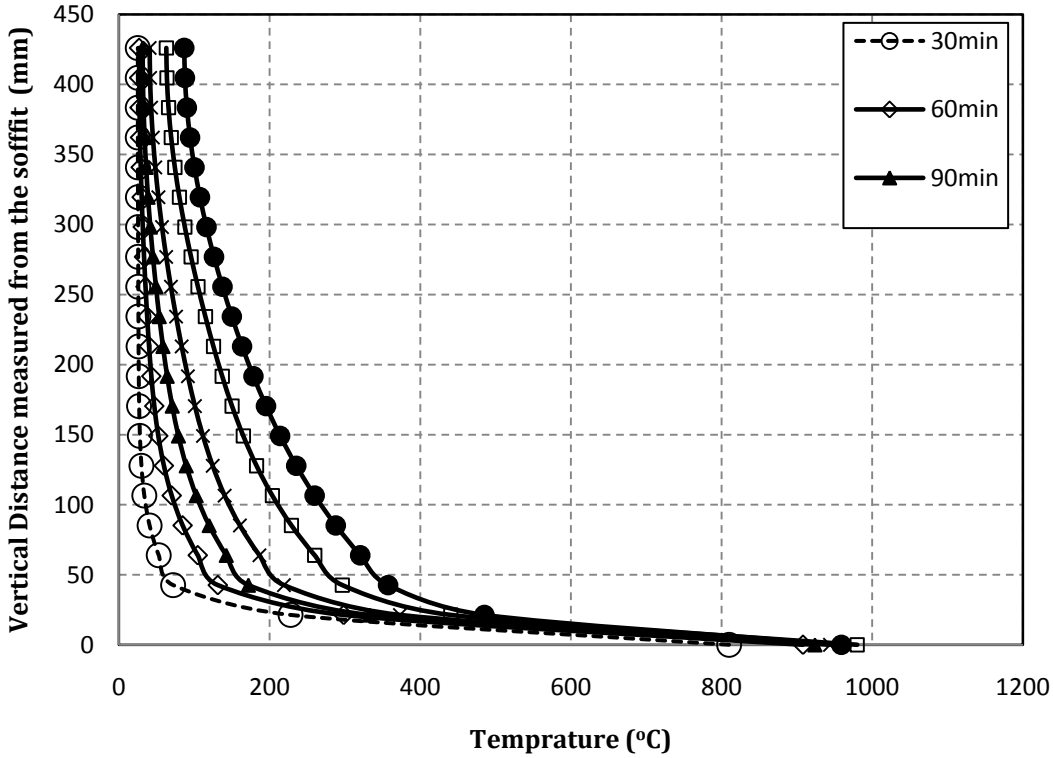

Figure 5.8 Temperature evolutions in path 2 at different exposure times

On the other hand, Fig. 5.8 provides better insight on the evolution of temperature along the vertical height of the beam's web. As expected, the temperatures at the lowest point of the VG insulation are those of the highest recorded temperatures, this due to the fact that the beam was mainly heated from below. Also, Fig. 5.8 shows that there is a large decrease in temperature in the first 25mm; on average in terms of 560°C between the bottom and top surfaces of the VG insulation. This decrease is mainly due to the presence of the VG insulation. Another kink is observed at around 35mm because of the change of materials from CFRP to concrete. Then, steady reduction in temperature is observed along the height of the beam which can be referred to the relatively low thermal properties of the concrete and other available materials. It is also clear from Figs. 5.7 and 5.8 that the variation of temperature is neither nonlinear nor scaled and mainly depends on the material available in the path line heating directions.

5.3.3 Structural Validation

In order to further validate the performance of the developed FE model. The structural performance of the tested beams and simulated FE models is compared. The mid-span deflection response of the measured and predicted results is shown in Fig. 5.9. It should be noted that there was a sudden drop in deflection because of an accidental loss of hydraulic pressure in the loading rig during the fire test. The sustained applied load was equal to 34kN/m as calculated by Williams et al. [**4**]. It should be noted that this load corresponds to 56 and 48% of the theoretical ultimate capacity of the RC beam and ultimate capacity of the strengthened beam, respectively.

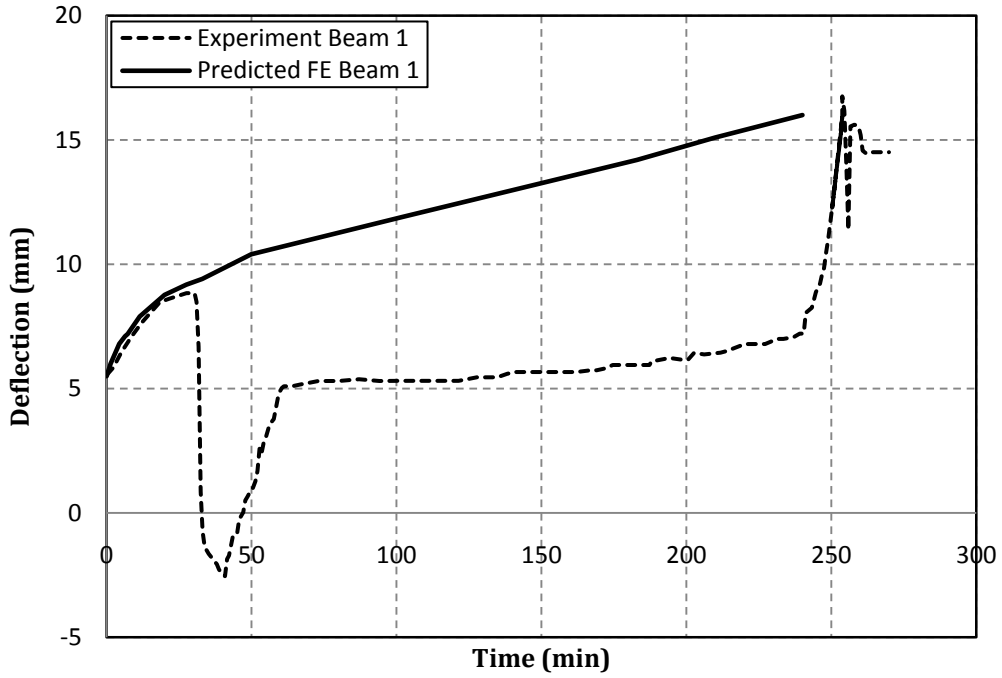

(a) Beam 1

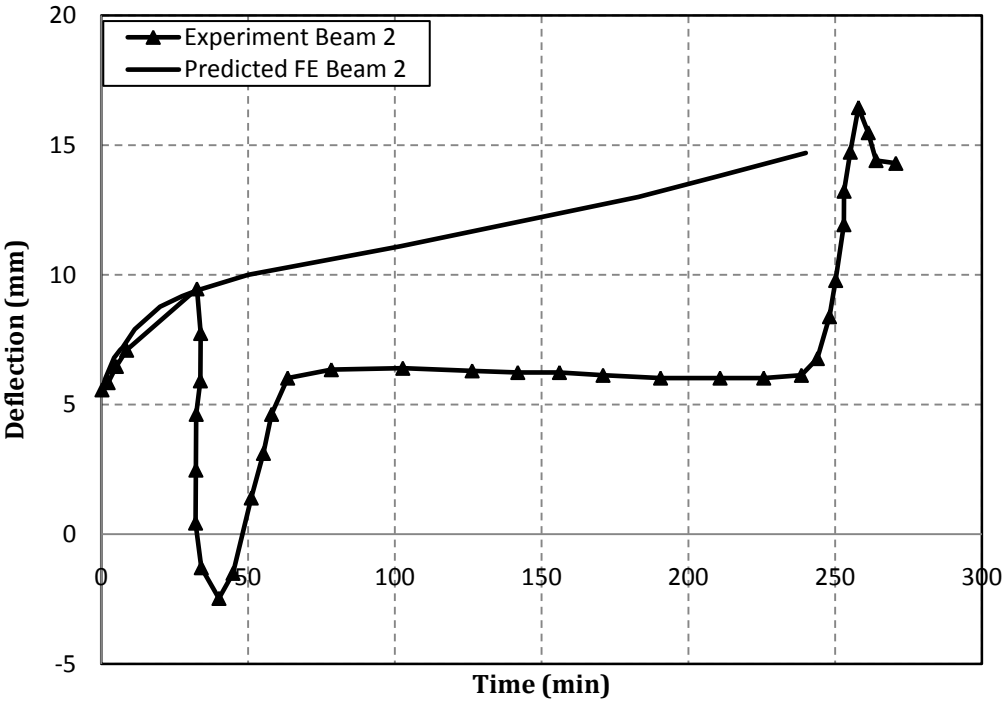

(b) Beam 2

Figure 5.9 Comparison of the FE predicted and measured mid-span deflection

A closer look to Fig. 5.9 shows the good agreement between the measured and predicted FE results up to loss of the hydraulic pressure and end of the fire test at 240min. In the FE model, the mid-span deflection increases under the sustained load during the whole course of the fire test. On the other hand, the measured mid-span deflection is significantly reduced once the pressure was lost then slightly increased after the restore of the applied pressure. Then, the mid-span vertical displacement steadily increased, yet did not retain its initial level up to the end of the test which resulted in relatively lower deflections.

5.3.4 Structural Behavior

Viewing of the full fields of vertical deflection, stresses is possible in the FE model. This provides a great advantage over experimental testing in evaluating the fire tested beams. For example, the limited numbers of Linear Variable Differential Transformers (LVDTs) used in the experimental program would not allow measuring deflections at different locations. Furthermore, the calculation of stresses and strains may not be applicable. However the FE simulation provides access to multiple numbers of results that are 3D-in nature, for example Figs. 5.10 and 5.11 show the mid-span deflection and crack patterns at failure.

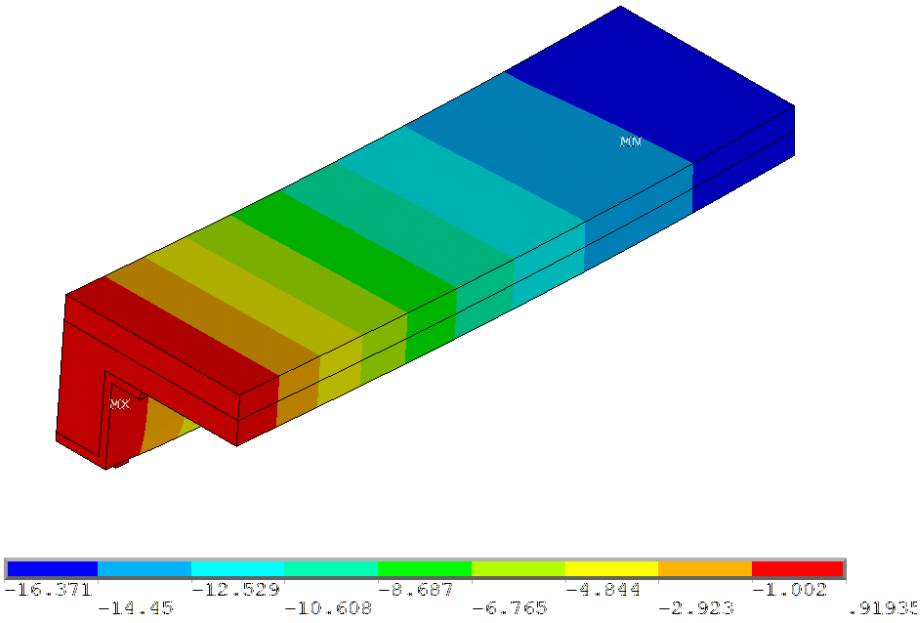

Figure 5.10 Mid-span deflection at failure (in mm)

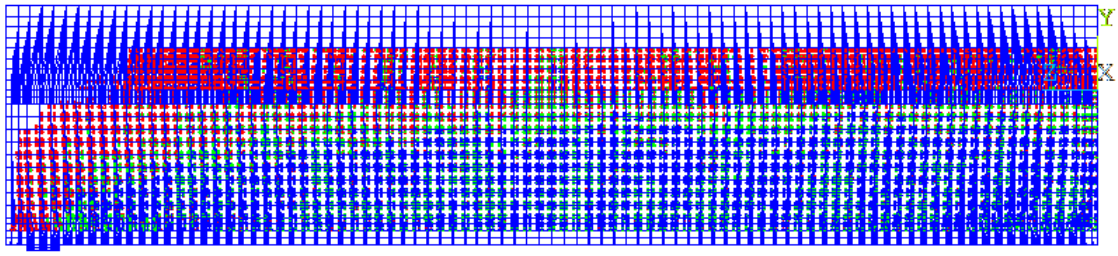

Figure 5.11 Crack patterns at failure

Figures 5.12 to 5.15 show the axial stresses in the concrete, steel, CFRP plate and insulation materials. Fig. 5.12 shows that low tensile stresses were on the flange; hence it seems that the flanges of the beam did not experience any serious cracking, this is also shown in Fig. 5.11. On the other hand, Fig. 5.13 and 5.14 show the axial stress in the main tension steel rebar and CFRP plate. As expected the axial stress is maximum at the mid-span of the beam. Finally, Fig. 5.15 provides an insight on the axial stresses in the VG insulation. The VG insulation does not provide any structural stiffness due to its very low mechanical properties, thus it is only used for insulation purposes.

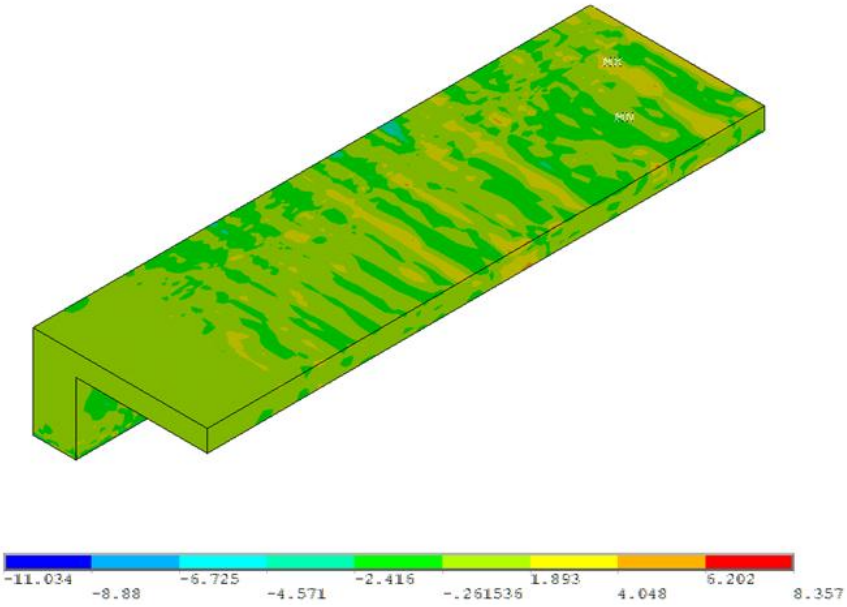

Figure 5.12 Axial stress in the concrete material (in MPa)

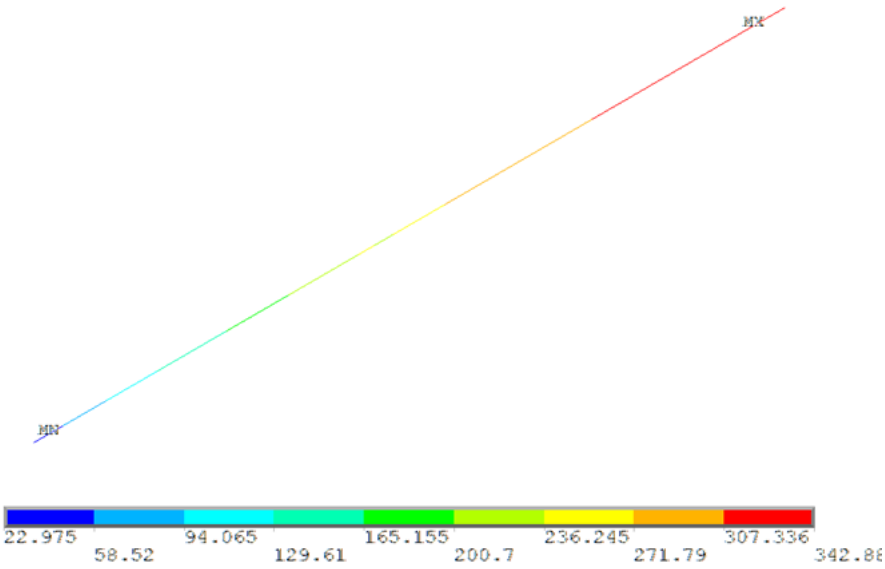

Figure 5.13 Axial stress in the steel rebars (in MPa)

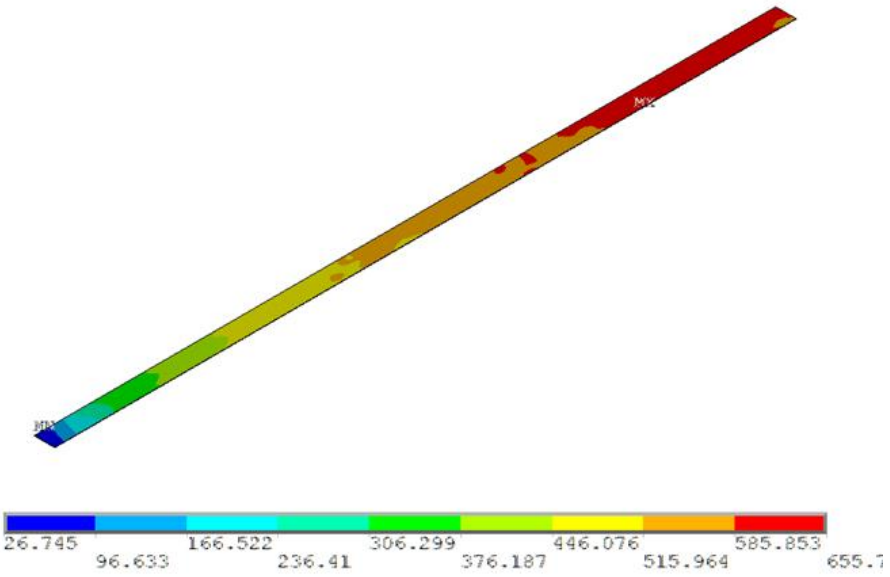

Figure 5.14 Axial stress in the CFRP plate (in MPa)

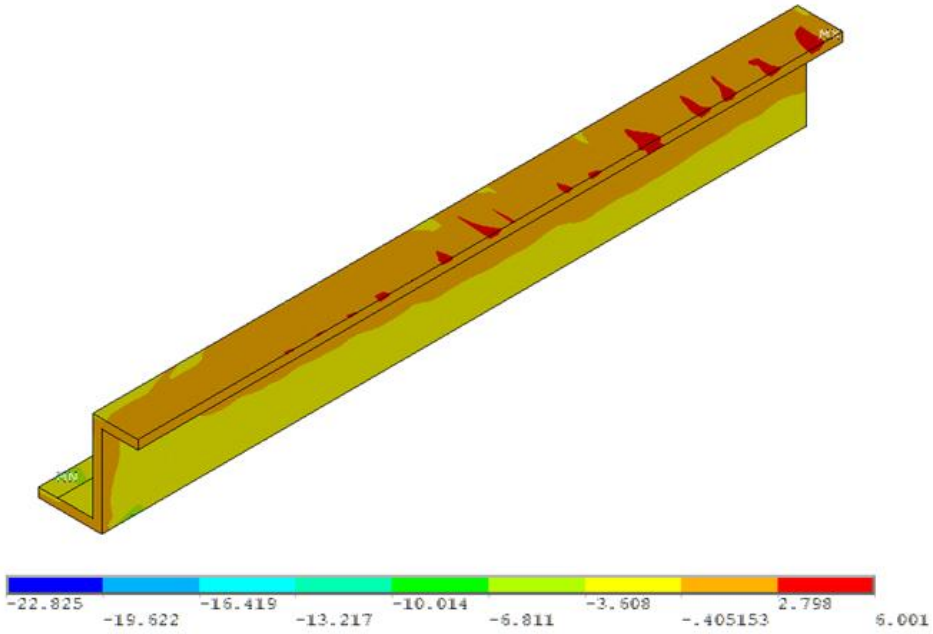

Figure 5.15 Axial stress in the concrete material (in MPa)

A path line has been defined along the CFRP plate length to capture the variation of axial stress with time. As expected, the CFRP plate experiences larger stresses at the mid-span region which tend to decay away from the maximum moment region. Also, it can be seen from Fig. 5.16 that CFRP plate experiences larger stresses with time. At the beginning of the fire test, the CFRP plate was experiencing axial stress of 361.26MPa at mid span and decays at a length of 1100mm. This indicates that 1100mm of the CFRP plate's length was utilized to carry the loads, because the stresses beyond this location rapidly decreased from 195 to 28MPa in a distance of approximately 250mm.

Furthermore at higher temperature it is clear that the stresses increase at mid-span and decay at a longer length compared to that at ambient temperature. Figure 5.16 shows a large jump of the increase in the axial stress of almost 93MPa from 361.26 to 455.27MPa within the first 30min. On the other hand, the axial stress within the CFRP plate increased on average by 15MPa on the fourth hour than that on the third hour of the fire exposure. This clearly shows that the CFRP plate was unable to carry any extra load due to the degradation of its mechanical properties.

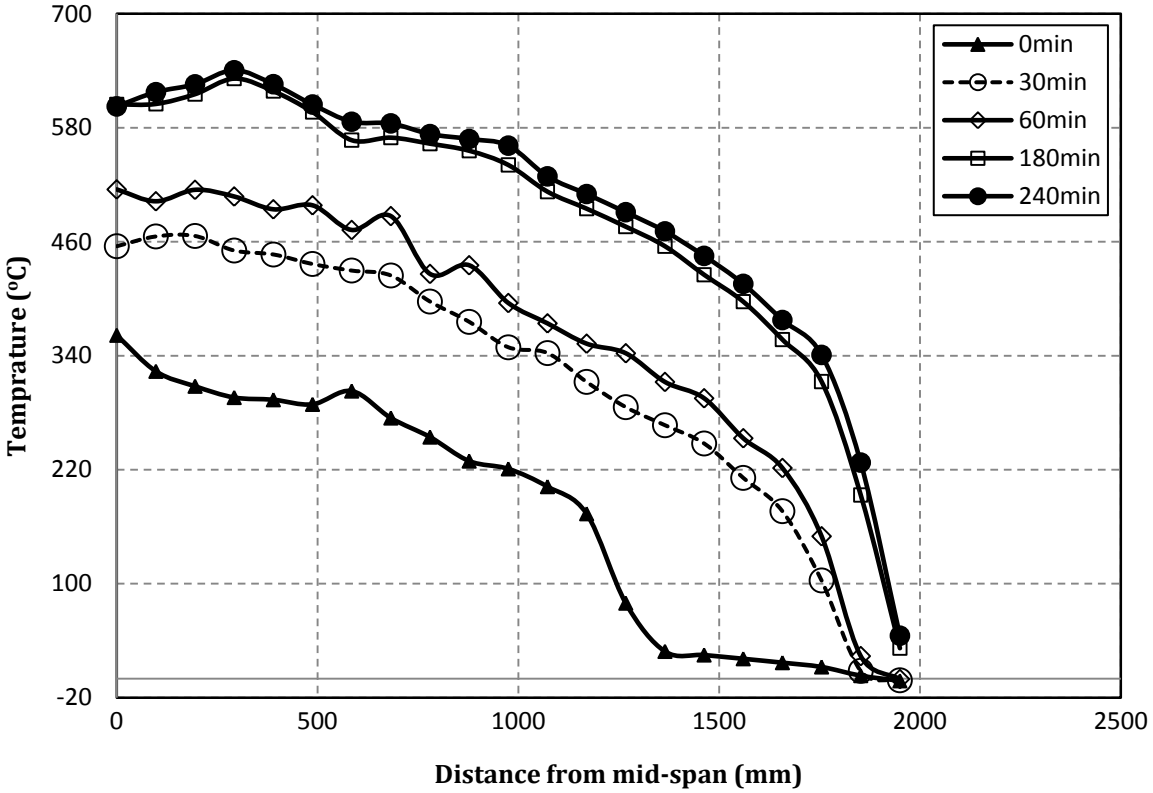

Figure 5.16 Predicted stress along the CFRP plate

Figure 5.17 shows the shear stress at the CFRP/Concrete interface. According to Varastehpour and Hamelin [**99**], once the shear stress at this interface reaches 4.5MPa, debonding is assumed to take place. Still, no debonding was reported in the experimental program. However, the FE model predicts localized deboning at the maximum moment region. The debonding occurred on a small area of a rectangular cross-section 10×44mm, compared to the total area of the CFRP plate of 100×3900mm. Such localized debonding would not affect the fire performance of the beam. Hence, the assumption of using perfect bond between the CFRP and concrete was valid in this study.

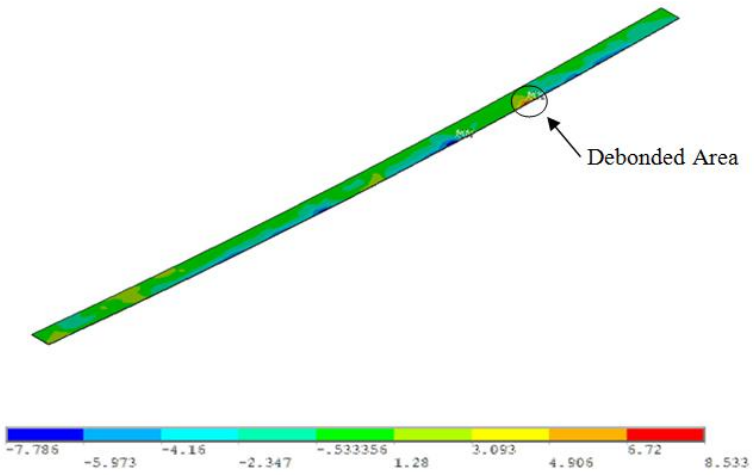

Figure 5.17 Shear stress at the CFRP/Concrete interface at the end of heating

5.3.5 Time to Failure

A developed failure criteria to predict the time to failure of the tested beams is shown in Fig. 5.18. The strength approach in which the damage of the FRP material is predicted by comparing the axial stresses available in the CFRP plate during the fire testing with its degraded strength at elevated temperature is used herein. As shown in Fig. 5.18, the FE model predicts the failure of the CFRP system after reaching a temperature of 224°C at 136min.

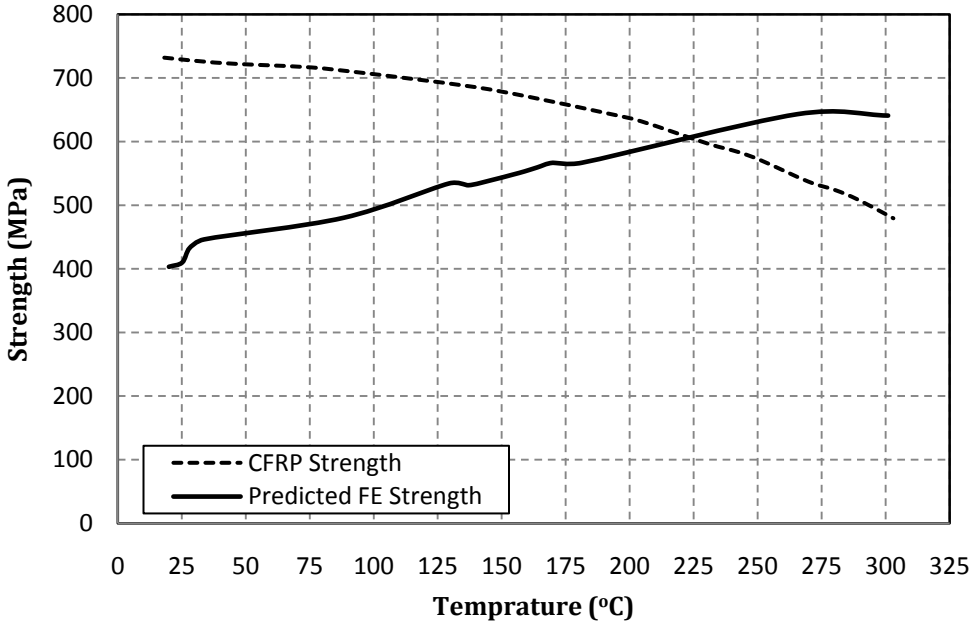

(a) Temperature at failure

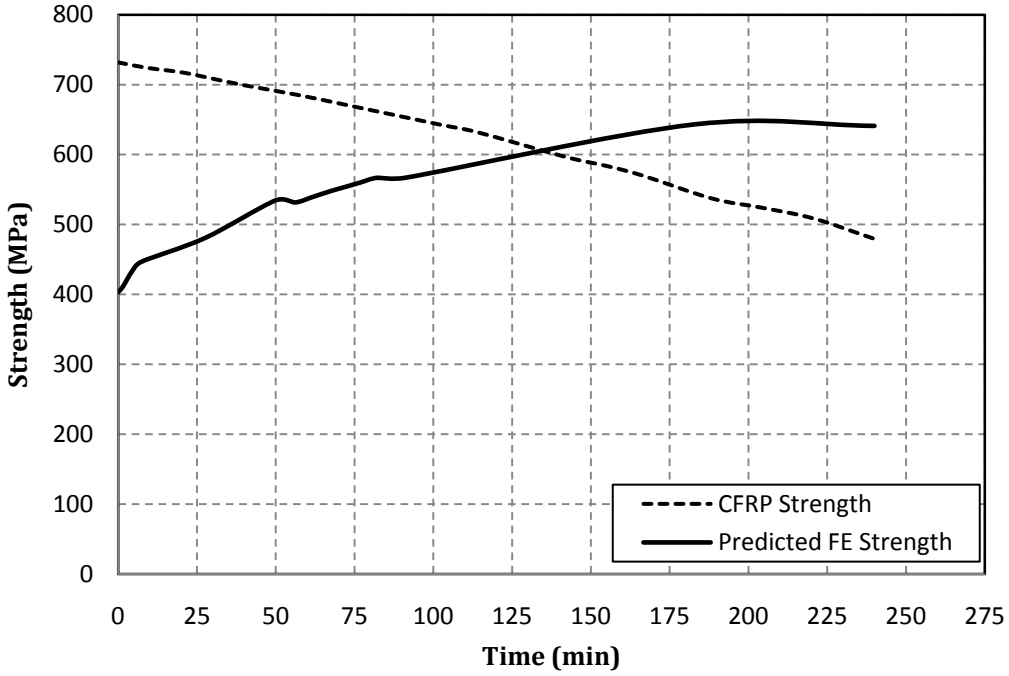

(b) Time to failure

Figure 5.18 Prediction of the fire endurance

It should be noted that the use of this technique is very useful if used in the FE simulation of such scenarios. Because the predicted stress in the CFRP system is a function of multiple parameters, this method requires accurate inputs in terms of material properties and loading/heating setup.

It was proven that although the temperature at the CFRP plate reached comparatively higher temperatures in the range of 300-400°C, the strengthening system was able to maintain its applied loads and achieved a 4 hours fire endurance in which the beam did not fail under the sustained loading. Thus, the author agrees with Williams [**59**] and Williams et al. [**4**] that the use of the temperature at the bond line as a failing criteria is very conservative, requires further investigation and does not represent the actual behavior of FRP strengthening systems. It should be noted that the thermal decomposition of the matrix/adhesive was determined to occur between 390 and 510°C [**2**].

5.4 Validation Model of Blontrock's et al. (2000) Experimental Program:

This section provides further validation of the proposed FE model by comparing its behavior to the experimental results of Blontrock et al. [**5**]. Blontrock's et al. [**5**] conducted tests on 10 RC beams, 8 under the ISO834 fire curve and the remaining two were used as control specimen tested at ambient temperatures.

5.4.1 Thermal Validation

Figures 5.19-5.25 show the validation of the thermal response of the developed FE models, namely Beam 3, Beam 4, Beam 5, Beam 6, Beam 7, Beam 8, Beam 9, and Beam 10. Although a more comprehensive description can be found in Blontrock et al. [**5**] and the previous chapter, a brief description of each specimen is provided herein.

a) Beam 1 is a control beam that is unstrengthened tested at ambient temperatures under monotonic loading

b) Beam 2 is a reference, strengthened beam with one CFRP plate attached to the soffit of the beam and tested under monotonic loading

c) Beams 3 and 4 are control beams which are unstrengthened, unprotected beams tested under the ISO834

d) Beam 5 through 10 are protected and strengthened specimen and tested at elevated temperatures (ISO834)

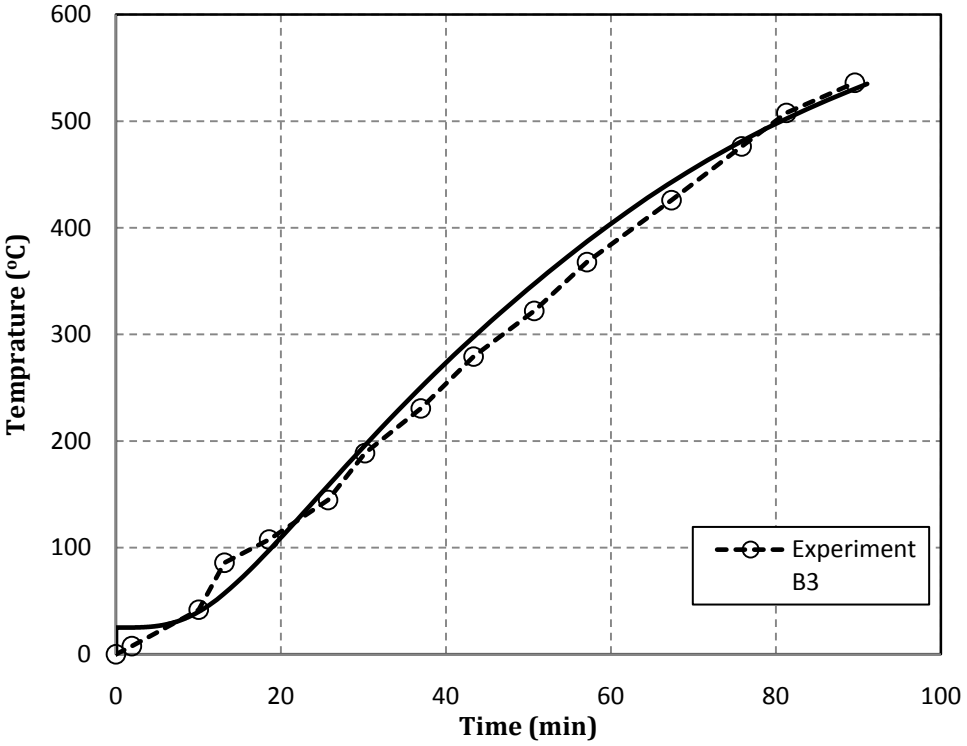

(a) Beam 3

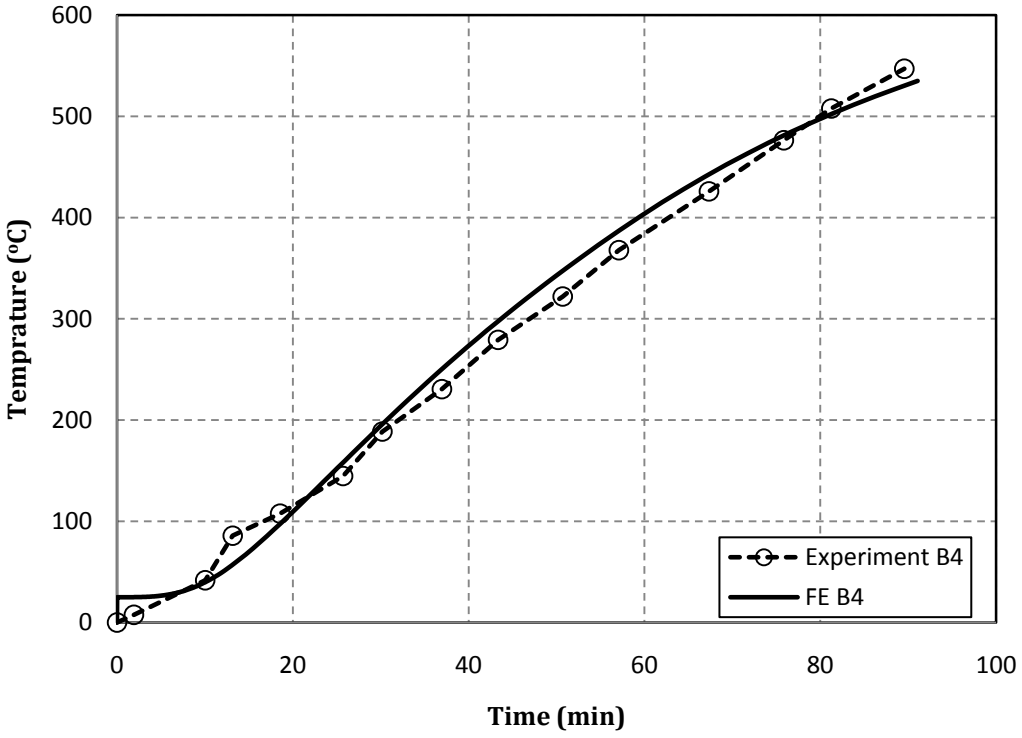

(b) Beam 4

Figure 5.19 Thermal validation at the steel reinforcement level of Beams 3 and 4

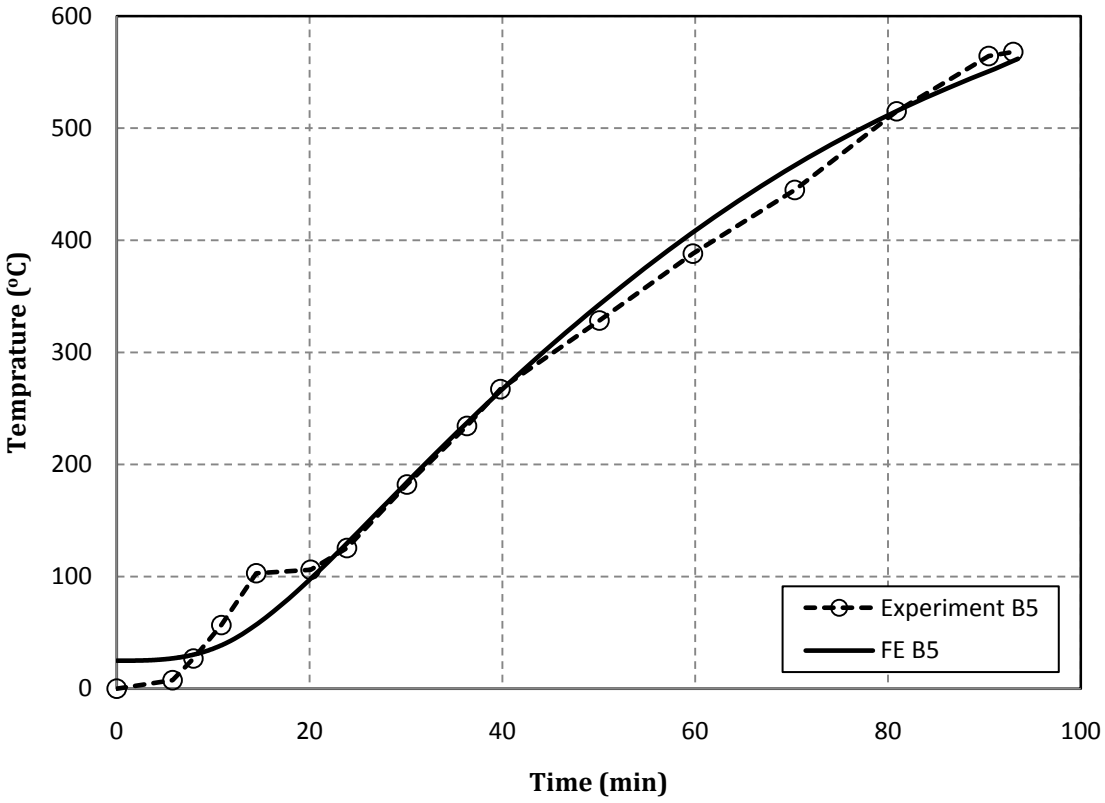

Figure 5.20 Thermal validation at the steel reinforcement level of Beam 5

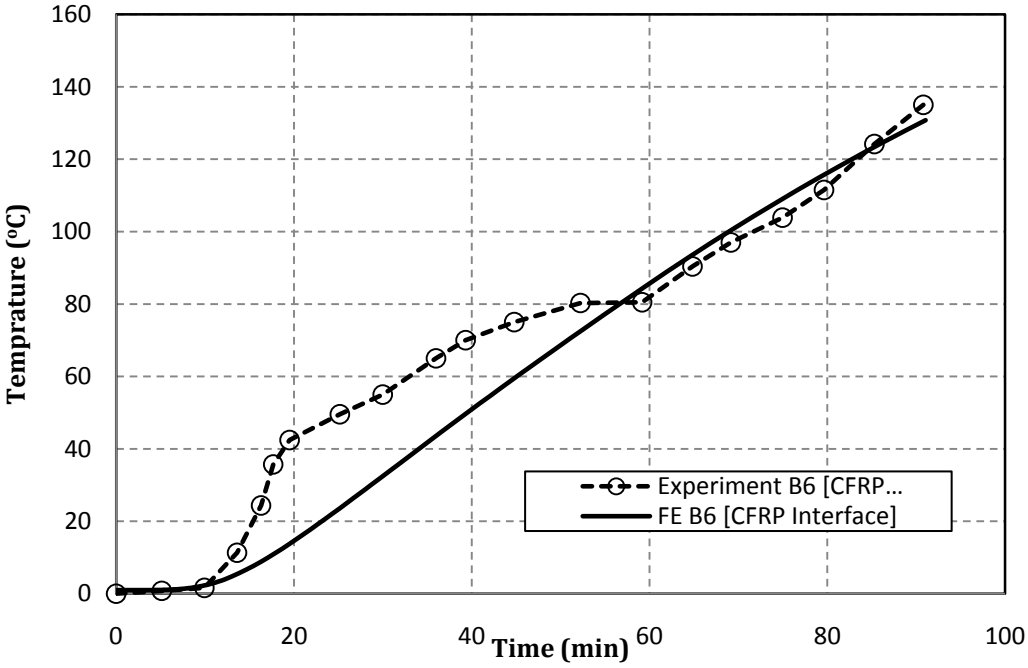

(a) CFRP interface

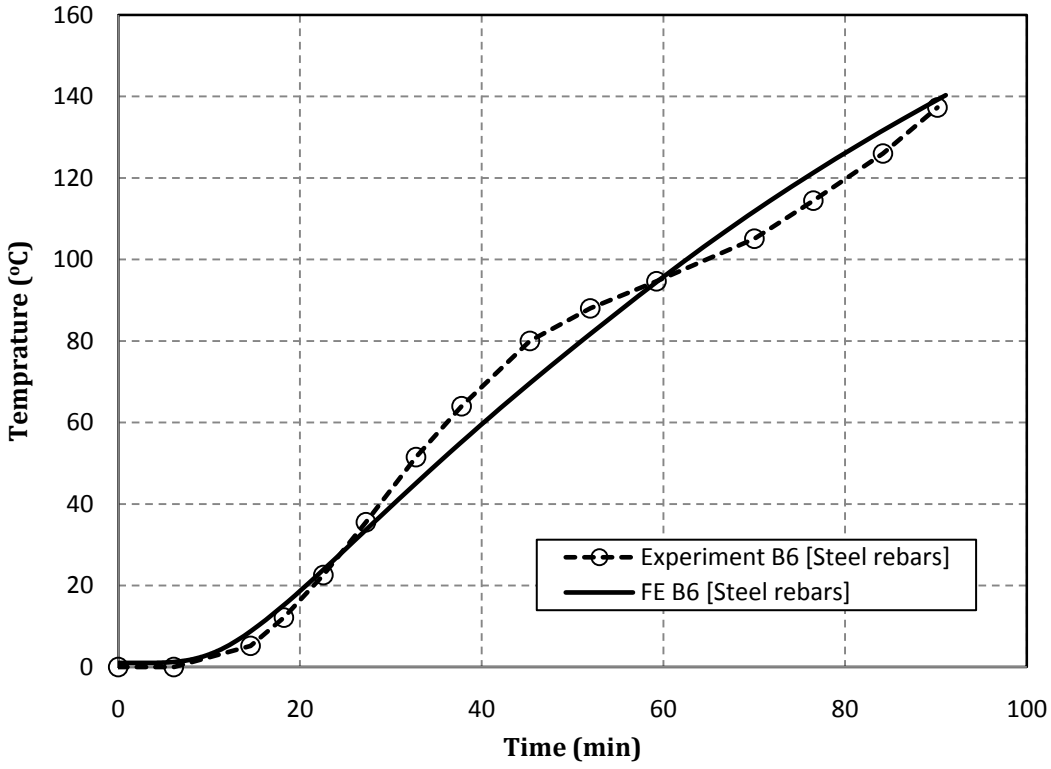

(b) Steel rebars

Figure 5.21 Thermal validation of Beam 6

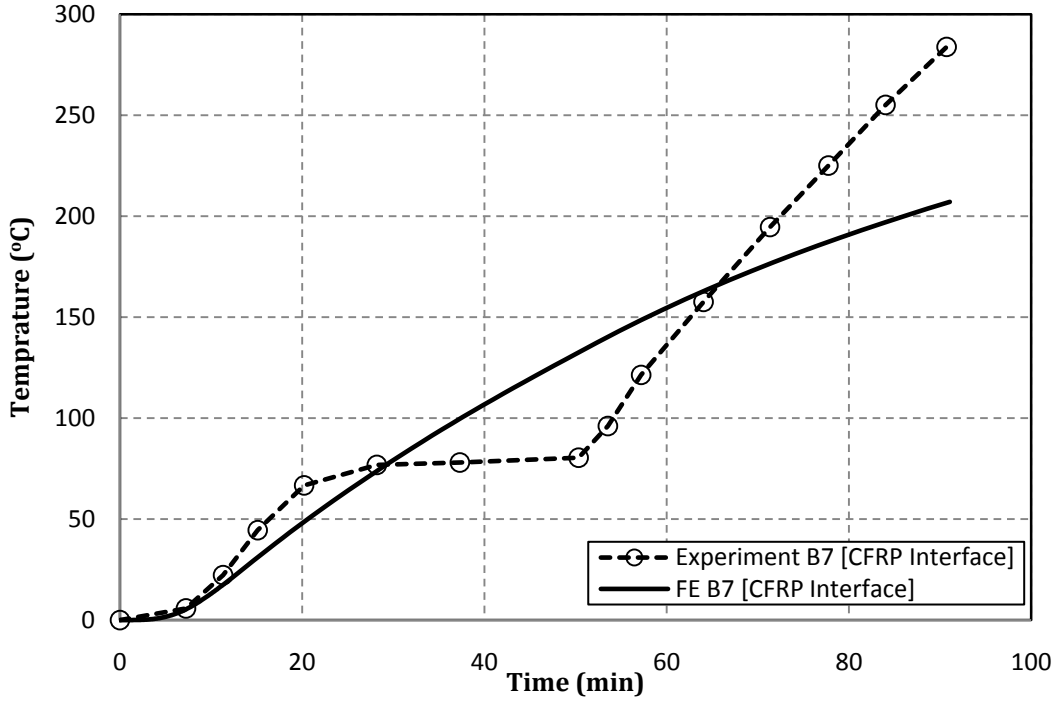

(a) CFRP interface

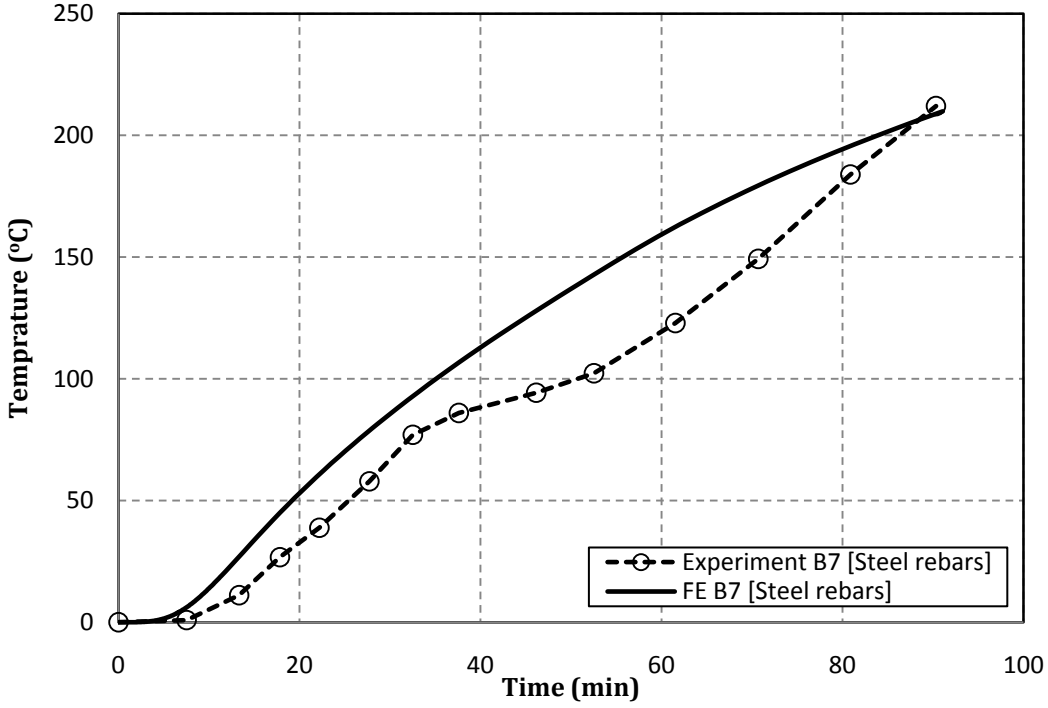

(b) Steel rebars

Figure 5.22 Thermal validation of Beam 7

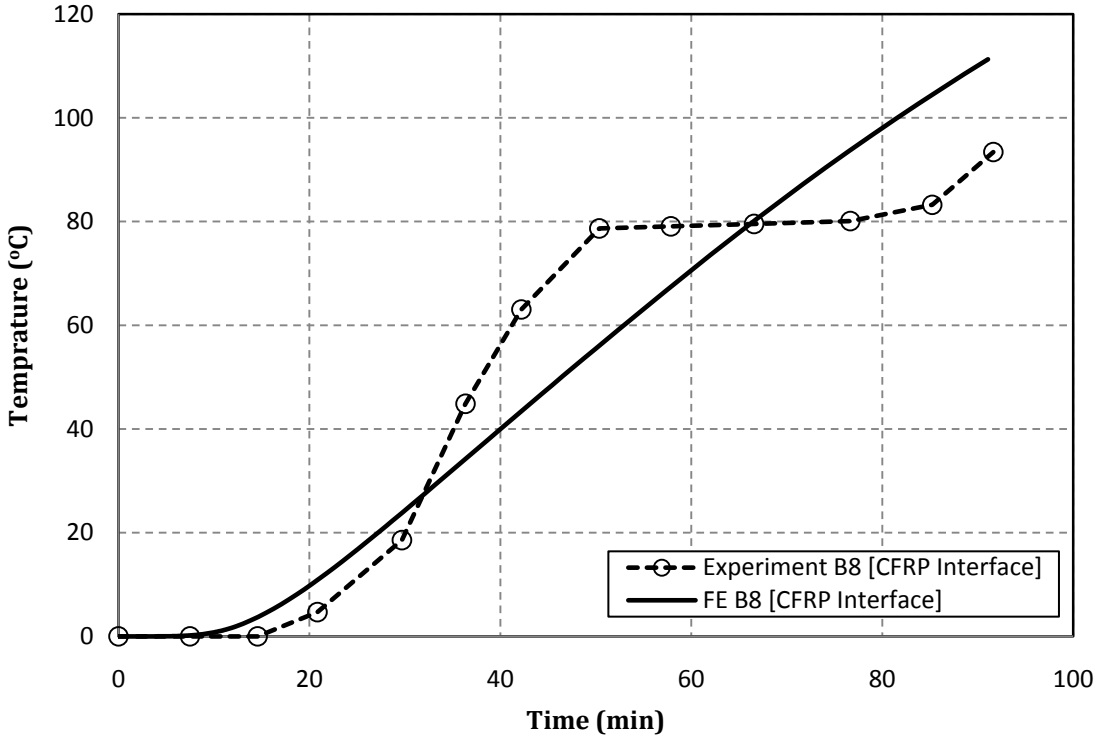

(a) CFRP interface

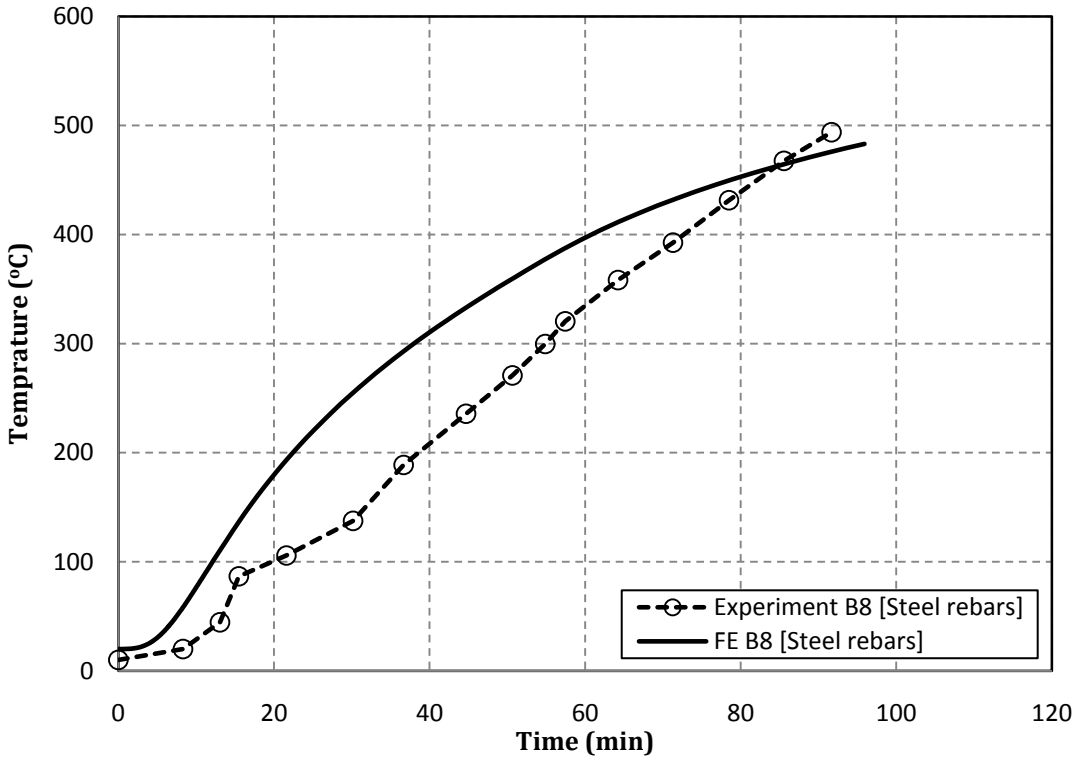

(b) Steel rebars

Figure 5.23 Thermal validation of Beam 8

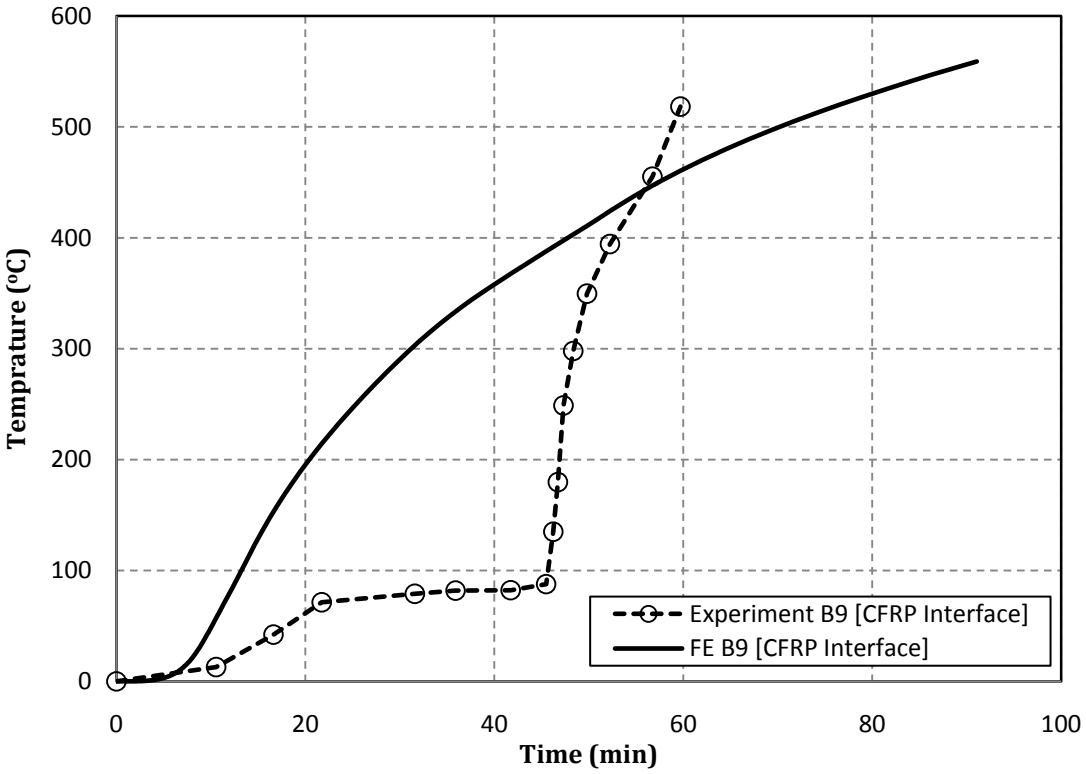

(a) CFRP interface

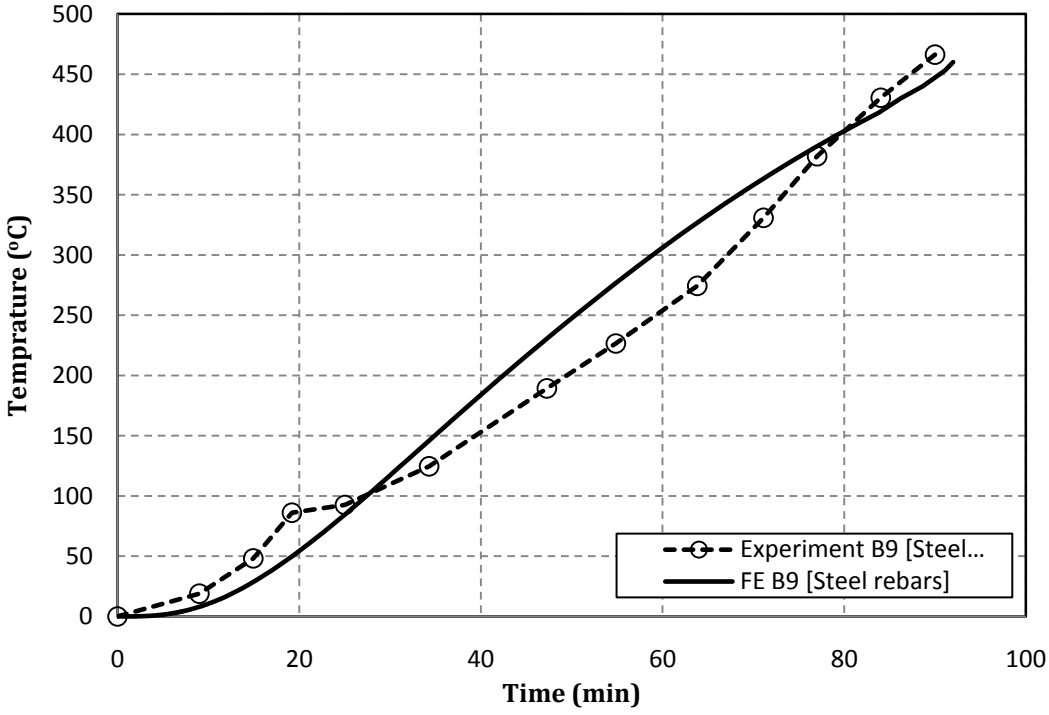

(b) Steel rebars

Figure 5.24 Thermal validation of Beam 9

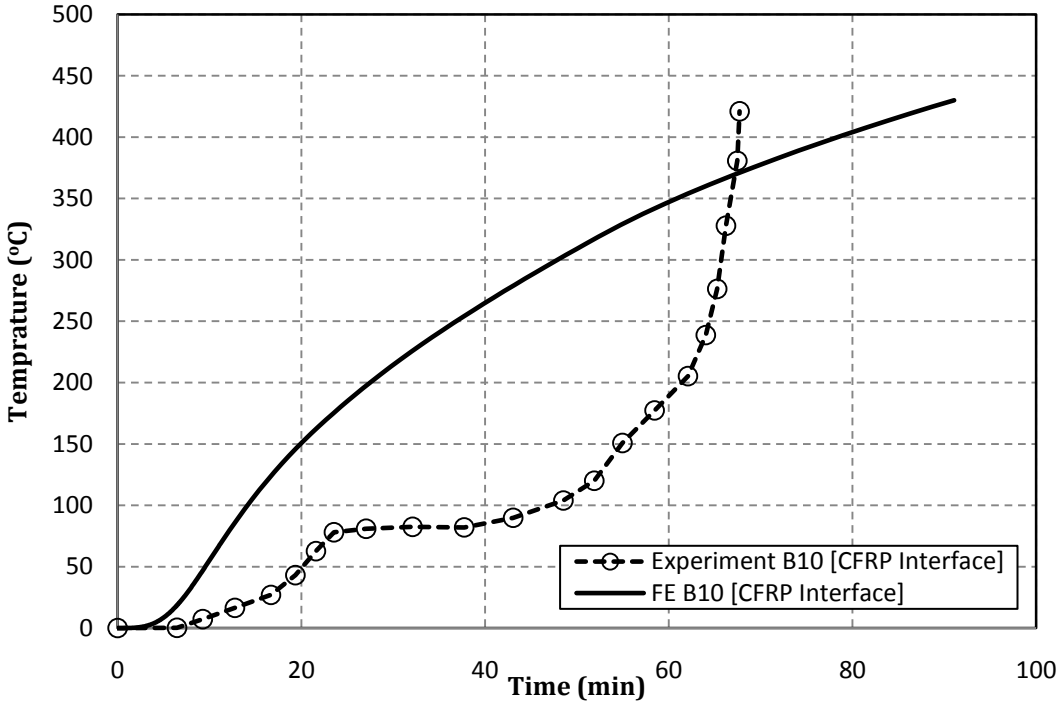

(a) CFRP interface

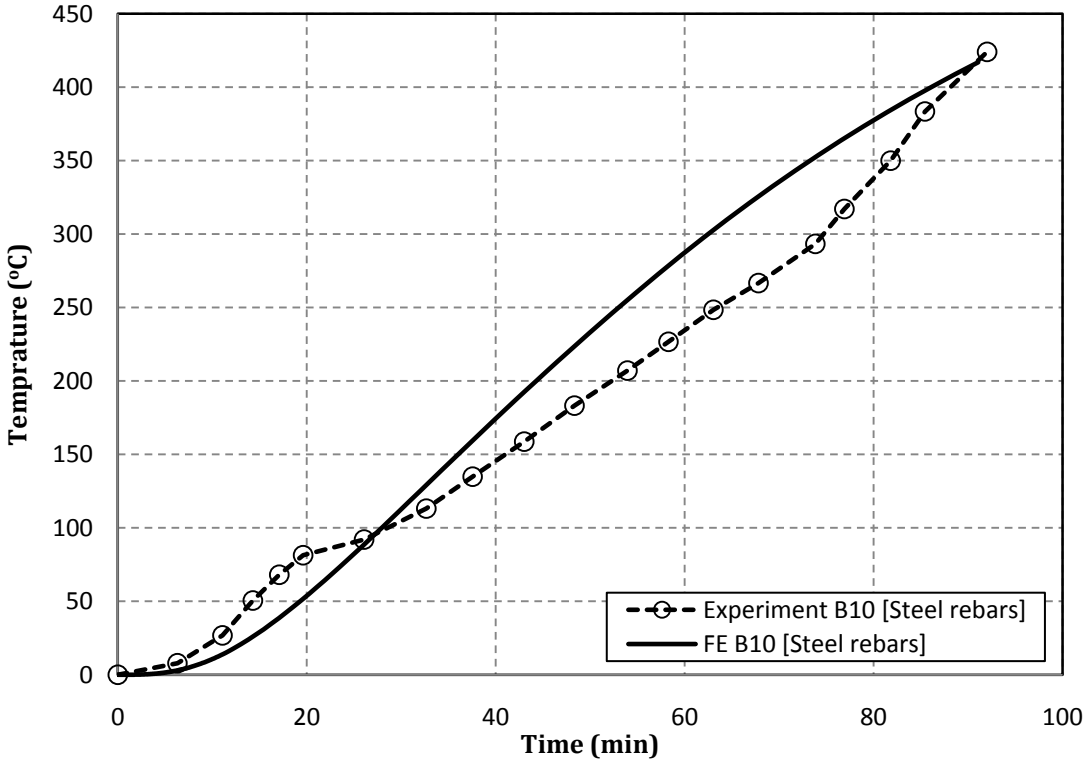

(b) Steel rebars

Figure 5.25 Thermal validation of Beam 10

It is clear that there is a good correlation between the experimental and predicted FE results. The FE models seem to capture the highly nonlinear phenomena of the fire testing. It can be seen that constant temperature in the CFRP plate for 30, 35, 25 and 28min in Figs. 5.21a, 5.22a, 5.23a and 5.24a respectively implies that the constant temperatures at the CFRP/concrete interface needs to be justified. Because a closer look to the adjacent 5.21b, 5.22b, 5.23b and 5.24b show that the temperature at the steel rebars linearly increased up to the end of the test. Since the beams were heated in both the soffit and sides of the beam and the CFRP plates are located below the steel rebars, in addition to the steady and linear increase in temperature at the steel reinforcement, then the constant temperatures and rapid jumps shown in Figs. 5.21a, 5.22a, 5.23a and 5.24a might be related to the inaccurate readings of thermocouples, or deficiency of the installation of the measuring devices. Hence, the use of FE simulation seems to avoid all time consuming and experimental preparation.

5.4.2 Structural Validation

Figures 5.26-5.30 present a comparison between the measured and predicted mid-span deflection of the tested and developed FE models. It can be concluded that there is a good agreement between the tested and predicted results for the entire experimental matrix. It seems that the FE model was able to capture the performance of the beams tested under ambient and elevated temperatures. Furthermore, the FE models incorporating FRP systems seem to be a little stiffer at the beginning of the test while matches well with the unstrengthened specimen. This is mainly due to the additional stiffness provided by the CFRP plate. Another reason might be regarding the material model used to illustrate the degradation of the CFRP material with temperature. Still, it is believed that such difference with the tested data is a must due to the complex nature of the problem, thus have minor effects and show that the presented data are in close agreement with the tested results.

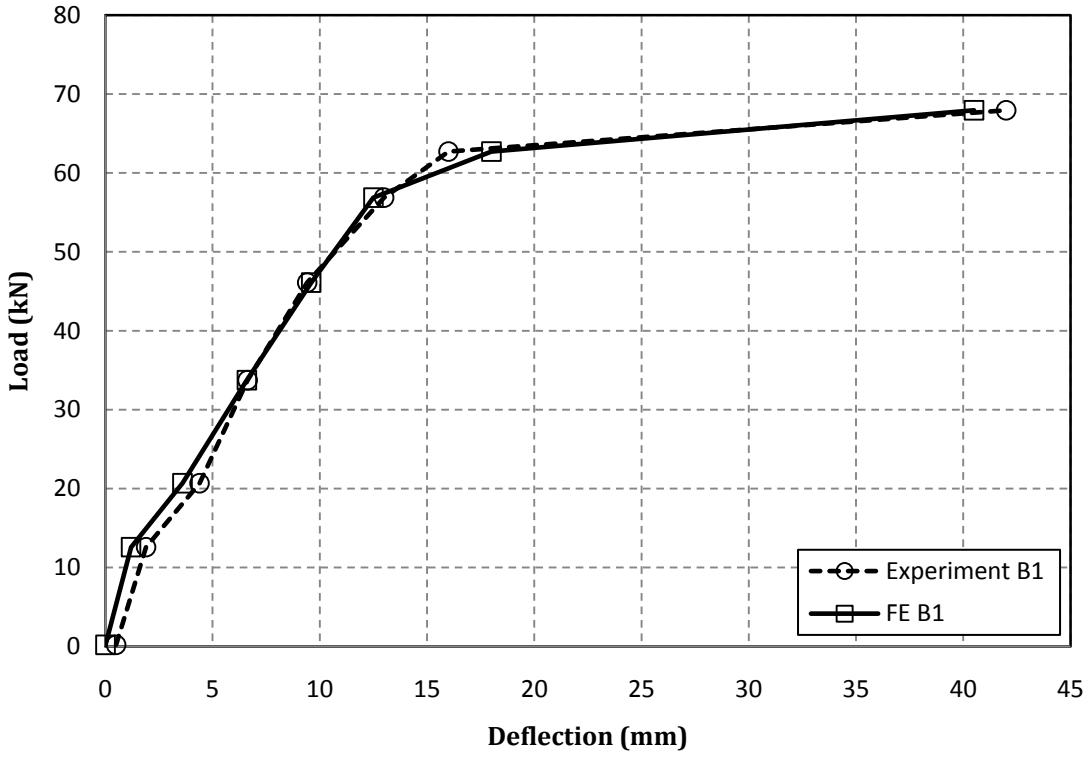

(a) Beam 1

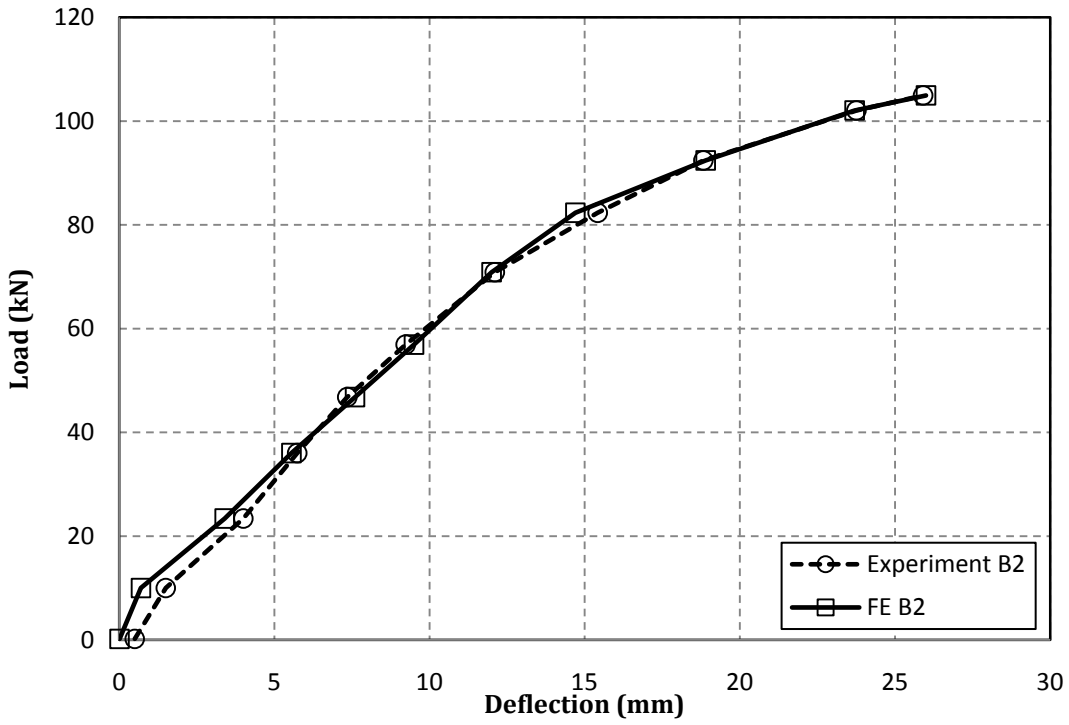

(b) Beam 2

Figure 5.26 Structural validation of Beams 1 and 2

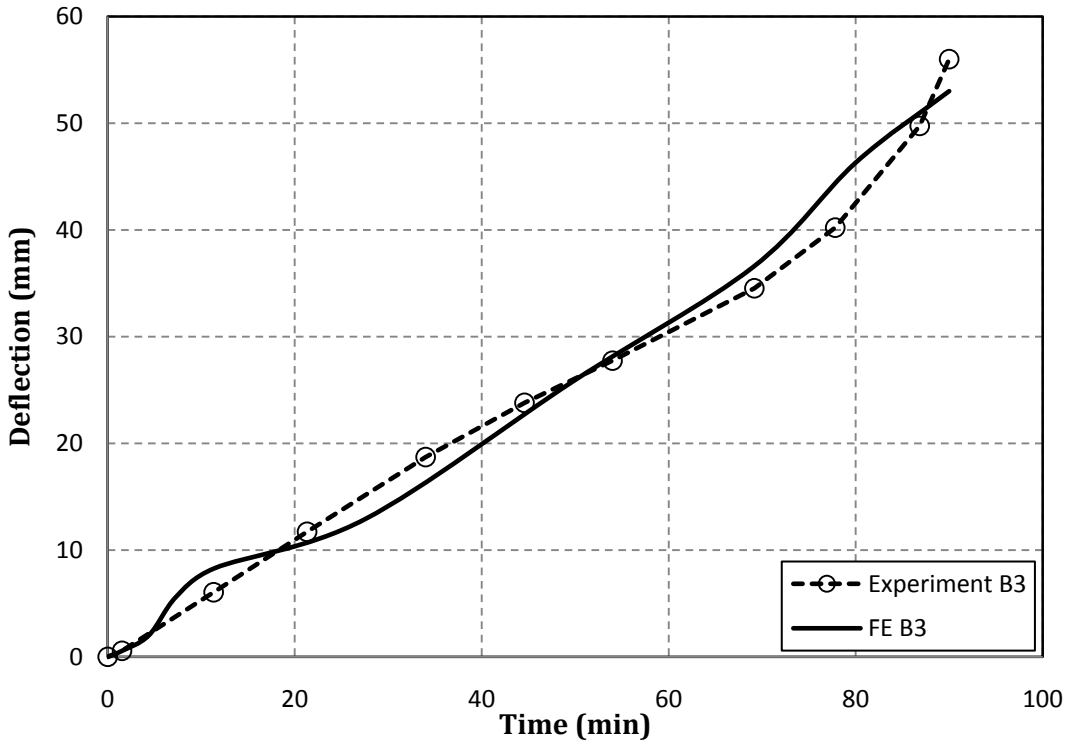

(a) Beam 3

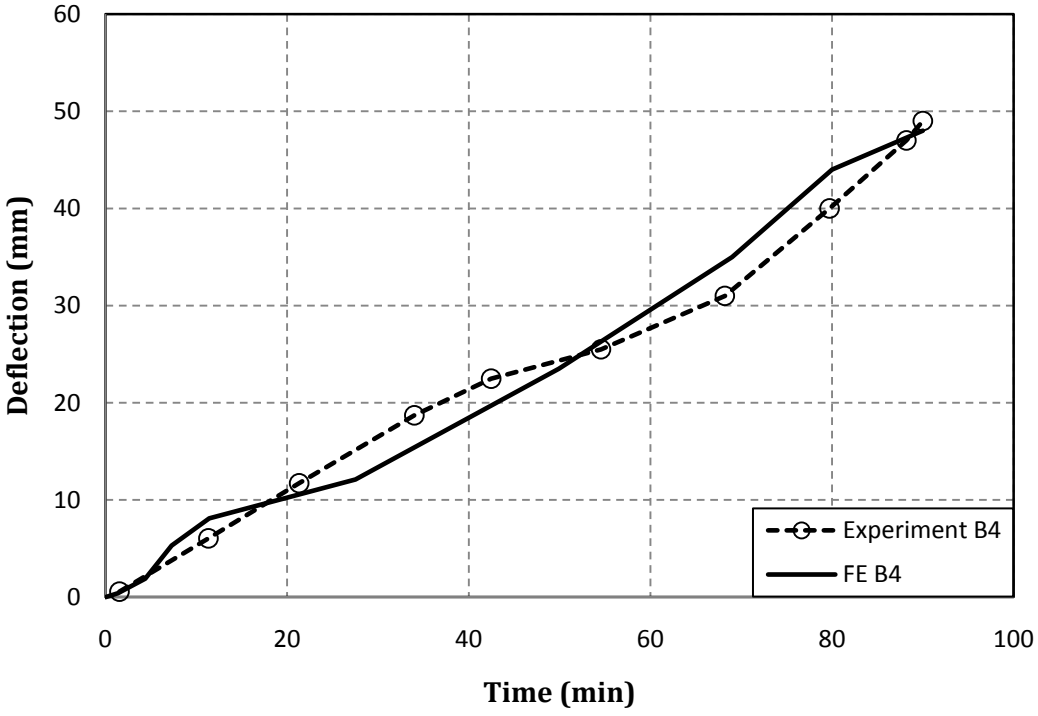

(b) Beam 4

Figure 5.27 Structural validation of Beams 3 and 4

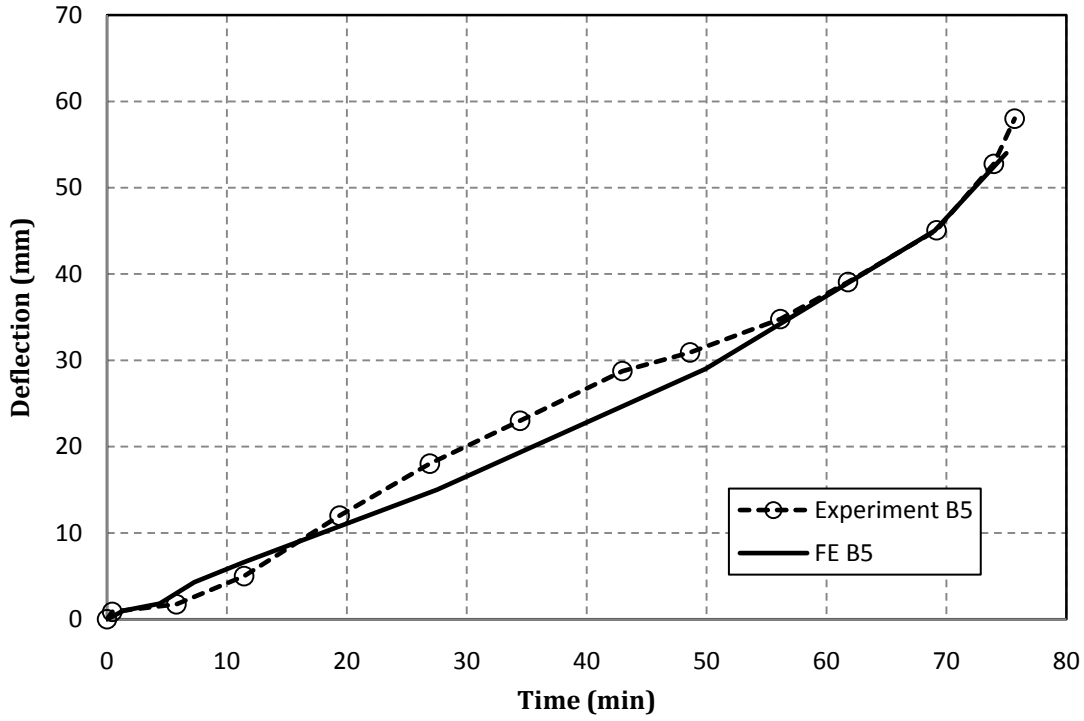

(a) Beam 5

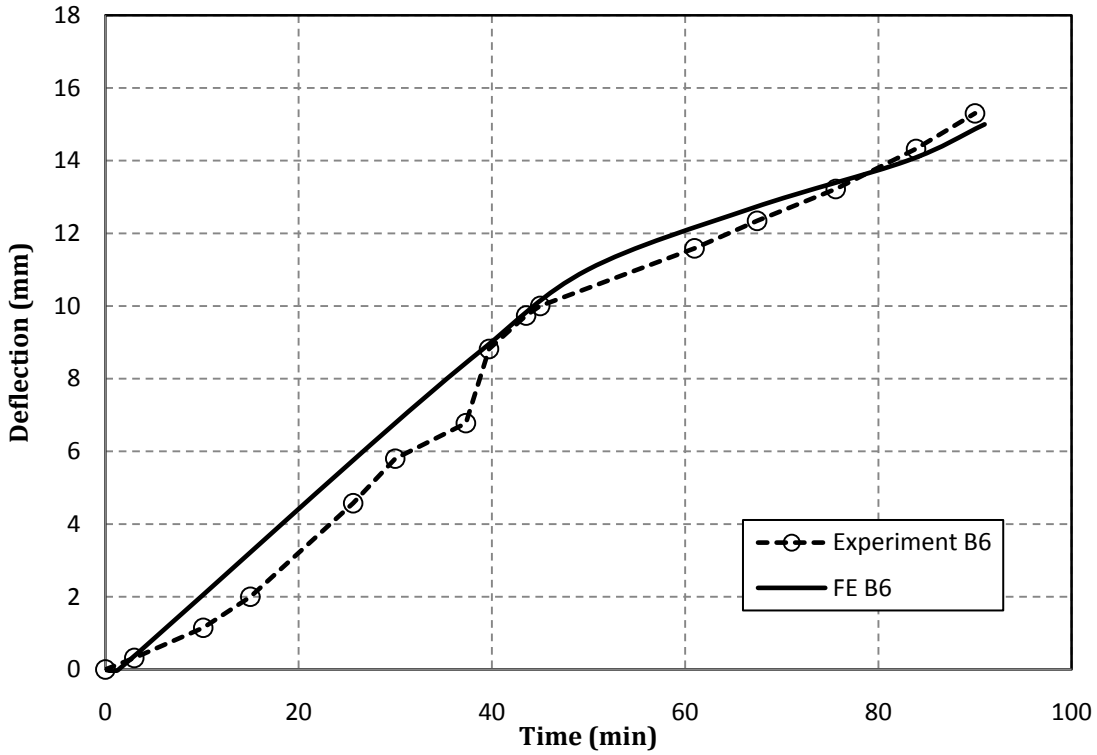

(b) Beam 6

Figure 5.28 Structural validation of Beams 5 and 6

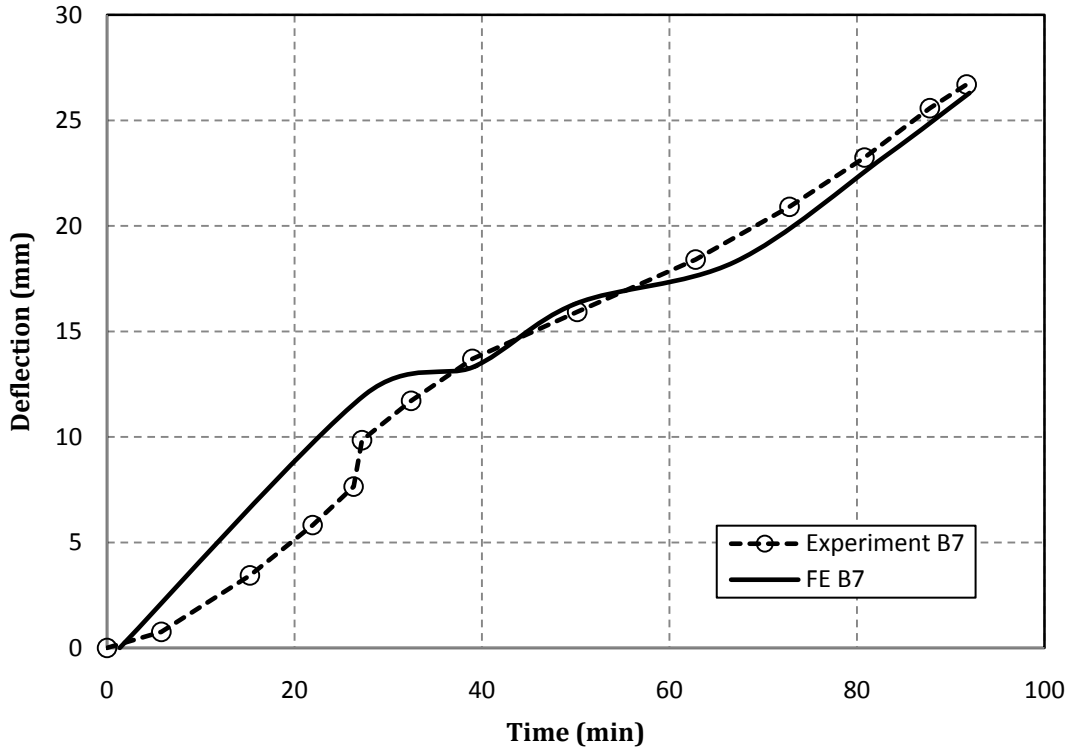

(a) Beam 7

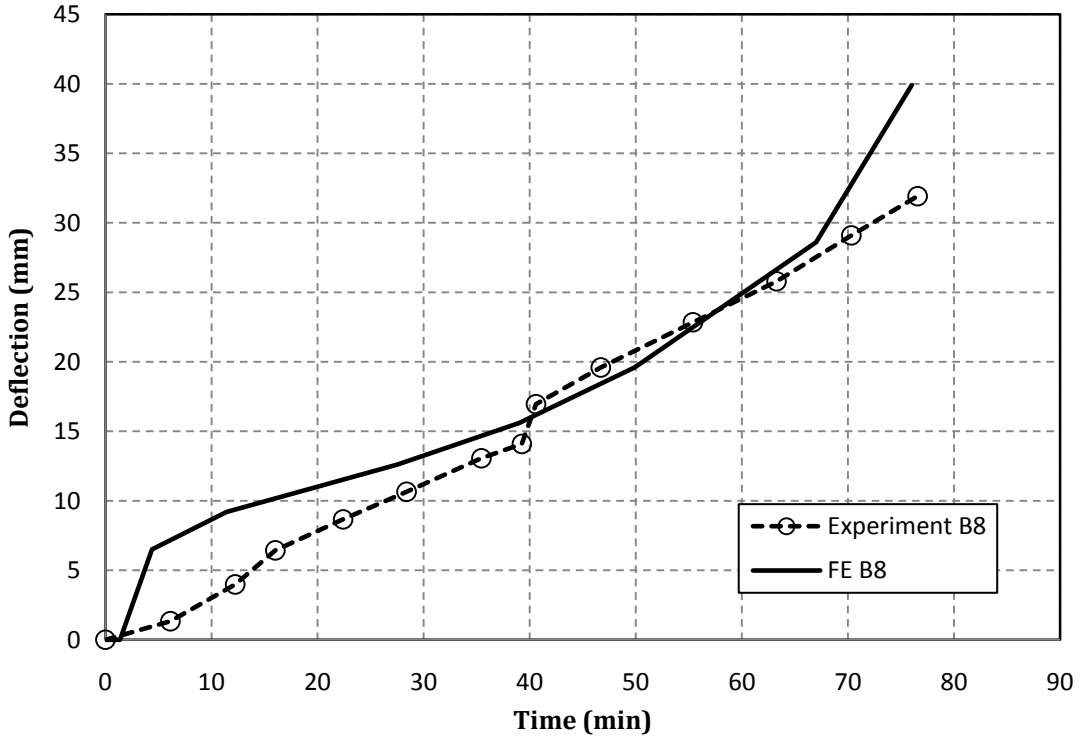

(b) Beam 8

Figure 5.29 Structural validation of Beams 7 and 8

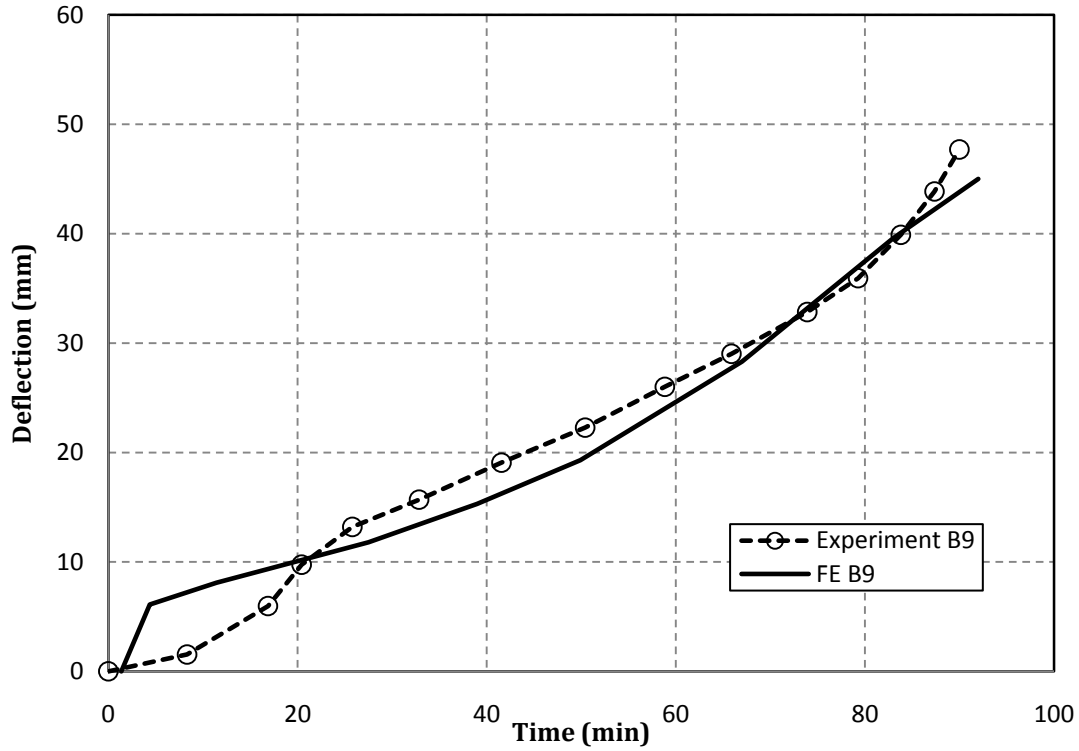

(a) Beam 9

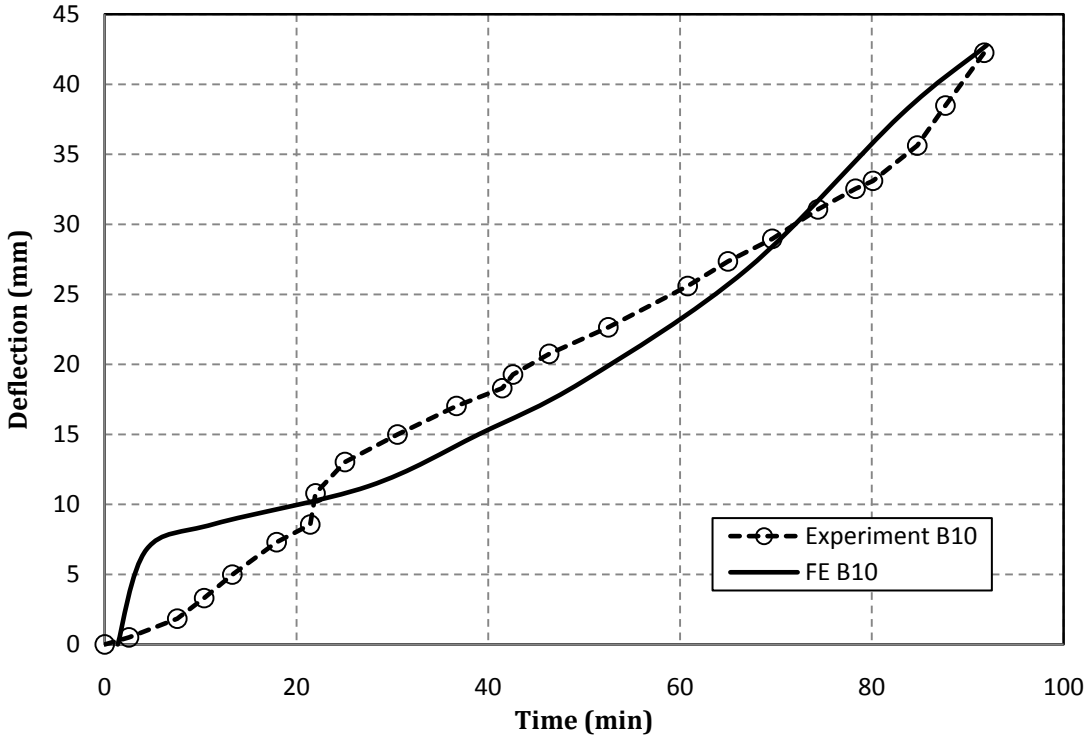

(b) Beam 10

Figure 5.30 Structural validation of Beams 9 and 10

5.4.3 Model Behavior

Figure 5.31 shows the initiation and completion of the debonding at the interface of the CFRP/Concrete of Beam 5 during fire. Table 5.1 shows the measured and predicted failure loads, mid-span deflection and debonding occurrence. It is clear that the deviation between the measured and predicted mid-span deflection at failure is less than 8.5% for all the tested specimens except for Beam 8. The deviation between measured and predicted mid-span deflection at failure for Beam 8 is 18%. Thus, it is clear that the developed FE models were able to accurately predict the performance of the tested beams under fire exposure and could be used as an alternative to the expensive and time consuming experimental testing.

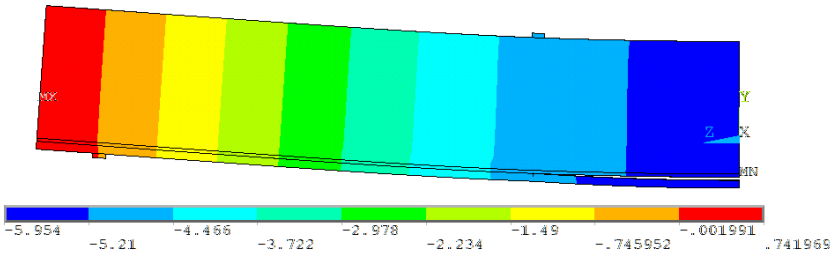

(a) Initiation of debonding (after 2min of fire exposure)

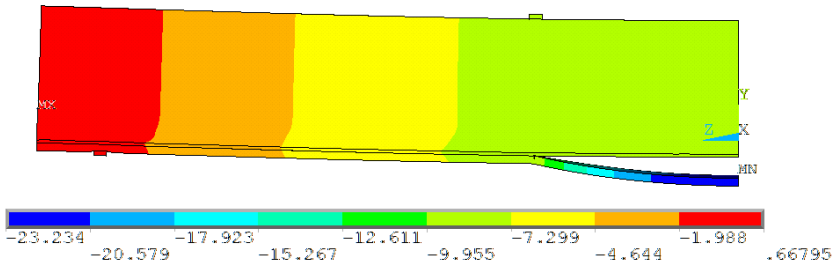

(b) Completion of debonding (after 7min of fire exposure)

Figure 5.31 Debonding of CFRP plate in Beam 5 (in mm)

Table 5.1 Comparison between the measured and predicted debonding occurrence, temperature at the steel reinforcement and deflection after 90min of testing.

Specimen	*FE Model*	*Debonding Occurrence (min)*		*Percentage Difference*	*Temperature at the steel after 90min(°C)*		*Percentage Difference*	*Deflection after 90min (mm)*		*Percentage Difference*
		Exp.	*FE*	*1-(Exp./FE)*	*Exp.*	*FE*	*1-(Exp./FE)*	*Exp.*	*FE*	*1-(Exp./FE)*
Beam 1	***FE B1***	-	-	-	-	-	-	42.5	41.1	-3.4
Beam 2	***FE B2***	-	-	-	-	-	-	26.0	26.0	0.0
Beam 3	***FE B3***	-	-	-	536.2	534.0	-0.4	56.0	53	-5.7
Beam 4	***FE B4***	-	-	-	547.5	540.5	-1.3	49.4	54	8.5
Beam 5	***FE B5***	7	7	0.0	560.0*	552.0	-1.4	54.0*	55	1.8
Beam 6	***FE B6***	38	37	-2.7	137.3	140.0	1.9	15.3	15	-2.0
Beam 7	***FE B7***	26	25	-4.0	212.8	209.1	-1.7	26.1	26.3	0.8
Beam 8	***FE B8***	39	42	7.1	493.0*	485.2	-1.6	32.0*	39.0	18.0
Beam 9	***FE B9***	18	19	5.2	466.4	455.0	-2.5	47.7	45.0	-6.0
Beam 10	***FE B10***	22	20	-9.5	419.5	416.0	-0.8	40.7	42.0	3.0

*Results were digitized from the experimental program.

5.5 Parametric Study Using the Validated FE Model of Williams et al. (2008) Experimental Program

After the developed FE achieved a good agreement with the experimental program, a parametric study is designed to further investigate several different parameters associated with the behavior of CFRP strengthened RC members under elevated temperatures. The designed parametric study investigate the effect of applying different fire curves and scenarios, different applied live load combinations as well as the effect of using different insulation schemes, types and thicknesses. The following subsections will discuss each part of the parametric study individually.

5.5.1 Effect of Different Fire Curves

The use of the ASTM E119 and/or ISO834 fire curves were exclusively used in most of the experimental program conducted so far. This section aims to study the effect of using different fire curves on the performance of the T-beams validated previously. The use of the ASTM E1529, RWS, Hydrocarbon Modified (HCM), Compartment fire 1 and 2 was implemented herein. As mentioned in Chapter Three, all of the ASTM E1529, RWS, Hydrocarbon Modified (HCM) are considered as standard fire curves used for different purposes i.e. petroleum and chemical industries, tunnels, etc. while, the compartment fire curves are those most likely to occur in buildings and follows a unique trend. Figure 5.32 shows the different fire curves used in this section. To show the variety of the available fire curves, it can be seen that the compartment fire curves were chosen to reach as higher temperatures than the standard ASTM E119 fire curve or more, have short durations in addition to a decaying period.

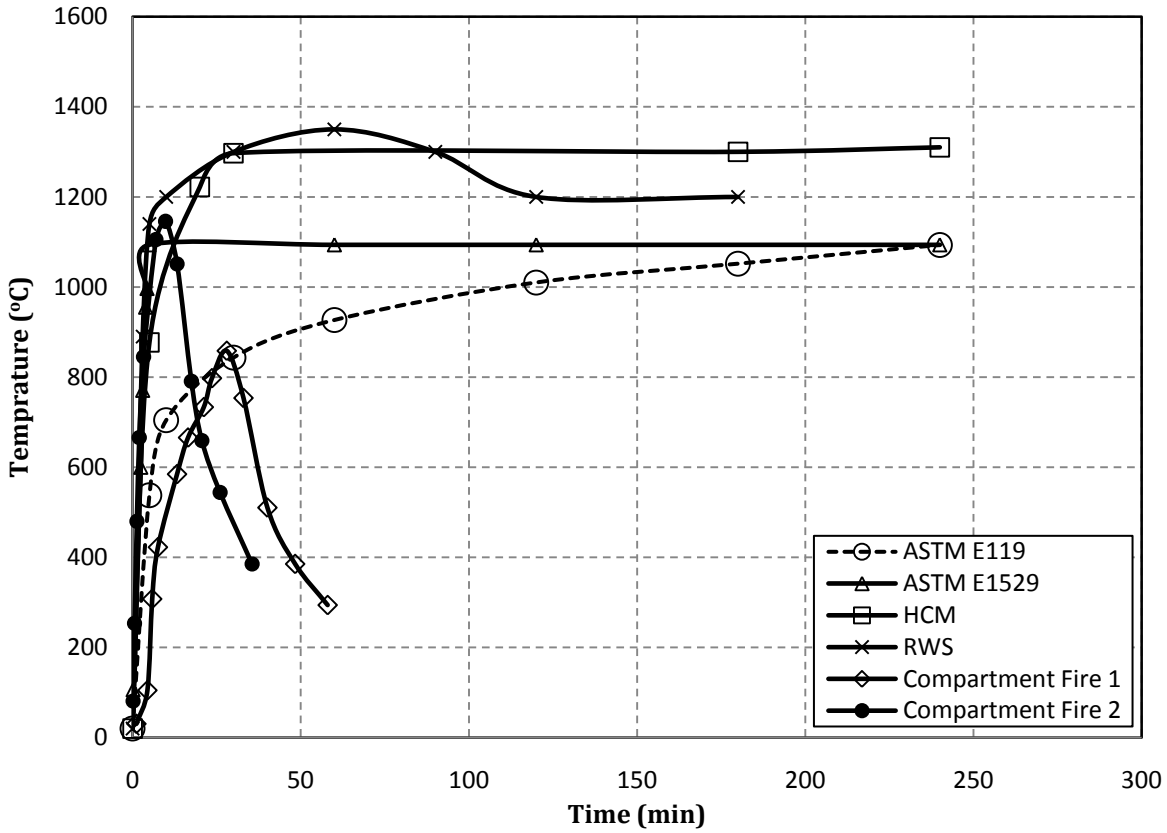

Figure 5.32 Different fire curves used in the parametric study

5.5.1.1 Thermal Response

The temperatures at the VG/CFRP and CFRP/Concrete are shown in Figs. 5.33 and 5.34, respectively. It can be seen that although the RWS fire curve is most severe fire curve compared to the other fire curves, the temperature at the interfaces of the model exposed to the HCM fire curve was the highest temperature. This is due to the fact that the RWS only lasts for 180min, while the HCM lasts for 240min. In addition, the RWS curve tends to decrease its temperature from 1350°C at 60min to 1200°C at 180min. Because of the short durations of the compartment fire curves, the temperatures at the interfaces seemed not to increase beyond 110°C. This implies that the duration of fire and its severity are the key parameters that should be considered in fire performance analysis and design of such structures.

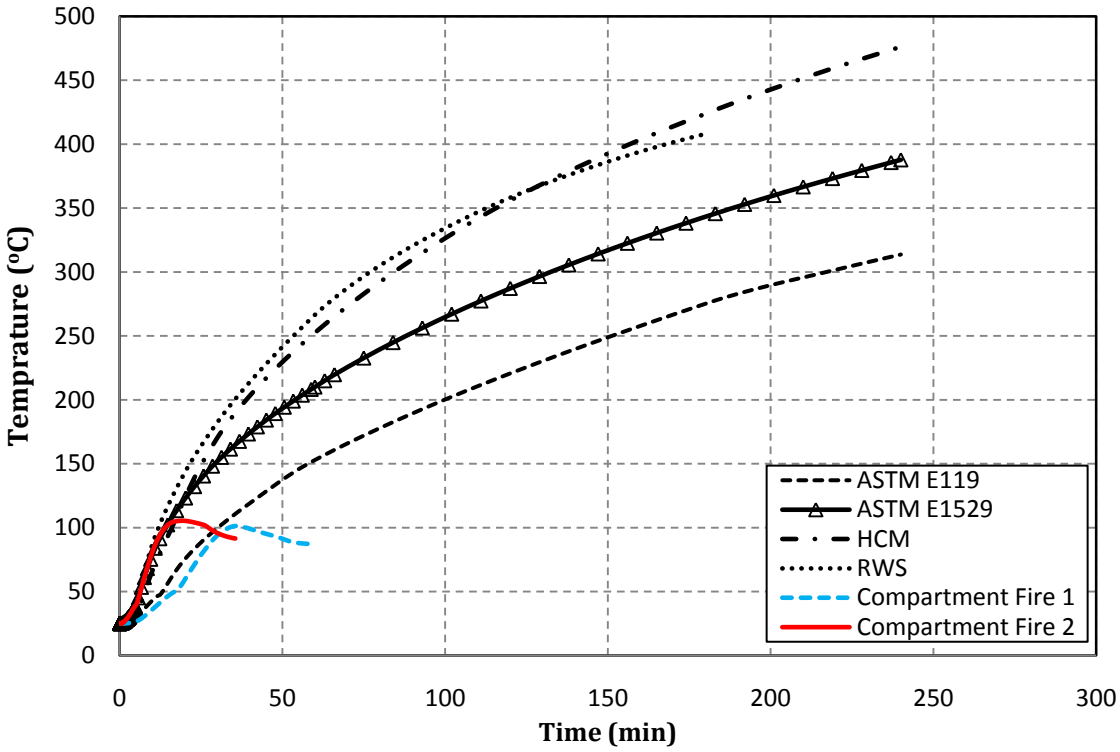

Figure 5.33 Temperature at the VG/CFRP interface for different fire curves

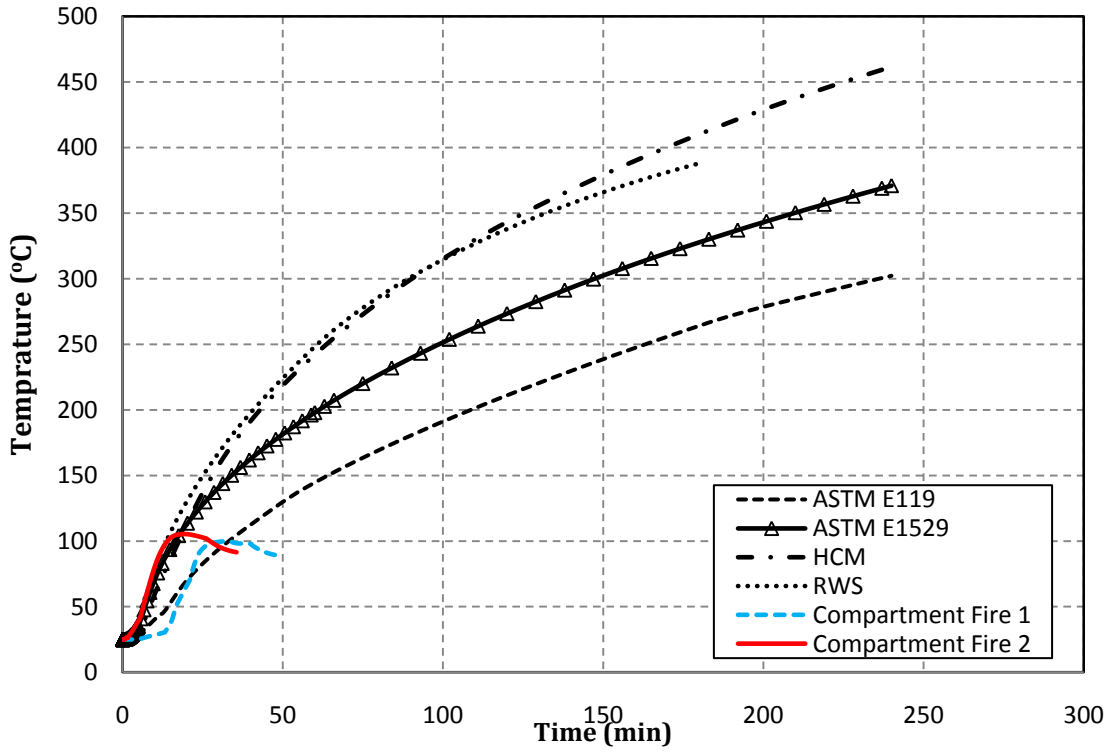

Figure 5.34 Temperature at the CFRP/Concrete interface for different fire curves

5.5.1.2 Structural Response

The structural response of the RC beam when exposed to the different fire curves was predicted by comparing the mid-span deflection with that of the ASTM E119 fire curve. As mentioned previously, the severe temperature exposure of both RWS and HCM led to the large increase in the mid-span deflection of the RC beam. The mid-span deflection of the specimen when exposed to the RWS and HCM was greater than the rest of the other fire exposures.

On the other hand, both compartment fire curves achieved the lowest mid-span deflections during the fire exposure, although they have the same peak temperature as of the ASTM E119 (Compartment Fire 1) or higher (Compartment Fire 2). This was mainly due to their short duration and presence of the decay period during the second phase of exposure. Figure 5.35 shows the mid-span deflection of the different models associated with the different fire curves used in this study.

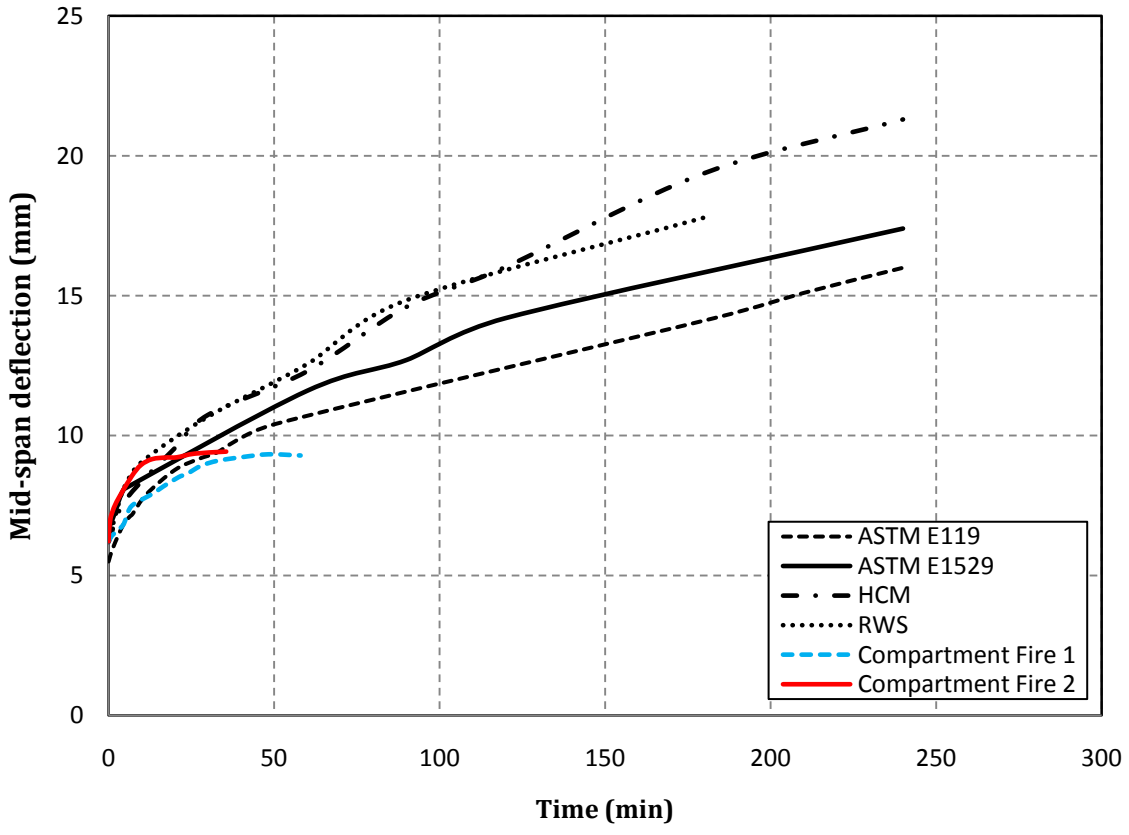

Figure 5.35 FE predicted mid-span deflection when exposed to elevated temperatures

The same developed failure criteria used previously to predict the time to failure of the validated T-beams are used herein. Table 5.2 shows the temperature and time to failure of the strengthened beams exposed to different fire curves.

Table 5.2 Fire performance of the RC beams subjected to different fire curves

	E119	***E1529***	***RWS***	***HCM***	***Comp. Fire 1***	***Comp. Fire 2***
Time to failure (min)	136	98	85	86	NF	NF
Temperature at failure (°C)	224	221	202	214	NF	NF

5.5.2 Effect of Different Fire Scenarios

This section discusses the effect of using different fire scenarios on the behavior of RC beam. The different fire scenarios are shown in Fig. 5.36. They were chosen as if the fire was localized on certain percentages of the span length of the T-beam. The span percentages are 5, 25, 50 and 90% of the beam's span. Such cases might occur in RC beams spanning between two rooms or apartments. Once fire initiated in a room, the soffit of the beam will be exposed to elevated temperatures while the rest of soffit; spanning to adjacent room with ambient temperature, will still experience ambient temperatures. Additional cases were chosen in which the fire is applied on the top flange of the RC beam and restraining the beams expansion/movement from both sides. The corresponding FE models associated with this section are called FE 5%, FE 25%, FE 50%, FE 90%, FE Top Fire and FE Restrained, respectively.

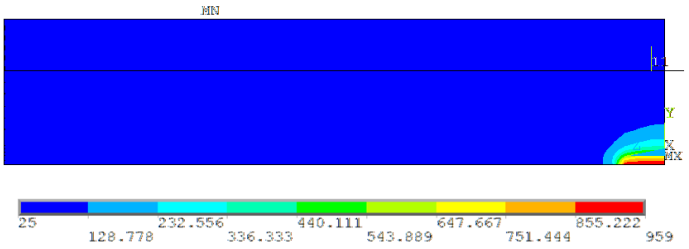

(a) 5% exposure

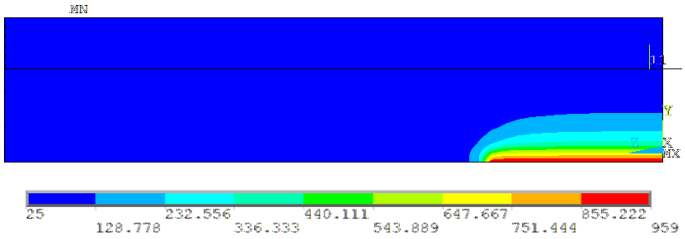

(b) 25% exposure

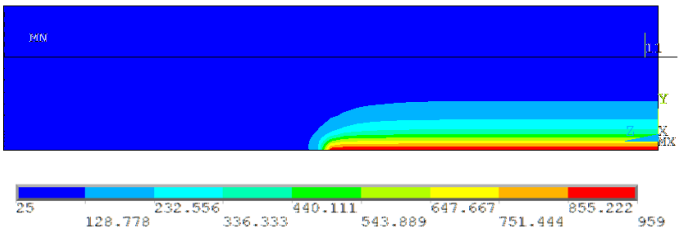

(c) 50% exposure

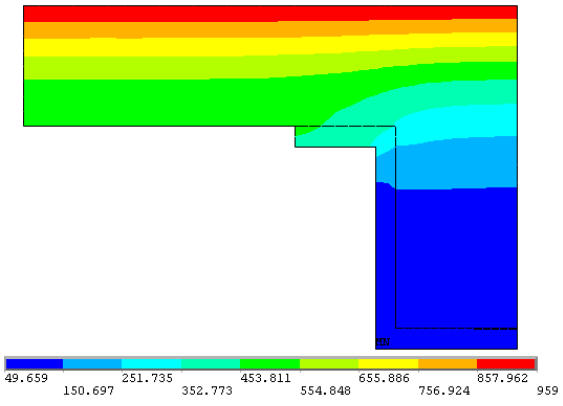

(d) Top fire

Figure 5.36 Temperature variation of different fire scenarios

5.5.2.1 Thermal Response

Figure 5.37 shows the temperature at the VG/CFRP interface for the different fire scenarios used herein. It can be seen that the temperature at the interface of both specimen exposed to the 50 and 90% are almost identical. On the other hand, the temperature at the same interface seems to reduce with smaller exposed percentages as shown in FE 25% and FE 5%. Furthermore, the temperature at the interface of the VG/CFRP of the model exposed to the ASTM E119 applied on the top flange seems to be very low compared to that of the FE 90% case. At the end of heating, the temperature at the interface was approximately 59.7°C.

Figure 5.38 provides the temperature at the VG/CFRP, CFRP/Concrete interfaces as well as at the steel rebars. The temperature at those locations was constant for the first 60min or so, and then started to increase. As expected, the temperature at the steel rebars is higher than those at the VG/CFRP, CFRP/Concrete interfaces since the fire temperature was applied from the top. In addition, the temperature at the VG/CFRP, CFRP/Concrete interfaces are very similar because they are located close to each other.

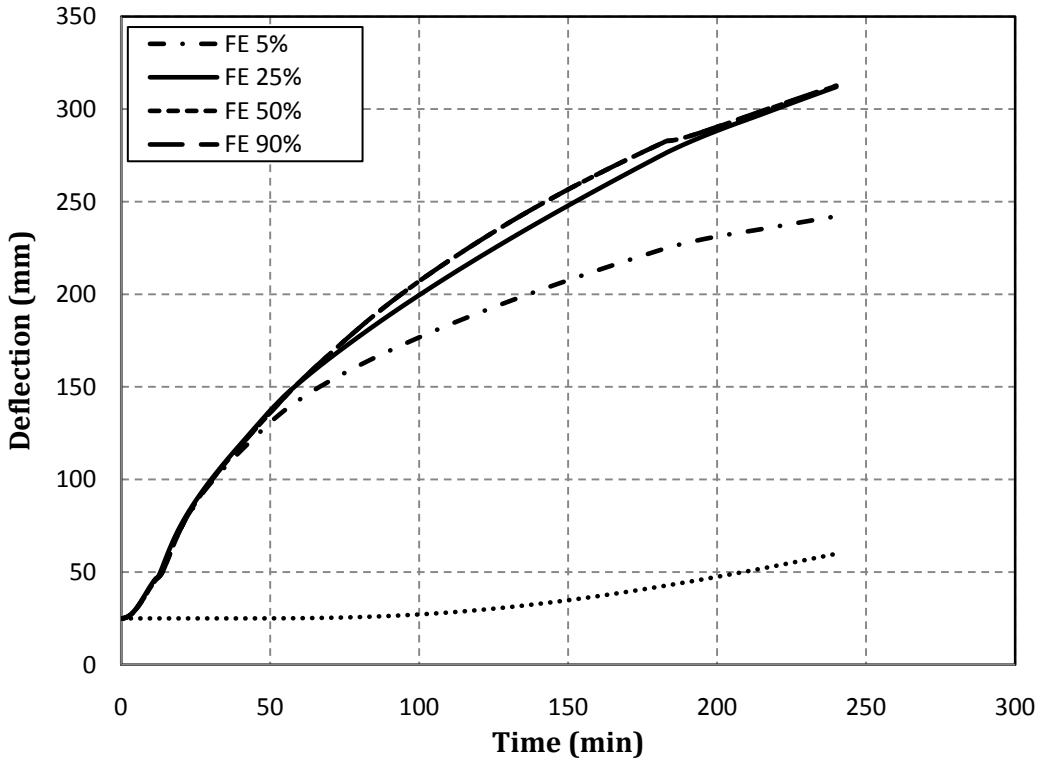

Figure 5.37 Temperature at the VG/CFRP interface

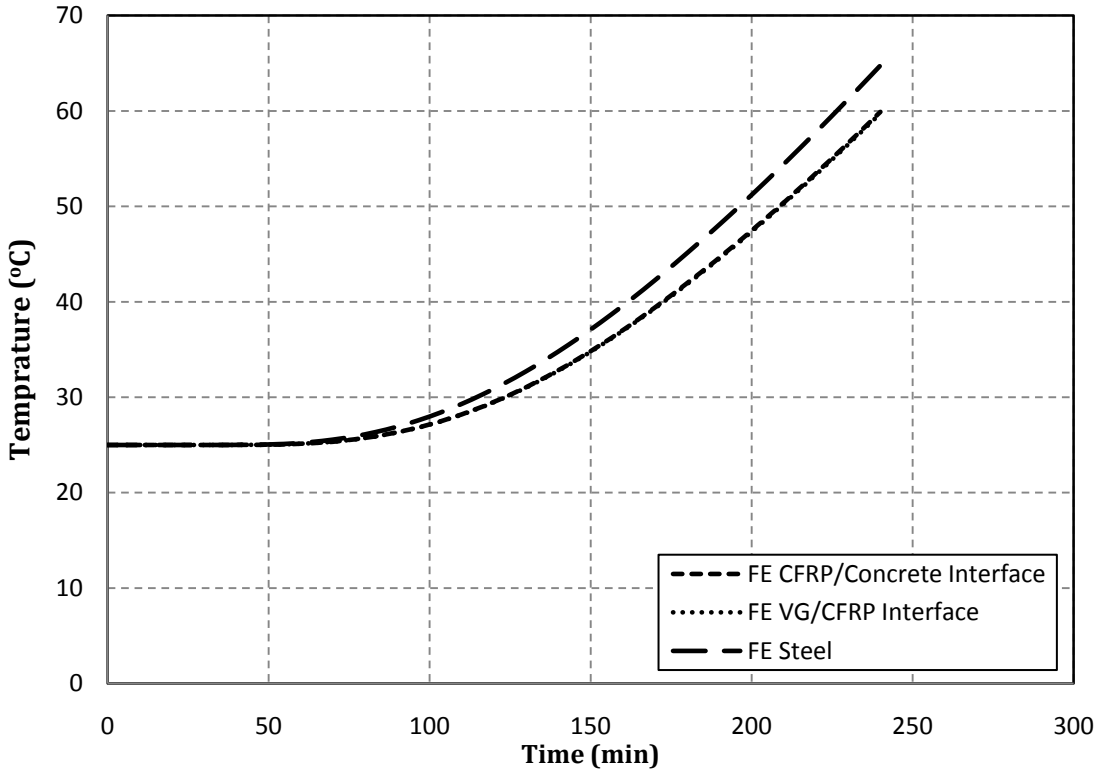

Figure 5.38 Temperature variation of the FE Top Fire model

5.5.2.2 Structural Response

The structural behavior of the specimen can be found in Fig. 5.39. Figure 5.39 shows the predicted mid-span deflection with time of the models exposed to different fire scenarios. It can be seen that the lower the exposed area to the temperature, the lower the mid-span deflection. This is because the smaller the exposed area to fire, the more the damage become localized and its effects barely affect the whole member. Furthermore, the camber effect is clearly seen in the case of FE Top Fire shown in Fig. 5.40. Basically, the camber effect is the result of heating the top fibres of the concrete beam, thus reducing its mechanical properties. Such reduction in the concrete strength and stiffness will shift the member's neutral axis downward which will result in reducing its mid-span deflection. The camber effect acts in a similar manner to pre-stressed concrete beams.

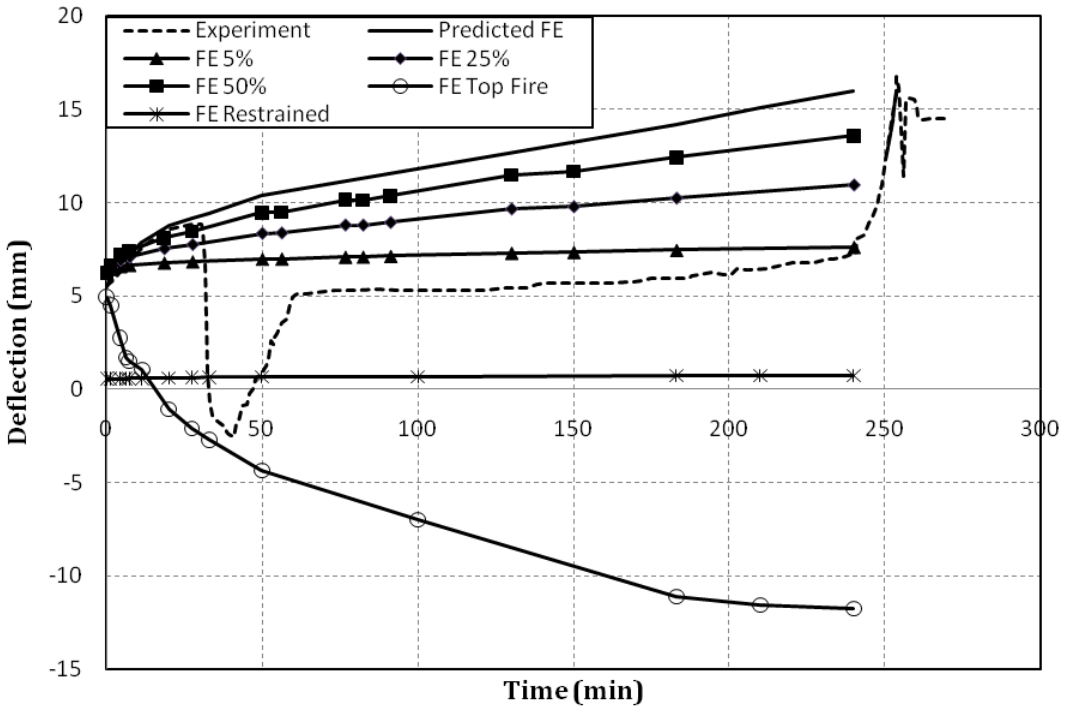

Figure 5.39 Comparison of the mid-span deflection with time of the models exposed to different fire scenarios

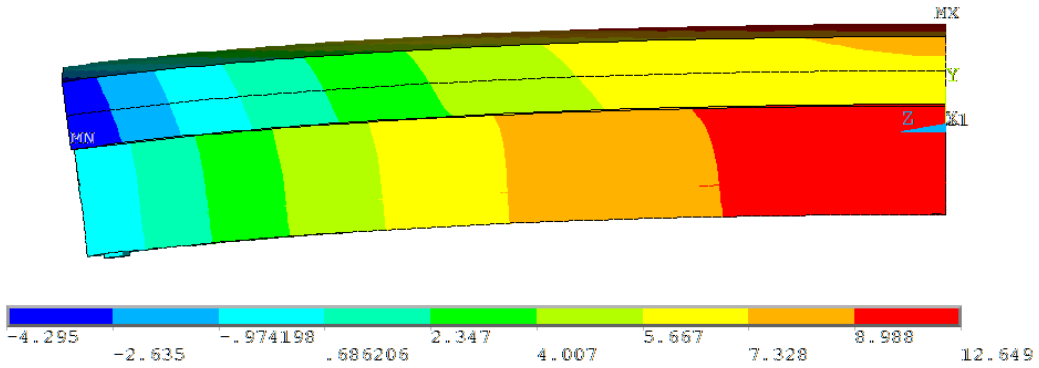

Figure 5.40 Camber effect shown in FE Top Fire model (in mm)

On the other hand, the failure mode of the two models in which the first was restrained from expansion and the other experienced fire from the top side was determined based on the strength approach. It should be noted that up to 4 hour fire exposure, either specimen failed due to the loss of the capacity in the CFRP plate.

5.5.3 Effect of Different Applied Live Load Levels

In order to investigate the performance of the tested beam under different applied load, a matrix was designed. The matrix consisted of four different applied loads. The applied loads were based on the service loads carried by the tested RC beam. The loads were varied to represent the presence of only self weight of the beam (0kPa), 25% increase in the live load (2.4kPa), 50% increase in the live load (4.8kPa), 60% increase in the live load (7.68kPa) and 75% increase in the live load (8.4kPa). The FE models associated with each case are designated, FE 00-LL, FE 25-LL, FE50-LL FE 60-LL and FE 75-LL, respectively. It should be noted that the tested beam was strengthened to a way to represent a 50% increase in the live load; hence this case is similar to the validated model.

5.5.3.1 Thermal Response

Since the FE thermal simulation does not acquire any structural inputs i.e. mechanical material properties or applied sustained loading, the response of the modeled beam did not change from that of the validated model. Please refer to Figs. 5.3, 5.4 and 5.6 to refer to the thermal response of the FE models.

5.5.3.2 Structural Response

Nevertheless, the structural response is shown in Fig. 5.41. Figure 5.41 shows the mid-span deflection versus time. Since the model FE 00-LL did not carry any live loads, its mid-span deflection started very close to zero, unlike the rest of the models which they experienced larger deflections with the increase of the applied live load. Furthermore, the shape of the mid-span deflection of specimen FE 00-LL is different than the rest, in which it starts by a linear increase rather than a parabolic increase. This is mainly due to the flexibility of the RC beam since it does carry and external loading loads.

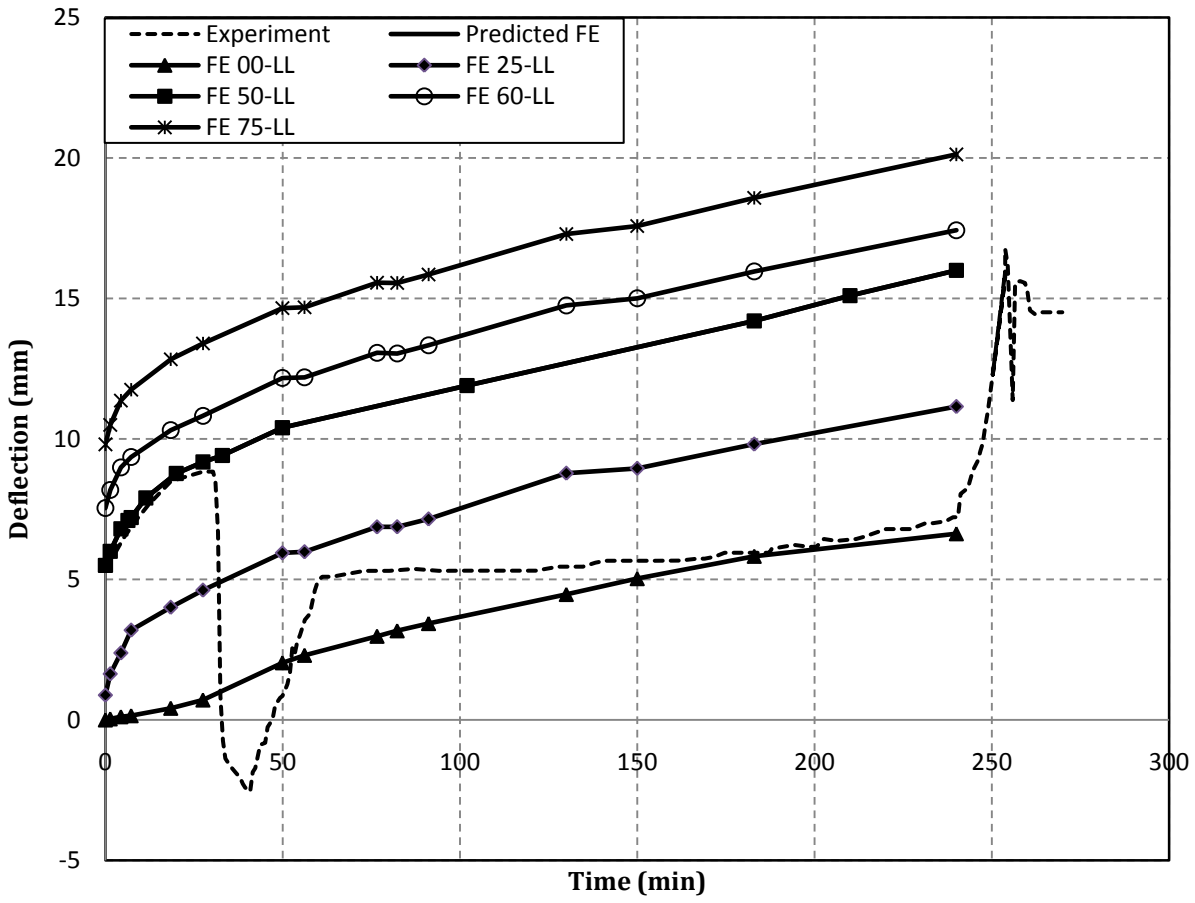

Figure 5.41 Mid-span deflection of the models with different applied live loads

The failure of the different specimens was based on the strength approach discussed earlier. Figures 5.42 and 5.43 show the predicted axial stresses in the CFRP plate and that available in the CFRP material. It is clearly shown that model FE 00-LL did not fail up to 4 hours from the fire exposure. This is because the axial stress in the CFRP plate did not reach the degraded strength of CFRP material. Hence, a defined critical temperature for the CFRP material must be defined. Table 5.3 shows the predicted time and temperature at failure of each of the models. It is clear now that the higher the applied loads, the shorter the fire endurance the beam experience.

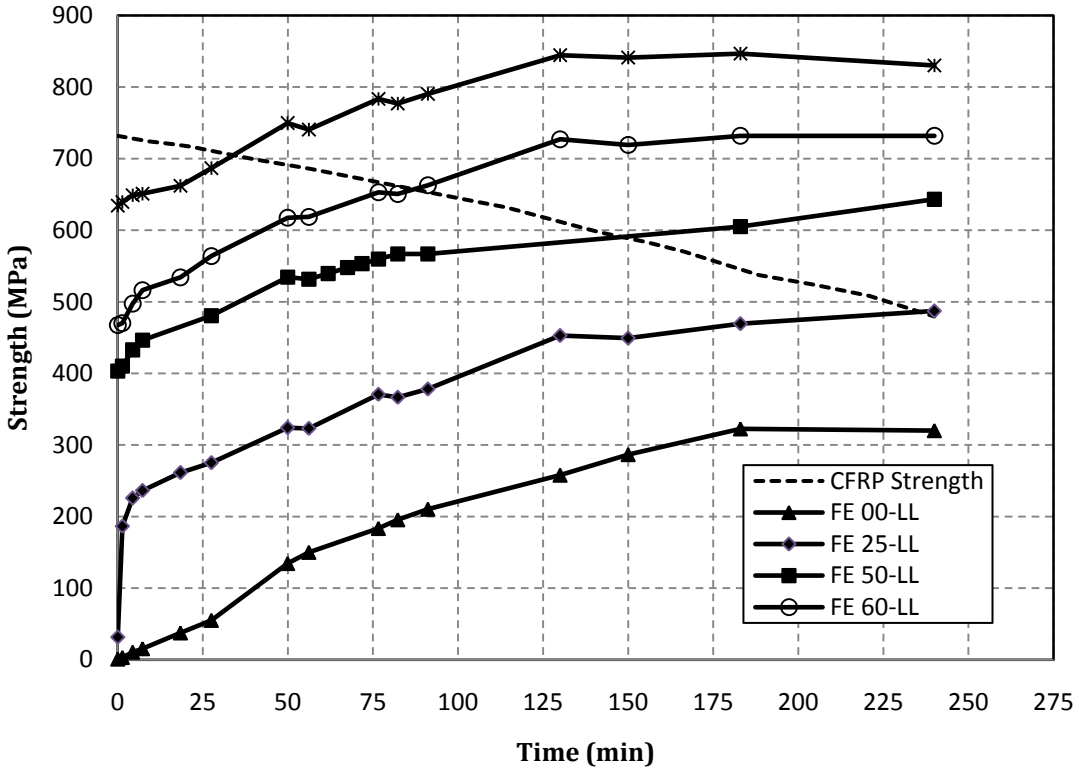

Figure 5.42 FE prediction of the time to failure

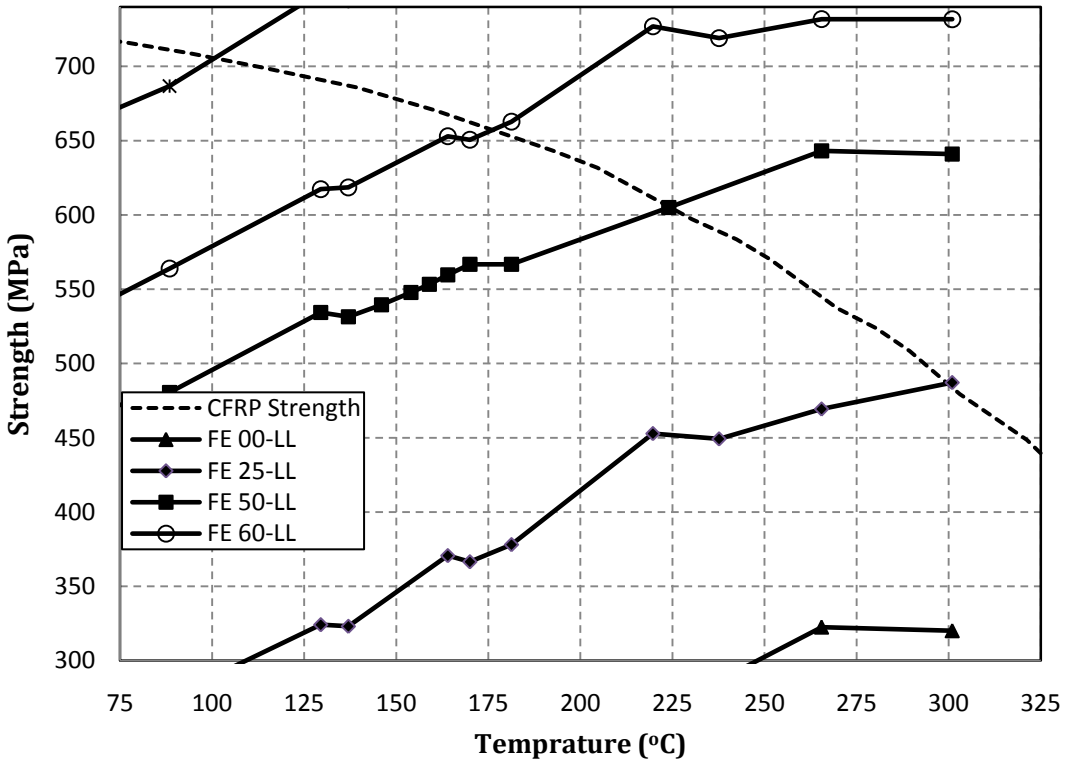

Figure 5.43 FE prediction of the temperature at failure

Table 5.3 Fire performance of the RC beams subjected to different applied live load levels

	FE 00-LL	*FE 25-LL*	*FE 50-LL*	*FE 60-LL*	*FE 75-LL*
Time to failure (min)	>240	240	136	87	33
Temperature at failure (°C)	NA	300	224	177	105

5.5.4 Effect of Different Insulation Schemes, Types and Thicknesses

The use of insulation materials was proved to be very important for the CFRP strengthened RC beam. This section investigates the different parameters involved in the insulation systems i.e. schemes, types and thicknesses. The developed matrix is composed of four FE models in which (FE Soffit) explore the insulation covering the web of the beam's soffit. The (FE PROMAGLAF) study the effect of insulation material types. Finally the last two models vary the insulation thickness between 35 and 50mm. The corresponding FE models are (FE 35mm) and (FE 50mm), respectively. The developed FE models for the parametric study were compared against the (FE Validation) validated FE model that has a 25mm thick VG insulating material wrapped in a U-Shape scheme.

5.5.4.1 Thermal Response

The thermal response of the developed FE models can be found in Fig. 5.44. It is clearly shown that the temperature at the CFRP/Concrete interface dropped with the use of thicker insulations. On a similar manner, the temperature at CFRP/Concrete interface of the FE model that used PROMAGLAF insulation material performed better than VG insulation for the same insulation thickness. This is due to the better thermal properties of the PROMAGLAF insulation which can be found in Table 5.4.

Table 5.4 PROMAGLAF Insulation material properties

Property	***PROMAGLAF***
Density (Kg/m^3)	100
Thermal Conductivity (W/m.K)	@ 200°C => 0.06 @ 400°C => 0.10 @ 600°C => 0.14 @1000 => 0.20
Specific heat (kJ/Kg.K)	1.13

On the other hand, the FE model in which the thermal insulation was only applied to the soffit of the beam; FE Soffit, faced rapid increase in the temperature at the same interface which concludes that the use of U-Shape wrapped insulation is better. This is because the U-Shaped insulation will protect both the sides and soffit of the beam, unlike the insulation applied to the soffit of the beam.

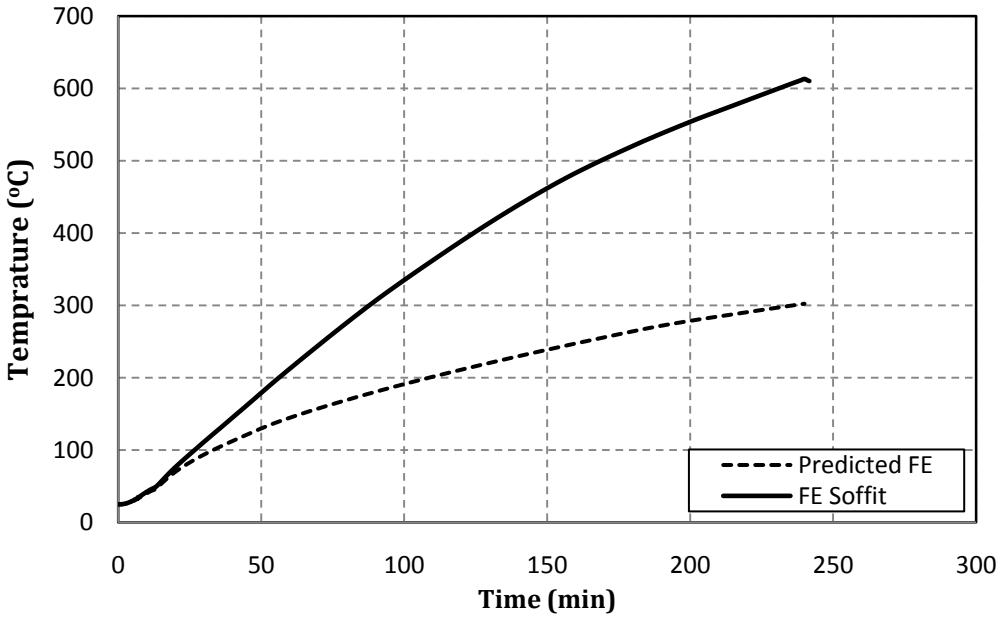

(a) Different insulation schemes

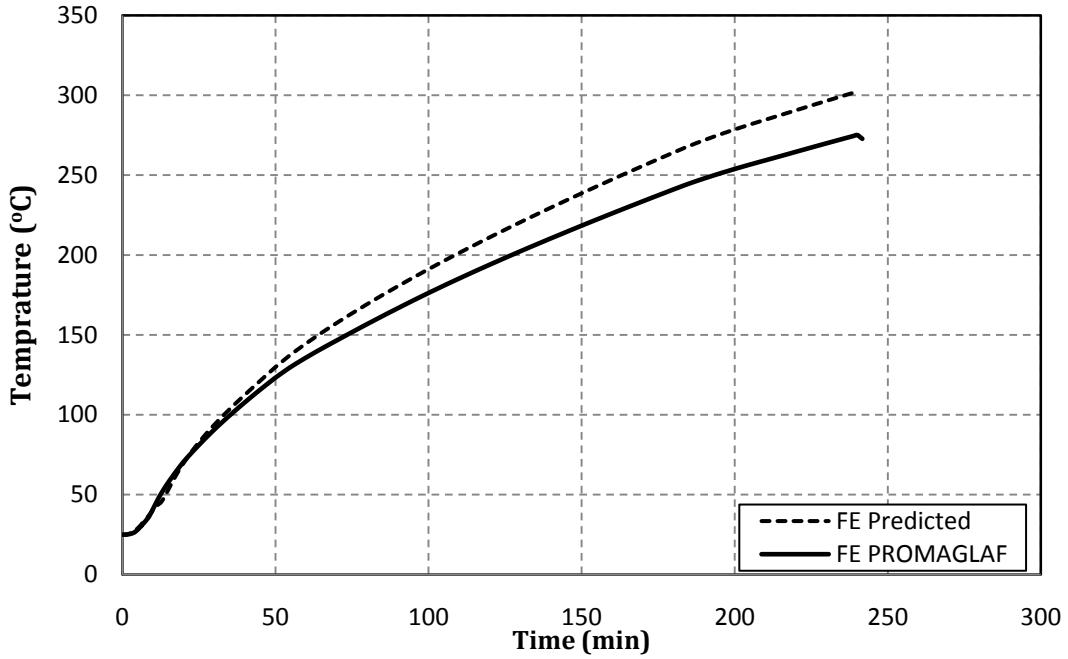

(b) Different insulation types

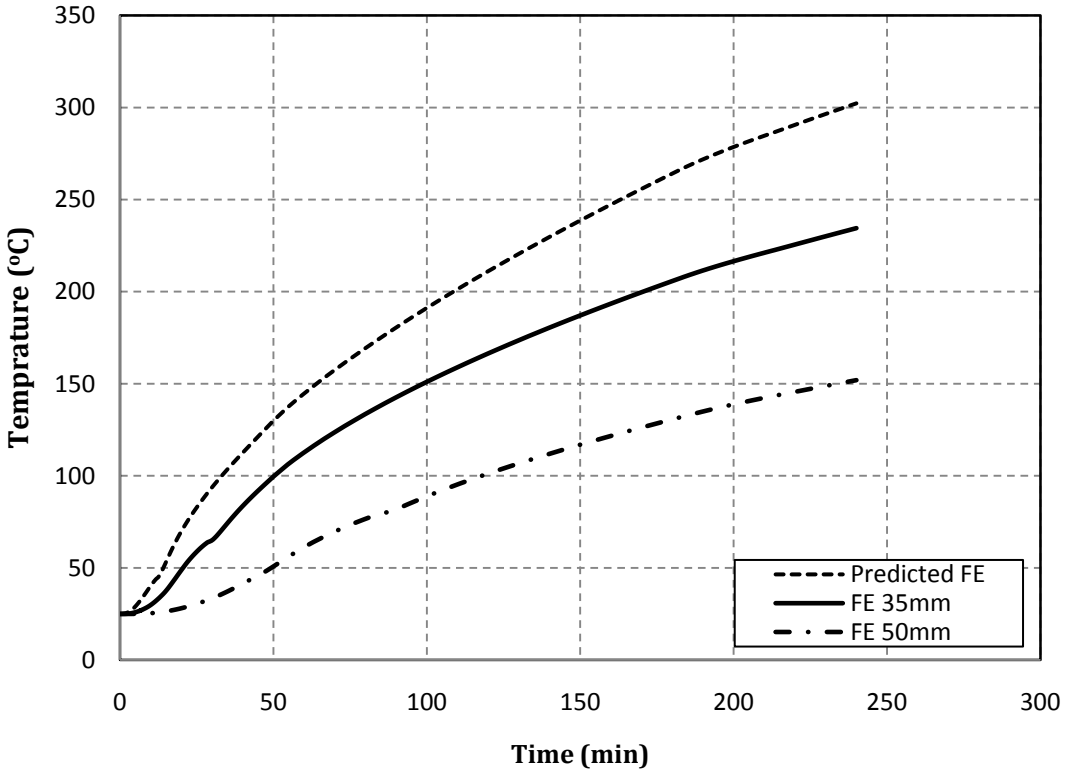

(c) Different insulation thickness

Figure 5.44 Thermal responses at the CFRP/Concrete interface of the different FE models

5.5.4.2 Structural Response

As mentioned earlier, the validation model had a 25mm thick VG insulation, installed in a U-Wrap shape. As expected, the structural response of the FE models insulated with thicker 35 and 50mm insulation is better than that of the validation model. Furthermore, the response of the model that used PROMAGLAF insulation is also better than the validation model. The only case where the performance dropped was shown in the FE Soffit.

It is the absence of the insulation on the web's sides that led the temperature to rapidly increase across the member which led to early failure of the CFRP plate attached to the RC beam. Figure 5.45 shows the mid-span deflection of different cases studied herein.

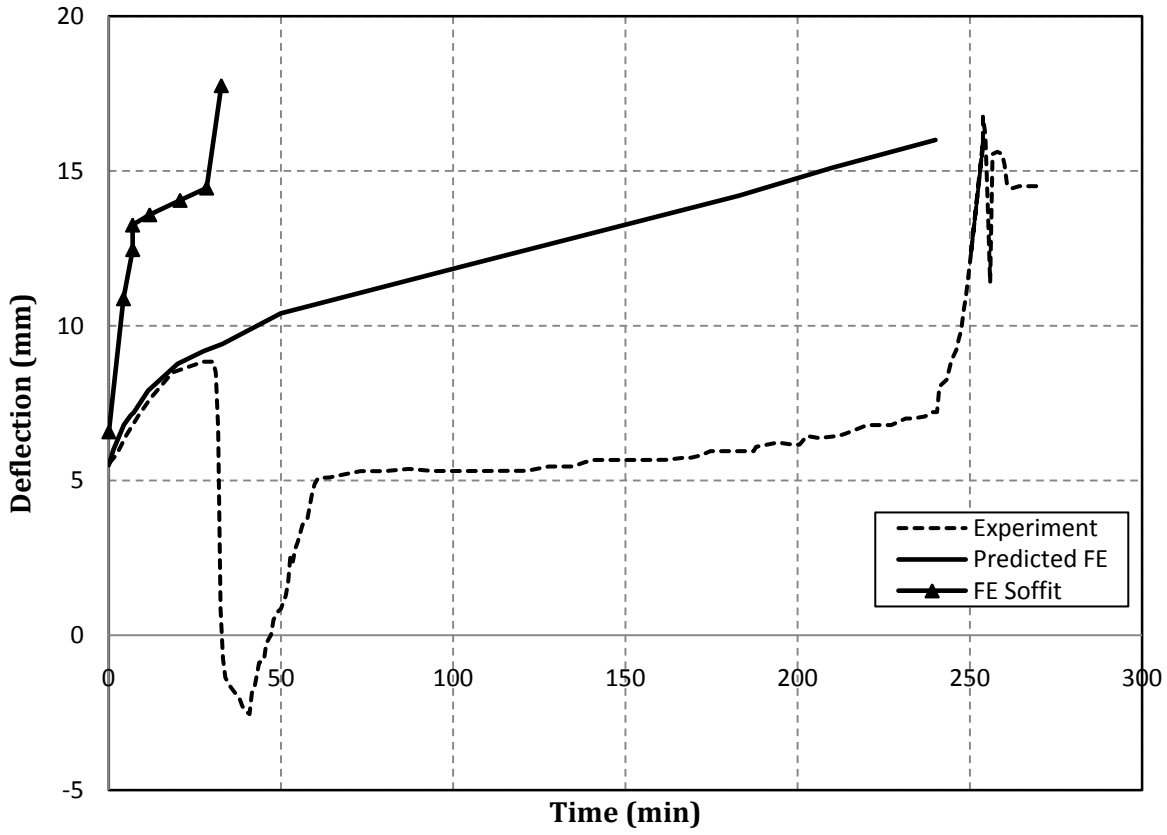

(a) Different insulation schemes

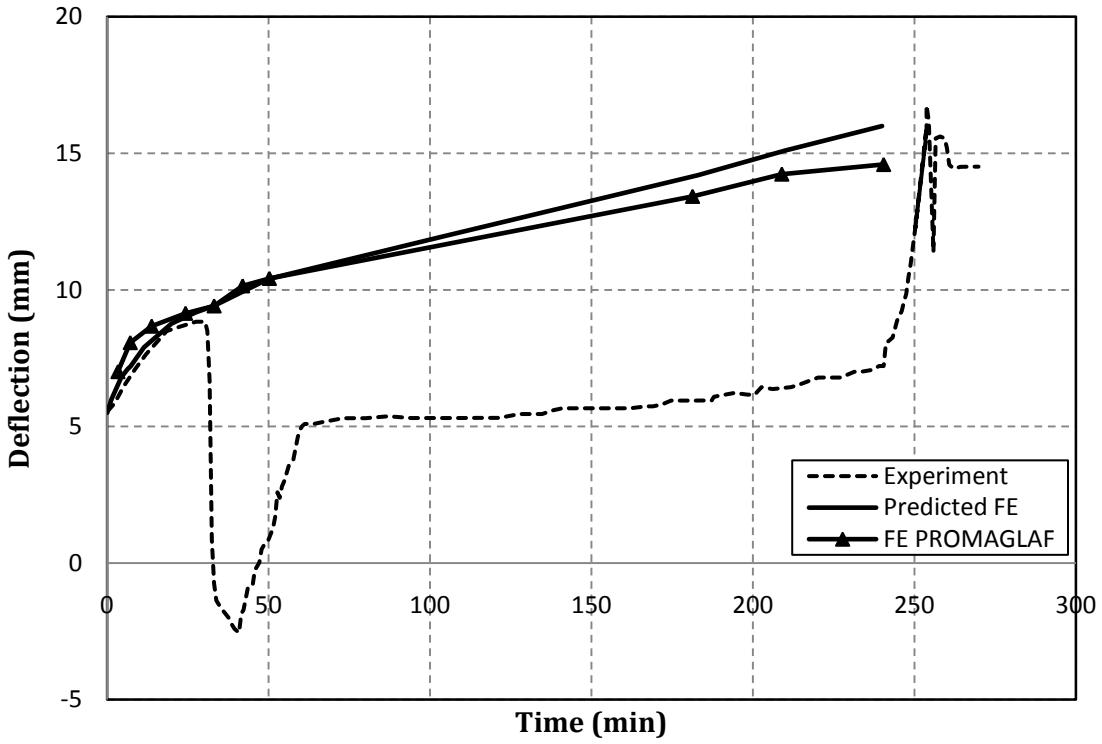

(b) Different insulation types

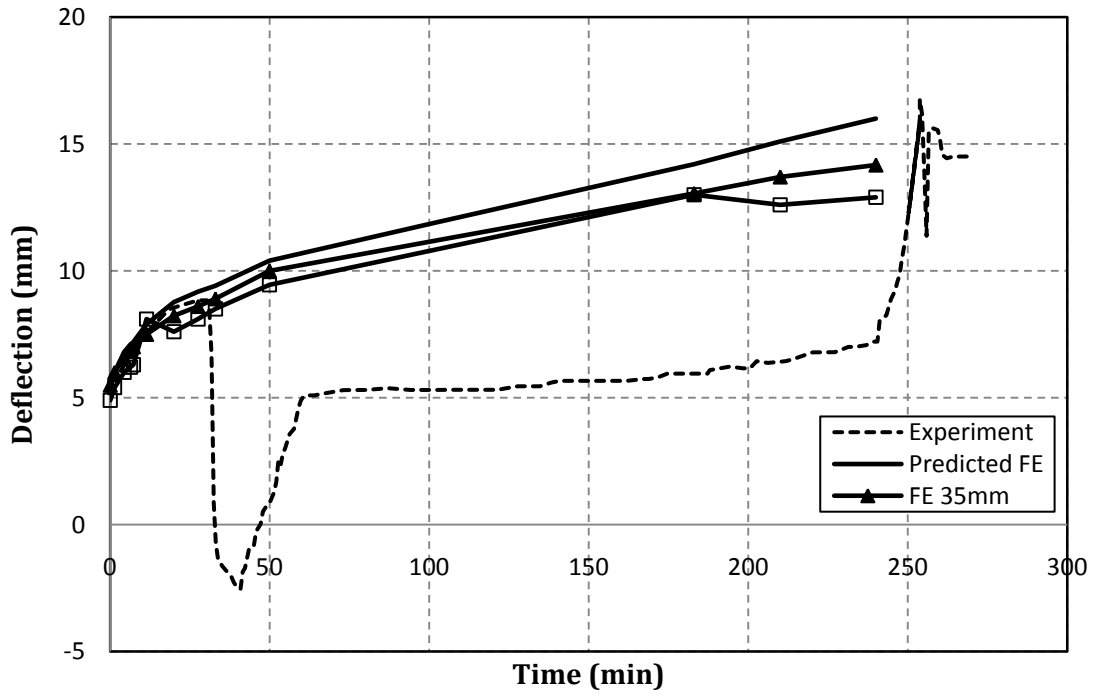

(c) Different insulation thickness

Figure 5.45 Structural responses of the different FE models

Specimen FE 50mm, FE 35mm and FE PROMAGLAF took 144, 140 and 137 min, respectively to fail. On the other hand, FE Soffit failed very maturely at approximately 18min. In addition, the FE model predicts the temperature at the CFRP/Concrete interface of FE 35mm, FE PROMAGLAF and FE Soffit to be 202, 217 and 309°C, respectively.

5.5.5 Proposed Chart for Different Insulation Thicknesses

This section provides further discussion on the use of different insulation thicknesses on the thermal response of the simulated T-beam. Multiple thermal simulations were carried out in this section to provide a further insight on the thermal performance of the tested beams using different insulation thicknesses. Twenty-nine different insulation thicknesses were chosen, starting from 10 to 40mm in a 2.5mm increment, then continued up to 125mm in 5mm increment. It should be noted that the presented results in this section were purely based on thermal analysis of the validated FE model subjected to the ASTM E119. Furthermore, the thermal simulation was carried out up to two hours, since most structural elements are required; by standards and building codes, to have two hours fire endurance. The thermal simulation resulted in 116 data points which were used to develop a chart that can aid designers and engineers. In addition they can provide preliminary idea on the temperature at the CFRP/Concrete interface when different insulation thicknesses are used.

Such chart can be used according to designers' critical temperature i.e. the critical temperature at the CFRP/Concrete interface is up to the designers' choice; hence the proposed chart was not based on any limiting temperatures. Simply, they provide rational sense to designers and engineers. A detailed example is provided at the end of the section.

Figure 5.46 shows the evolution of temperature at the CFRP/Concrete interface with time. The time increments were chosen to be 30min. It should be noted that the applied temperature-time curve for both thermal simulations in this sub-section is the ASTM E119.

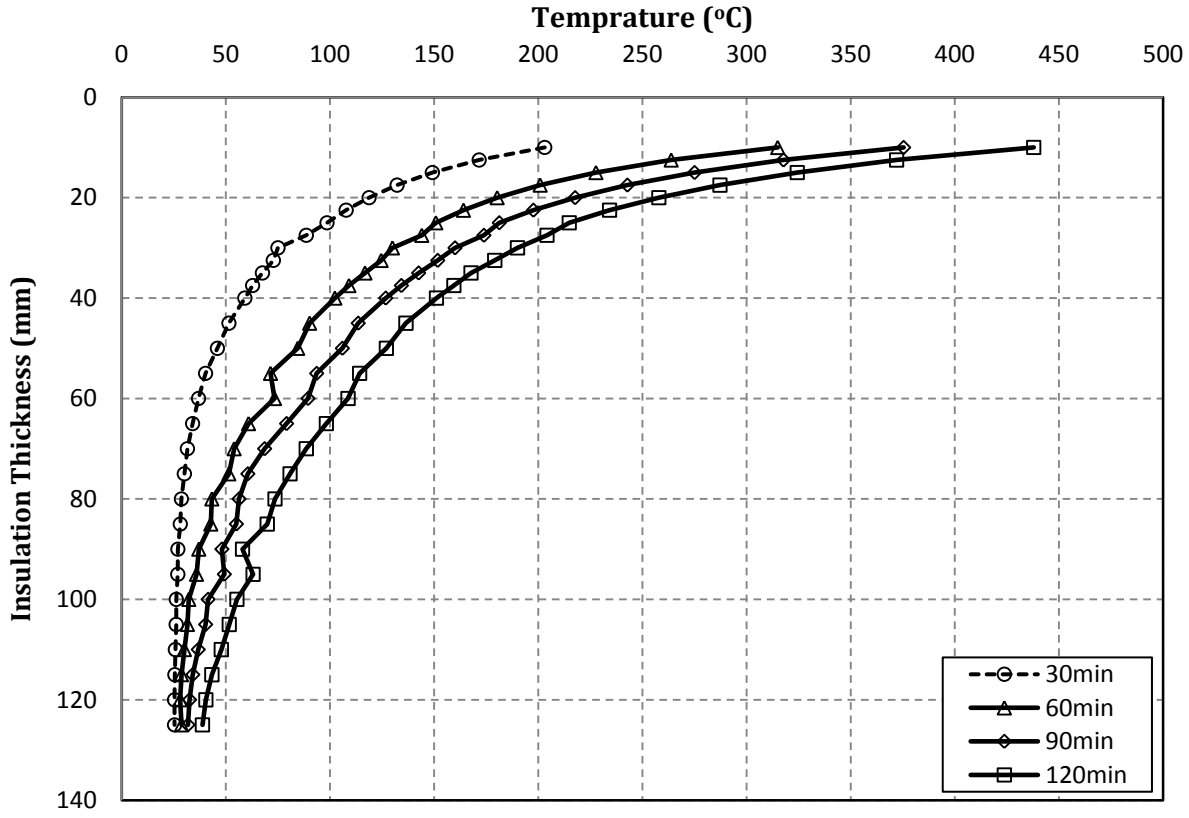

Figure 5.46 Evolution of temperature with time

In addition, it is clear that the temperature in the VG insulation rapidly increases up to the thickness of 40mm. However, it is observed that there is a threshold in which any increase of the insulation thickness does not seem to significantly change the temperature at the CFRP/Concrete interface. This thickness is found to be approximately 100mm for both materials.

Detailed Design Example:

Assuming that a designer needs to figure out the temperature at the CFRP/Concrete interface insulation using 20, 60 and 100mm VG insulation to a T-Beam exposed to the ASTM E119 fire curve. Table 5.5 shows the predicted temperature at the CFRP/Concrete interface with time.

Table 5.5 Predicted temperature at the CFRP/Concrete interface with time

	30 min	***60 min***	***90 min***	***120 min***
20mm	118.7	180.2	217.6	257.8
60mm	36.8	73.38	89.4	108.6

CHAPTER 6 CONCLUSION

6.1 Summary

A detailed Finite Element model is developed in this numerical study to investigate the performance of strengthened RC beams with CFRP plates under fire loadings. The developed FE models were validated against the experimental programs of Williams et al. [**4**] and Blontrock et al. [**5**]. The validation process was based on both thermal and structural criteria i.e. temperature distribution at key points across the beam cross section, mid-span deflection response, and time to failure. Up to date, these two programs are considered to be the most comprehensive experimental studies conducted on the behavior of strengthened RC beams exposed to fire loading. Full scale fire testing of RC beams strengthened with CFRP plates and insulated using special protection systems were tested in the referred experimental programs.

This study developed a FE model that can accurately predict the behavior of strengthened RC beams. This was shown by the good correlation achieved between the measured and predicted results. Upon the good validation, a parametric study was conducted to investigate the effect of different fire curves and scenarios, different sustained loads levels and different insulating materials, schemes and thickness.

6.2 Conclusions

The following conclusions could be drawn from the results of the numerical study conducted herein:

1. Good correlation was obtained between the experimental and predicted results (both thermal and structural) at all stages of the fire loading up to failure of the tested specimens.

2. The developed models would be used as alternative to the time consuming and very expensive fire testing, especially in design oriented parametric studies.

3. The FE models used to simulate Blontrock et al. [**5**]. were able to predict debonding at the CFRP/concrete interface during the fire exposure.

4. The FE modeling can be a great tool to aid designers and researchers in the process of investigating the different aspects of the structural fire engineering. In addition, FE simulation well controlled environment can be used in a new technique to alternative, costly and time consuming experimental programs.

5. The FE modeling can provide full field of results, in terms of temperature distribution, mechanical stresses, deflections, and investigation of the failure modes.

6. The temperature variation with time is highly dependent on the fire exposure scenario.

7. The type of fire scenario plays a critical role on the fire performance of concrete beams and should be considered in both analysis and design.

8. Severe fire curves i.e. HCM and RWS produce larger mid-span deflections and damage to the FRP system compared to both standard building and compartment fire curves presented herein.

9. The mid-span deflection increases during the fire exposure for most of the studied cases presented herein, except when the fire was applied to the top fibres of the beams.

10. The mid-span deflection increases as the applied local fire exposure area increases.

11. The use of U-Wrap insulation enhances the fire endurance of the insulated, strengthened beams. On the other hand, the use of insulating materials attached to the soffit of the beam would compromise the strengthening system.

12. Mid-span deflection usually decreases with the increase of insulation thickness.

13. The developed chart might serve as a good tool to predict the temperature at the FRP/Concrete interface.

REFERENCES

[1] ACI, Building code requirements for structural concrete ACI-318-05, 2005.

[2] Luke Alexander Bisby, *Fire Behaviour of Fibre-Reinforced Polymer (FRP) Reinforced or Confiend Concrete*. 2003.

[3] J. Barros and J. Figueiras, "Model for the analysis of steel fibre reinforced concrete slabs on grade," vol. 79, no. 1, pp. 97-106, 2001.

[4] B. Williams, V. Kodur, M. Green, and L. Bisby, "Fire Endurance of Fiber-Reinforced Polymer Strengthened Concrete T-Beams," *J ACI Structural* , vol. 105, no. 1, pp. 60-67, 2008.

[5] H. Blontrock, L. Taerwe, and P. Vandevelde, "Fire Tests on Concrete Beams Strengthened with Fibre Compasite Laminates.," in *Third PhD Symposium.*, Vienna, Austria, 2000, p. 10.

[6] Ershad Ullah Chowdhury, "Performance in Fire of Reinforced Concrete T-Beams Strengthened with Externally Bonded Fibre Reinforced Polymer Sheets," *Queen's University*, 2005.

[7] United States of America. Federal Highway Administration FHWA, *Status of the Nation's Highways, Bridges, and Transit: 2004 Conditions and Performance*, 2004.

[8] H. GangaRao, T. Narendra, and P. Vijay, *Reinforced Concrete Design with FRP Composites*.: CRC Press, 2007.

[9] L.C. Hollaway, "Polymer, fibre, and composite material properties and manufacturing techniques.," in *In Polymers and Polymer Composites in Construction,*.London, England, 1990, pp. 5-29.

[10] R.M. Jones, *Mechanics of Composite Materials*. Washington, D.C.: Scripta Book

Company (Taylor and Francis), 1975.

[11] Y.A. Cengel, *Heat Transfer: A Practical Approach.*: WCB/McGraw-Hill, 1998.

[12] H. Blontrock, L. Taerwe, and S. Matthys, "Properties of Fiber Reinforced Plastics at Elevated Temperatures with Regard to Fire Resistance of Reinforced Concrete Members.," in *In Fibre Reinforced Polymer Reinforcement for Reinforced Concrete Structures.*, Detroit, Michigan, 1999, pp. 43-54.

[13] T. Uomoto, "Durability considerations for FRP reinforcements.," in *In The Fifth Annual Symposium on Fibre-Reinforced-Plastic Reinforcement for Concrete Structures (FRPRCS-5).* , London, England, 2001, pp. 17-32.

[14] A. Braimah, *Long-term and fatigue behaviour of carbon fibre reinforced polymer prestressed concrete beams.*: Department of Civil Engineering, Queen's University, Kingston, Ontario., 2000.

[15] U. Meier, "Rehabilitation of Concrete Structures with the CFRP Sheet Bonding Technique," in *Proceedings of Advancing with Composites '94: Materials and Technologies, Vol. 1, May 3-5th*, Milan, Italy, 1994, pp. 169-181.

[16] L. De Lorenzis and J. Teng, "Near-surface mounted FRP reinforcement: an emerging technique for strengthening structures.," *J Compos, Part B*, vol. 38, pp. 119–43., 2007.

[17] S. Smith and J. Teng, "FRP-strengthened RC beams. I: review of debonding strength models.," *Eng Struct* , vol. 24, no. 4, pp. 385–95., 2002.

[18] S. Smith and J. Teng, "FRP-strengthened RC beams. II: assessment of debonding strength models. ," *Eng Struct*, vol. 24, no. 4, pp. 397–417., 2002.

[19] S. Asplund, "Strengthening bridge slabs with grouted reinforcement," *J Am Concr Inst* , vol. 20, no. 6, pp. 397-406, 1949.

[20] O. Buyukozturk, B. Hearing, and O. Gunes, "FRP strengthening and repair: where do we go from here? Structural Faults and Repair," in *Proceedings of the 8th international*

conference on extending the life of bridges, civil, and building infrastructure, London, England, 1999, p. 12.

[21] T.T. Lie, "Structural Fire Protection," American Society of Civil Engineers Manuals and Reports on Engineering Practice No. 78. 1992. ASCE, New York, NY.

[22] U. Schneider, "Modelling of Concrete Behaviour at High Temperatures. ," *In Design of Structures Against Fire.* , pp. 53-70, 1986.

[23] Eurocode, "Eurocode 2, Design of Concrete Structures, ENV EC2 Part 1.2.," Eurocode, 2004.

[24] P.K. Mallick, *Fibre-Reinforced Composites: Materials, Manufacturing, and Design.* New York, NY.: Marcel Dekker Inc., 1988.

[25] G. Cooke, "An introduction to the mechanical properties of structural steel at elevated temperatures.," *Fire Safety Journal*, vol. 13, pp. 45-54, 1988.

[26] Y. Anderberg, "Properties of Materials at High Temperatures-Steel, RILEM," University of Lund, Sweden., 1983.

[27] J. Purkiss, *Fire Safety Engineering Design of Structures,* 2nd ed.: Butterworth-Heinemann, 2007.

[28] T.Z. Harmathy, "A Comprehensive Creep Model.," *Journal of Basic Engineering*, vol. 89, 1967.

[29] A. Buchanan, *Structural Design for Fire Safety*. England: John Wiley & Sons Ltd., 2001.

[30] M. Fardis and H. Khalili, "FRP-encased concrete as a structural material.," *Magazine of Concrete Research*, vol. 34, no. 121, pp. 191-202, 1982.

[31] C.E. Bakis, "FRP Reinforcement: Materials and Manufacturing, Fiber-Reinforced-Plastic (FRP) Reinforcements for Concrete Structures: Properties and Applications," pp. 13-58, 1993.

[32] L. Bank, "Properties of FRP Reinforcements for Concrete," Fibre-Reinforced-Plastic (FRP) Reinforcements for Concrete Structures: Properties and Applications," pp. 59-86, 1993.

[33] Y. Uematsu, T. Kitamura, and R. Ohtani, "Delamination of a Carbon-Fibre-Reinforced Thermoplastic Polymer at High Temperatures," *Composites Science and Technology*, vol. 53, pp. 333-341, 1995.

[34] Y. Dimitrienko, *Thermomechanics of Composites under High Temperatures*. London, UK: Kluwer Academic Publishers, 1999.

[35] T. Fujisaki, T. Nakatsuji, and M. Sugita, "Research and Development of Grid Shaped FRP Reinforcement," in *International Symposium on Fiber Reinforced Polymer Reinforcement for Reinforced Concrete Structures*, Detroit, Michigan, 1993.

[36] V. Kodur and D. Baingo, "Fire Resistance of FRP Reinforced Concrete Slabs," National Research Council of Canada, Ottawa, Ontario, IRC Internal Report No. 758 1998.

[37] A. Ahmed and V. Kodur, "Effect of bond degradation on fire resistance of FRP-strengthened reinforced," *Composites Part B: Engineering*, vol. 42, no. 2, pp. 226-237, 2011.

[38] C. Griffis, R. Masmura, and C. Chang, "Thermal response of graphite epoxy composite subjected to rapid heating," *In Environmental Effects on Composite Materials*, vol. 2, pp. 245-260, 1984.

[39] G.L. Nelson, "Fire and Polymers: An Overview.," in *Fire and Polymers II: Materials and Tests for Hazard Prevention. American Chemical Society Symposium Series 599*, Washington, DC., 1995, pp. 1-26.

[40] K. Neale and P. labossière, in *Proceedings of the First International Conference on Advanced Composite Materials in Bridges and Structures*, Sherbrooke, Quebec., p. 1992.

[41] F. Apicella and M. Imbrogno, "Fire performance of CFRP-composites used for repairing and strengthening concrete," in *In Materials and Construction: Exploring the Connection.*

Proc. 5th ASCE Materials Engineering Congress, Cincinnati, OH, 1999, pp. 260-266.

[42] A. Katz, N. Berman, and L. Bank, "Effect High Temperature on the Bond Strength of FRP Rebars," *Journal of Composites for Construction, ASCE*, vol. 3, no. 2, pp. 73-81, 1999.

[43] A. Sumida, T. Fujisaki, K. Watanabe, and T. 2001.. Edited by C. Burgoyne, Thom Kato, "Heat Resistance of Continuous Fiber Reinforced Plastic Rods," in *In The Fifth Annual Symposium on Fibre-Reinforced-Plastic Reinforcement for Concrete Structures (FRPRCS-5)*, London, 2001, pp. 557-565.

[44] Rockwool (n.d.). (2011, March) Advantages of Rockwool Products. [Online]. "http://www.rockwool.ru/sw5200.asp" http://www.rockwool.ru/sw5200.asp

[45] Fiberfrax (n.d.). (2011, March) Fiberfrax: Woven and Non-Woven Materials for High Temperature Insulation, Sealing and Filtering Applications. [Online]. "http://www.fiberfrax.com/" \l "Fiberfrax-1" http://www.fiberfrax.com/#Fiberfrax-1

[46] Isolatek (n.d.). (2011, March) Spray-Applied Fire Resistive Materials. [Online]. "http://www.isolatek.com/category_search.asp?categoryID=1" http://www.isolatek.com/category_search.asp?categoryID=1

[47] Underwriters Laboratories (n.d.). (2010, June) The Significance of the UL Classification Mark on Intumescent Coatings. [Online]. http://www.ul.com/regulators/coating.html" http://www.ul.com/regulators/coating.html

[48] M. Deuring, "Brandversuche an Nachtraglich Verstarkten Tragern aus Beton," Swiss Federal Laboratories for Materials Testing and Research, Dubendorf, Switzerland., Research Report EMPA No. 148’795, 1994.

[49] ASTM, Standard Test Methods for Fire Tests of Building Construction and Materials, ASTM Standard E119, 2002, American Society for Testing of Materials, West Conshohocken, PA.

[50] L. Bisby, M. Green, and P. Burke, "Structural Performance of Near Surface Mounted FRP

Strengthened Concrete Slabs al Elevated Tempratures," 2008.

[51] M. Yaqub and C. Bailey, "Cross sectional shape effects on the performance of post-heated reinforced concrete columns wrapped with FRP composites," *Composite Structures*, vol. 93, no. 3, pp. 1103-1117, 2011.

[52] N. Raut and V. Kodur, "Response of high-strength concrete columns under design fire exposures," *J. Struct. Engrg.*, vol. 139, no. 69, 2011.

[53] B. Williams, L. Bisby, V. Kodur, M. Green, and Chowdhury E., "Fire insulation schemes for FRP-strengthened concrete slabs ," *Composites Part A: Applied Science and Manufacturing*, vol. 37, no. 8, pp. 1151-1160, 2006.

[54] S. Lamont, *The Behavior of Multy-storey Composite Steel Framed Structures in Response to Compartment Fires*. University of Edinburgh, 2001.

[55] M. Rafi and A., Faris, A. Nadjai, "Finite Element Modeling of Carbon Fiber-Reinforced Polymer Reinforced Concrete Beams under Elevated Temperatures," *ACI Structural*, vol. 105, no. 6, 2008.

[56] NEFCOM Corporation, "Fire resistance of concrete slabs reinforced by NEFMAC," NEFCOM Corp., Tokyo, Japan, 1998.

[57] T. Okamoto, S. Matsubara, M. Tanigaki, and K. Hasuo, "Practical Application and Performance of PPC Beams Reinforced with Braided FRP Bars," in *In Fibre-Reinforced-Plastic Reinforcement for Concrete Structures: An International Symposium.*, Detroit, Michigan, 1993.

[58] A. Abbasi and P. Hogg, "Fire testing of concrete beams with fibre reinforced plastic rebar," *Composites: Part A.* , vol. 37, no. 8, pp. 1142–1150, 2006.

[59] B. Williams, "Fire Performance of FRP-Strengthened Reinforced Concrete Flexural Members," Queen's University, Ontario, 2004.

[60] G. Craighead, *High-Rise Security and Fire*, 3rd ed. Oxford: Butterworth-Heinemann, 2009.

[61] International Code Council, "International Building Code," 2009.

[62] International Code Council, "International Fire Code," 2009.

[63] National Research Council, "National Building Code of Canada," 2010.

[64] ASTM 2002. Test Method E119-01: Standard Methods of Fire Test of Building Construction and Materials. American Society for Testing and Materials, West Conshohocken, PA..

[65] V. Kodur, "Fire Resistance Requirements for FRP Structural Members," in *Annual Conference of the Canadian Society for Civil Engineering*, Regina, Saskatchewan, 1999, pp. 83-94.

[66] A. Abbasi and P. Hogg, "Temperature and environmental effects on glass fibre rebar: modulus, strength and interfacial bond strength with concrete. ," *Composites: part B*, vol. 36, no. 5, pp. 394-404, 2005.

[67] J. Franssen, V. Kodur, and R. Zaharia, *Designing Steel Structures for Fire Safety*. London, UK.: Taylor & Francis Group, 2009.

[68] D. Drysdale, *An Introductin to Fire Dynamics*, 2nd ed.: John Wiley and Sons, 1999.

[69] S. Fehérvári, "Characretistics of tunnel fires," *Concrete Structures*, 2008.

[70] Promat, Tunnel Fire Protection, 2004.

[71] E. butcher, T. Chitty, and L. Ashton, "The temprature attained by steel in building fires.," *Fire Research technical paper*, 1966.

[72] S. Ingberg, "Tests of the severity of building fires," *National Fire Protection*, vol. 22, no. 1, pp. 43-61, 1928.

[73] M. Law, "A relationship between fire grading and building design and contents," *Fire Research Note*, 1971.

[74] O. Pettersson, S. Magnusson, and J. Thor, "Fire engineering design of steel structures," Swedish Institute of Steel Construction, 1976.

[75] T. Lie and E. Denham, "Factors Affecting the Fire Resistance of Circular Hollow Steel Columns Filled with Bar-Reinforced Concrete," Ottawa, 1993.

[76] T. Lie and R. Irwin, "Method to Calculate the Fire Resistance of Reinforced Concrete Columns with Rectangular Cross-Section," *ACI Structural Journal*, vol. 90, no. 1, pp. 52-60, 1993.

[77] T. Lie and V. Kodur, "Fire Resistance of Steel Columns Filled with Bar-Reinforced Concrete," *Journal of Structural Engineering, ASCE*, vol. 122, no. 1, pp. 30-36, 1996.

[78] B. Fredlund, "Modeling of heat and mass transfer in wood structures during fire," *Fire Safety Journal*, vol. 20, no. 1, pp. 36-69, 1993.

[79] Quiter, "High-rise buildings ," in *Fire Protection Handbook. 20th ed.* Quincy, MA: National Fire Protection Association;, 2008.

[80] R. Custer and B. Meacham, Introduction to Performance based Design for Fire Protection Engineers, 1994-1996, Short course.

[81] S. Badger, "Large Loss Fires in the United States," National Fire Protection Association, Batterymarch Park, Quincy, MA, 2009.

[82] Council of Canadian Fire Marshals and Fire Commissioners, *Fire Losses in Canada*. 2002.

[83] n.d. (2011) Beijing Television Cultural Center fire. [Online]. "http://reference.findtarget.com/search/Beijing%20Television%20Cultural%20Center%20fire/" http://reference.findtarget.com/search/Beijing%20Television%20Cultural%20Center%20fire/

[84] The free encyclopedia Wikipedia. (2011, March) List of fires. [Online]. "http://en.wikipedia.org/wiki/List_of_fires" http://en.wikipedia.org/wiki/List_of_fires

[85] ANSYS – Release Version 11., ANSYS – Release Version 11. , 2007, A Finite Element Computer Software and User Manual for Nonlinear Structural Analysis, ANSYS 2007; Inc. Canonsburg, PA.

[86] H. Blontrock, L. Taerwe, and P. Vandevelde, "Fire Testing of Concrete Slabs Strengthened with Fibre Composite Laminates. ," in *In The Fifth Annual Symposium on Fibre-Reinforced-Plastic Reinforcement for Concrete Structures (FRPRCS-5)*, London , 2001, pp. 547-556.

[87] Y. Bai, T. Keller, and T. Vallée, "Modeling of stiffness of FRP composites under elevated and high temperatures," *Composites Science and Technology*, vol. 68, no. 15-16, pp. 3309-3106, 2008.

[88] C. Griffis, R. Masmura, and C. Chang, "Thermal response of graphite epoxy composite subjected to rapid heating," *In Environmental Effects on Composite Materials*, vol. 2, pp. 254-260, 1984.

[89] S. Park, S. Manzello, D. Bentz, and T. Mizukami, "Determining thermal properties of gypsum board at elevated temperatures," *Fire and Materials*, 2009.

[90] C. Bailey and E. Ellobody, "Fire tests on bonded post-tensioned concrete slabs," *Eng Struct*, vol. 31, no. 3, pp. 686-696, 2009.

[91] C. Zhou and F. Vecchio, "Nonlinear finite element analysis of reinforced concrete structures subjected to transient thermal loads," *J Comput Concrete* , vol. 2, no. 6, pp. 455-479, 2005.

[92] CAN/ULC-S101-M89, "Standard Methods of Fire Endurance Tests of Building Construction and Materials," Underwriters' Laboratories of Canada, Scarborough, Ontario, 1989.

[93] X. Lu, J. Teng, L. Ye, and J. Jiang, "Bond–slip models for FRP sheets/plates bonded to concrete," *Engineering Structures*, vol. 27, no. 6, pp. 920-937, 2005.

[94] K. Nabaka, T. Kanakubo, T. Furuta, and H. Yoshizawa, "Bond behavior between fiber reinforced polymer laminates and concrete," *ACI Structural Journal*, vol. 98, no. 3, pp. 359-367, 1998.

[95] M. Leone, S. Matthys, and M. Aiello, "Effect of elevated service temperature on bond between FRP EBR systems and concrete," *Composites: Part B*, vol. 40, pp. 85–93, 2009.

[96] X-P. Xu and A. Needleman, "Numerical simulations of fast crack growth in brittle solids," *Journal of the Mechanics and Physics of Solids* , vol. 42, pp. 1397-1434, 1994.

[97] ISO, "ISO 11357-2: Plastics - Differential scanning calorimetry (DSC) - Part 2: Determination of glass transition temperature," ISO, 1999.

[98] American Society of Civil Engineers, "Standard calculation methods for structural fire protection : ASCE/SEI/SFPE 29-05. ," , 2007.

[99] H. Varastehpour and P. Hamelin, "Strengthening of concrete beams using fiber-reinforced plastics. ," *Mater Struct*, vol. 30, pp. 160-166, 1997.

[100] The free encyclopedia Wikipedia. [Online]. "http://en.wikipedia.org/wiki/"] http://en.wikipedia.org/wiki/

VITA

Mohannad Z. Naser was born on 14 January 1986 in Abu Dhabi, United Arab Emirates. He studied his elementary school in Abu Dhabi's public schools and then transferred to Al Orooba high school in Sharjah. He received his Bachelor of Science in Civil Engineering from the American University of Sharjah, UAE in Fall 2008. In January 2009, he was enrolled in the Civil Engineering graduate program with emphasis in Structural Fire Engineering at the American University of Sharjah, UAE. At the American University of Sharjah, he worked as a teaching assistance for the Statics, Mechanics and Structural Analysis as well as Field Plane Surveying Laboratory and research assistance for different professors on multiple researches. He was awarded the Master of Science degree in Civil Engineering in 2011.